

Jørgen Avdal

# Model-Based Evaluation of Blood Velocity Estimation Techniques

Thesis for the degree of Philosophiae Doctor

Trondheim, December 2014

Norwegian University of Science and Technology  
Faculty of Medicine  
Department of Circulation and Medical Imaging





# Abstract

Pulsed Wave (PW) Doppler is a flow imaging modality in which the velocity distribution of the blood flow in a spatial region is displayed over time. In this work, methods for improvement of the conventional PW Doppler technique are evaluated using mathematical models, *in vitro* and *in vivo* studies. The first part of the thesis is an evaluation of the use of sparse sequences for simultaneous PW Doppler and B-mode imaging, the second part investigates properties of the recently proposed 2-D Tracking Doppler method, and in particular the feasibility of this method for cardiac applications.

In conventional PW Doppler/B-mode duplex ultrasound, packets of B-mode and Doppler transmissions are interleaved, producing undesirable gaps in the Doppler data. In this context, several sparse sequence methods have been proposed in which PW Doppler spectra are generated from observation windows containing missing samples. In this work we show that sparse sequence methods have two significant weaknesses. Firstly, it is shown that long reverberation times lead to discontinuities in the signal from stationary clutter after each B-mode interruption. Secondly, using frequency analysis, it is shown that clutter filtering of non-uniformly sampled data may introduce artifacts in the velocity spectrum. Methods are presented for quantification of these effects, and their severity in clinical applications are shown using *in vivo* examples.

Two-dimensional (2-D) tracking Doppler is a proposed alternative to PW Doppler, in which the sample volume follows the trajectory of the blood scatterers over time. Compared to PW Doppler, 2-D tracking Doppler has longer observation time of individual scatterers and therefore reduced transit time broadening. An extensive signal model is presented and is, in addition to *in vitro* and *in vivo* recordings, used to evaluate properties of the 2-D tracking Doppler technique. It is shown that the spectra have lowest bandwidth and maximum power when the tracking angle is equal to the beam-to-flow angle, which may be used for automatic angle correction. *In vitro* studies and simulations indicate that automatic angle correction using tracking Doppler may be more accurate than manual angle correction, especially for high beam-to-flow angles.

The feasibility of using 2-D tracking Doppler for maximum velocity estimation in cardiac jet flow was investigated using simulations, *in vitro* and *in vivo* recordings. The results indicate that the -6 dB relative broadening of tracking Doppler spectra is smaller than 5% for tracking angles up to 80°, and also that the maximum power is found when tracking in the flow direction.



# Preface

This thesis is submitted in partial fulfillment of the requirements for the degree of *Philosophiae Doctor* (Ph.D.) at the Faculty of Medicine of the Norwegian University of Science and Technology (NTNU). The research was funded by the *Medical Imaging Laboratory* (MI-Lab), and was carried out at the Department of Circulation and Medical Imaging. The main supervisor has been Professor Hans Torp from Department of Circulation and Medical Imaging, and co-supervisors have been Professor Lasse Løvstakken from Department of Circulation and Medical Imaging and Pål Erik Goa from the Department of Physics.

## Acknowledgements

There are many people who have supported me during my years as a PhD student. I would like to thank my first supervisor, Pål Erik Goa, for making me feel comfortable right from the start and for introducing me to the exciting world of MR physics, but also for being a great supervisor and a good friend. I would also like to thank my main supervisor Hans Torp, for many interesting discussions in which he always ends up being right. His knowledge of the ultrasound field is surpassed by few, and he has been a source of encouragement and stability during my work in the field. I also want to express my gratitude to my co-supervisor Lasse Løvstakken, who has always been a great motivator and has been of great help in my writing.

Then I would like to thank the many people who have made me feel comfortable and happy at work. In particular I would like to thank Helen for many interesting and fun conversations over the years, Solveig for always having time for distractions, and Tonje for our great collaboration and many fruitful discussions. I should also thank Tore and Bastien for spending countless hours helping me with scanners and simulations, it would never have worked out without you.

I would like to thank my family for their unconditional love and support. I would also like to thank Magnus for being my favorite distraction and greatest motivation the last year. Finally, thank you, my dear Ingvild, for always taking care of me and supporting me. You are my best friend and the love of my life.



# Table of Contents

Abbreviations . . . . .	ix
<b>1 Introduction</b>	<b>1</b>
1.1 The duplex challenge . . . . .	1
1.2 Challenges in spectral velocity estimation . . . . .	3
1.3 Aims of study . . . . .	5
1.4 Thesis outline . . . . .	6
1.5 Background . . . . .	6
1.5.1 Pulsed Wave (PW) Doppler . . . . .	6
1.5.2 Clutter rejection . . . . .	9
1.5.3 Blood flow modeling . . . . .	13
1.6 Summary of contributions . . . . .	14
1.6.1 Evaluation of the use of sparse sequences for clinical applications (Chapter 2) . . . . .	14
1.6.2 2-D Tracking Doppler (Chapters 3 and 4) . . . . .	15
1.7 Discussion . . . . .	16
1.7.1 The use of sparse sequences for duplex imaging . . . . .	16
1.7.2 2-D Tracking Doppler . . . . .	18
1.8 Concluding remarks . . . . .	20
1.9 List of publications . . . . .	21
References . . . . .	22
<b>2 Effects of reverberations and clutter filtering in pulsed Doppler using sparse sequences</b>	<b>29</b>
2.1 Introduction . . . . .	29
2.2 Theory . . . . .	32
2.2.1 Reverberation time . . . . .	32
2.2.2 Clutter filtering of sparse sequences . . . . .	34
2.3 Materials and methods . . . . .	35
2.3.1 Data acquisition and processing . . . . .	36
2.3.2 Reverberation quantification . . . . .	36
2.3.3 Quantification of clutter filtering effects . . . . .	37
2.3.4 In vivo and in vitro color Doppler . . . . .	38
2.4 Results . . . . .	39

2.4.1	In vivo reverberation quantification . . . . .	39
2.4.2	Impact of clutter filtering on the velocity spectrum . . . . .	39
2.4.3	Impact of clutter filtering on the mean frequency estimate . . .	41
2.4.4	Experimental validation of Color Doppler Imaging sequence . .	42
2.5	Discussion . . . . .	44
2.6	Conclusion . . . . .	47
	References . . . . .	48
<b>3</b>	<b>Investigations of Spectral Resolution and Angle Dependency in a 2-D Tracking Doppler Method</b>	<b>53</b>
3.1	Introduction . . . . .	53
3.2	Theory . . . . .	55
3.2.1	The 2-D Tracking Doppler Algorithm . . . . .	56
3.2.2	Signal Model . . . . .	57
3.3	Methods . . . . .	58
3.3.1	Field II Simulations . . . . .	59
3.3.2	Application of the Signal Model . . . . .	60
3.3.3	<i>In Vitro</i> Recordings . . . . .	60
3.3.4	Velocity Calibration Analysis . . . . .	61
3.3.5	<i>In Vivo</i> Recordings . . . . .	61
3.4	Results . . . . .	62
3.4.1	Validation of Signal Model . . . . .	62
3.4.2	Investigations of the Tracking Angle Sensitivity . . . . .	62
3.4.3	Velocity Calibration . . . . .	66
3.4.4	<i>In Vivo</i> Imaging . . . . .	66
3.5	Discussion . . . . .	68
3.6	Conclusion . . . . .	70
	References . . . . .	72
<b>4</b>	<b>2-D tracking Doppler for Cardiac Jet Flow Velocity Estimation</b>	<b>75</b>
4.1	Introduction . . . . .	75
4.2	Methods . . . . .	77
4.2.1	Doppler processing . . . . .	77
4.2.2	Signal model . . . . .	78
4.2.3	Simulations . . . . .	80
4.2.4	Spectral broadening . . . . .	80
4.2.5	Transmit apodization . . . . .	81
4.2.6	Dependency of tracking angle . . . . .	82
4.2.7	<i>In vitro</i> validation . . . . .	83
4.2.8	<i>In vivo</i> measurements . . . . .	83
4.3	Results . . . . .	84
4.3.1	Simulation results . . . . .	84
4.3.2	Spectral broadening vs beam-to-flow angle . . . . .	85
4.3.3	Transmit apodization . . . . .	85
4.3.4	<i>In vitro</i> validation . . . . .	85

## Table of Contents

---

4.3.5	Variation with tracking angle . . . . .	86
4.3.6	In vivo results . . . . .	87
4.4	Discussion . . . . .	87
4.5	Conclusion . . . . .	90
	References . . . . .	91



# Abbreviations

B-mode	Brightness mode
CCA	Common carotid artery
CFD	Computational fluid dynamics
CDI	Color Doppler imaging
CW	Continuous wave
ECA	External carotid artery
FFT	Fast Fourier transform
FIR	Finite impulse response
FWHM	Full width at half maximum
$F_{\#}$	F-number
fps	Frames per second
ICA	Internal carotid artery
IIR	Infinite impulse response
IQ	In-phase Quadrature
PHT	Pressure half-time
PRB	Parallel receive beams
PRF	Pulse repetition frequency
PRT	Pulse repetition time
PSF	Point spread function
PW	Pulsed wave
RF	Radio frequency
ROI	Region of interest
Rx	Receive
SNR	Signal-to-noise ratio
Tx	Transmit
VTI	Velocity-time integral



# Chapter 1

## Introduction

Ultrasound imaging of blood flow in the human body has become an important diagnostic tool in several fields, including gynecology, obstetrics, pediatrics, oncology, and in the cardiovascular field [1–5]. The use of ultrasound technology to measure velocities in the human body was first suggested by Satomura [6] in 1959, then by transmitting a single frequency signal into the body and using the Doppler shift to measure the movement of heart walls and valves. This technology is still in use today and is commonly referred to as Continuous Wave (CW) Doppler. The method was soon adapted to measure blood velocities [7, 8]. Since then, several techniques have been introduced, significantly improving velocity estimation in medical ultrasound imaging. In the late 1960s, Pulsed Wave (PW) Doppler was described [9], in which finite pulses are transmitted with regular intervals, allowing the use of range gating to measure blood velocities at several depths and thus to acquire velocity profiles. The first images of arteries came in the early 1970s [10], and the first 2-D gray-scale or B-mode (Brightness-Mode) scan of a human joint in 1972 [11]. The duplex systems, allowing for both flow measurements and B-mode images for navigation were developed shortly thereafter [12].

The two most common ways of displaying Doppler velocity measurements as of today are illustrated in Fig. 1.1. In Color Doppler Imaging (CDI), or *color flow imaging*, the mean velocity is calculated in a 2-D or 3-D region of interest, color coded and then overlaid a grayscale anatomical image. The other imaging modality is commonly referred to as *spectral Doppler*, and is based on the PW Doppler and CW Doppler techniques. In this modality, the full spectrum of blood velocities in a small spatial region is displayed as a function of time. In this work, we investigate recently proposed methods addressing two fundamental challenges of PW Doppler imaging. The first challenge is to achieve simultaneous B-mode images and velocity measurements without significantly degrading the two modalities. The second challenge is to avoid broadening of the estimated spectra due to the limited observation time of moving scatterers.

### 1.1 The duplex challenge

PW Doppler/B-mode duplex ultrasound is a modality in which the ultrasound system is used for simultaneous acquisition and visualization of B-mode images and PW Doppler data. The two modalities strongly differ in their requirements on the

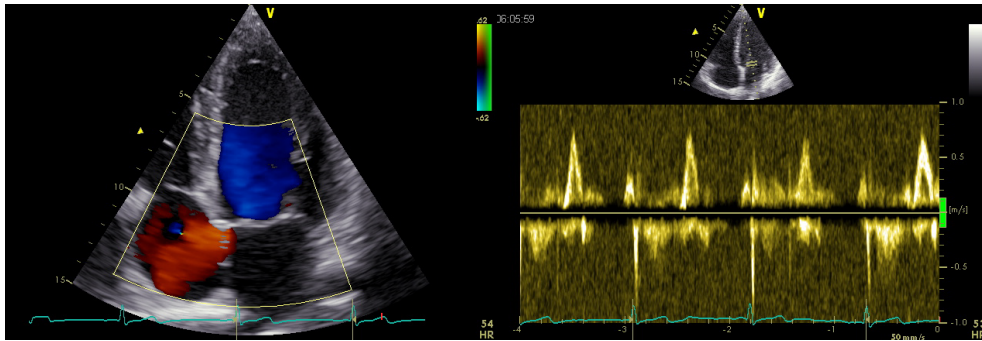


**Figure 1.1:** Left: example of a color Doppler image. A mean velocity color map is shown in a region of interest (ROI). Flow towards the probe is visualized as red, flow away from the probe is blue. Right: example of a PW Doppler image, where the flow velocity distribution in a sample volume is displayed over time. The sample volume is indicated by two parallel lines in the B-mode image above the spectral display.

transmitted pulses. B-mode images are used for navigation and anatomic assessment, and requires high resolution and contrast. High resolution is achieved by using pulses with high center frequency and short pulse length, and resolution can be traded off for contrast by using receive apodization. In PW Doppler imaging, however, the use of long pulses and low center frequency is preferred to increase the penetration depth and the Nyquist velocity limit. For this reason, separate pulses are typically used for the two modalities.

In conventional duplex imaging, the Doppler acquisition is interrupted regularly to acquire segments of B-mode images. However, this causes gaps in the Doppler data, which again lead to gaps in the velocity spectrum display. The gaps in the velocity spectrum are also larger than the gaps in the Doppler data, due to filter initialization and the use of overlapping windows for spectrum estimation.

Methods have been proposed to fill in the missing data in the Doppler signal before velocity spectrum estimation, in which the missing signal segments are essentially synthesized from preceding or successive samples [13, 14]. Ideally the interruptions should be short so that the signal can be assumed to be stationary throughout their duration. The number of interruptions should also be low to minimize the number of lost samples after each interruption. On the other hand, a minimum ratio of B-mode-to-Doppler insonations is required to maintain a decent B-mode frame rate and quality. Note that in addition to finding the right balance between Doppler and B-mode firings, an important part of duplex sequence design is the choice of clutter filter. Due to the samples lost to filter initialization after every interruption, it is desirable that the impulse response of the clutter filter should be as short as possible.

A number of proposed techniques have potential to influence the design of duplex sequences. One possibility is to use compounding of plane waves or diverging waves to produce B-mode images [15]. In this approach, received echoes from multiple

transmissions are coherently combined in post-processing to achieve higher contrast, resolution and SNR than the images generated from a single transmission. Lateral resolution increases with the maximum angles used, whereas contrast and SNR increases with the number of transmissions. A study performed by Bercoff *et al.* [16] shows that about 16 transmissions are enough to obtain higher SNR than focused imaging, and about 30 transmissions to achieve better anechoic contrast. However, on the order of 10 transmissions should result in an image quality comparable to that of focused imaging. A disadvantage of using plane wave compounding is that, similarly to other synthetic aperture techniques, rapid tissue motion leads to incoherency between the compounded signals and motion artifacts in the compounded image. The severity of this effect increases with the time lag between the first and last transmission used for each compounding frame [17, 18].

Also, some adaptive spectral estimation techniques like Power Spectral Capon [19], projection-based Capon [20] and BIAA [21, 22] have been proposed in which PW Doppler spectra are generated from shorter temporal observation windows. While this improves temporal resolution and thus the ability to depict rapid flow events, it can also decrease the length of the gaps in the velocity spectrum. In addition, the resulting spectra do not suffer from clutter sidelobes, and it has been shown that it is possible to produce high quality spectra without clutter rejection [20], avoiding the loss of samples due to filter initialization after B-mode interruptions. However, also these methods have notable drawbacks. The Capon methods are not robust without spatial or temporal averaging, unless a diagonal loading parameter is used for the covariance matrix. In addition, the projection-based Capon method is parametric - requiring an estimate of the number of signal components for every timestep. The BIAA method is less dependent on averaging, but being an iterative method, it is very computationally expensive.

Finally, a number of sparse sequence methods [22–25] have been proposed as potential solutions to the duplex problem. Common for all these methods is that the spectra are estimated from observation windows containing short and frequent gaps due to B-mode interruptions, as opposed to the longer gaps of conventional duplex acquisition. This eliminates the gaps in the spectral display, on the cost of potential artifacts due to the degraded observations windows. However, most of these techniques have only been validated on fully sampled data which have been synthetically undersampled in post-processing, and thus may face additional challenges when applied to data acquired by ultrasound systems using sparse sampling.

## 1.2 Challenges in spectral velocity estimation

The maximum velocity of blood flow is an important parameter used for grading stenosis, both in the carotid artery and in heart valves. It is also commonly used in the assessment of cardiac function. By using the simplified Bernoulli equation  $\Delta P = 4v^2$  [26], the maximum jet flow velocity in stenosed or insufficient valves is used to estimate the peak pressure gradient between heart chambers. Delineation of the maximum velocities in the spectral display of jet flow provides an estimate of the velocity-

time integral (VTI), which multiplied with cross-sectional area at the jet location gives an estimate of stroke volume. Maximum velocities are also used to estimate the pressure half-time (PHT), which is related to the severity of mitral stenosis and aortic regurgitation [27, 28]. To assure the diagnostic value of the maximum velocity estimates, ideally they should be accurate, or at least be minimally dependent on parameters that vary between observers and subjects. However, the conventional PW Doppler and CW Doppler spectral estimators have several weaknesses that makes this difficult to achieve in practice.

One such weakness is that only the velocity in the axial direction is measured. In order to estimate the true velocity, the beam-to-flow angle needs to be estimated manually by the observer. This may cause significant errors in velocity estimates, especially for large beam-to-flow angles. To limit errors in velocity estimation, clinical guidelines recommend against the use of beam-to-flow angles above  $60^\circ$  [29, 30]. Moreover, angle correction is not recommended in cardiac jet flow measurements, as it is likely to introduce more erroneous velocity estimates given the unpredictable jet direction [31].

The angle dependency problem of Doppler ultrasound have been subject to research since the early 1970s, and several techniques have been proposed for estimating two or three vector velocity components, either by using multiple beams from different angles [32], by using correlation techniques [33–36], or by studying the symmetry properties [37] or the bandwidth of the Doppler spectrum [38, 39]. This is a rapidly developing field, and one might argue that vector velocity imaging techniques also have the potential to determine maximal velocities in blood flow, and may therefore soon replace PW Doppler and CW Doppler in some applications. A notable challenge, however, would be to achieve high enough spatial resolution to accurately determine the maximal velocities. In most techniques used for vector velocity imaging, the mean velocity in each sample volume is estimated. Thus if the sample volumes containing the maximum velocities also contain notable velocity gradients, the maximum velocities would be underestimated by such approaches. In peripheral arteries, however, high enough resolution might be achievable.

Generation of velocity spectra for flow in the transversal direction has been investigated in a recent work by Jensen [40]. In this method, the received signals at left and right subapertures are combined in such a way that an oscillating field is generated in the transversal direction. Because the lateral velocity component is estimated, angle correction is performed relative to the transversal direction rather than the beam direction. This significantly decreases the sensitivity to errors in angle correction for high beam-to-flow angles. The spectral quality degrades when the beam-to-flow angle deviates from  $90^\circ$ , however, and use of the lateral spectrum is not recommended for beam-to-flow angles below  $75^\circ$ .

Another challenge in spectral Doppler is that the estimated spectra are subject to spectral broadening, due to the limited observation time of individual scatterers. This causes overestimation of maximum velocities, but also introduces intra-observer and inter-observer variation as the apparent maximum velocity depends on the beam-to-flow angle. Two notable techniques for reducing spectral broadening in the spectral display are the multifrequency Doppler technique [41] and the velocity-matched

spectrum technique [42]. In the former technique, Doppler spectra are generated from several ultrasound frequencies transmitted simultaneously and then averaged to reduce the variance of the spectral estimates. In the latter technique, the samples used for estimating the power at each velocity are following the axial position of scatterers over time, maximizing observation time for each velocity and thus minimizing spectral broadening. Even though the motivation for the two techniques were different, it turned out that they have essentially the same properties. A limitation of both techniques, however, is that they do not reduce transit time broadening for high beam-to-flow angles when the observation time is limited by the lateral extent of the sample volume.

A recently published technique for the reduction of spectral broadening is based on the use of plane waves [15]. In this technique, termed Doppler Frequency Spatial Analysis (DFSA) [43], the mean frequency is calculated from every spatial point in a region of interest, and mean velocity histograms are displayed over time, similar in appearance to velocity spectra produced by PW and CW Doppler. Provided that the velocity spectrum in each resolution cell is symmetric, this effectively reduces spectral broadening. A notable drawback, however, is that the velocity variations need to be small within each resolution cell. This makes the use of the technique difficult in for example cardiac applications, where the resolution is limited by the acquisition depth and the size of the transducer aperture. High velocity gradients within each sample volume would then contribute to underestimation of the maximum velocities.

Another notable technique addressing the estimation of maximal blood velocities in blood vessels is that of Ricci et al [44]. In this work, the velocity spectrum is estimated from a large sample volume, covering the entire vessel in the axial direction, and more than 30% of the diameter in the lateral direction. Through a model-based analysis, it is shown that the maximal velocity is then found at the half power, or -6 dB threshold, in the descending slope located at the higher frequencies of the spectrum. According to the model, this estimate is accurate for a wide range of beamwidths, velocities and flow profiles. However, the velocity estimates are still prone to errors due to angle correction. Also, further work is needed to understand the performance of the technique for more complex patterns.

Two dimensional (2-D) tracking Doppler [45] is a recently proposed extension of the velocity-matched spectrum technique, in which the sample volume follows both the axial and lateral movement of the blood scatterers over time. This was made possible by an increase in the number of available receive channels, facilitating the use of broad beams on transmit and parallel beams on receive. Compared to PW Doppler, the use of 2D tracking Doppler results in an increased observation time of individual scatterers, and therefore reduced transit time broadening.

### 1.3 Aims of study

The overall objective of this thesis is to investigate the practical applicability of recently proposed methods for improvement of the PW Doppler modality. The first part concerns the duplex challenge, the second part the quality of the velocity

spectrum. In short, the papers included in this thesis aimed to:

**1. Investigate the use of sparse sequences for duplex imaging:**

Several techniques have been proposed in recent years for spectral estimation from non-uniformly sampled Doppler data. This potentially solves the problem of gaps in the spectral display, but may degrade the quality of the resulting spectra. This study aims to investigate the use of sparse sequences in cardiac and carotid applications, considering both pulsed wave Doppler and color Doppler imaging modalities.

**2. Investigate the angle dependency of 2-D tracking Doppler:**

The 2-D tracking Doppler method is an extension of the velocity matched spectrum technique where tracking of scatterers is done across several receive beams. The new method has been shown to significantly decrease spectral broadening due to the transit time effect when the tracking angle coincides with the beam-to-flow angle. This study aims to investigate the dependency of the 2-D tracking method on the tracking angle and the beam-to-flow angle, and the potential use of this knowledge to perform automatic angle correction.

**3. Adapt the 2-D tracking Doppler technique to cardiac applications:**

Promising results have been presented using the 2-D tracking Doppler technique for velocity estimation in the carotid artery. The ability of the method to suppress effects of aliasing and the potential for automatic angle correction makes it a candidate for use in cardiac flow imaging. This work therefore aims to investigate the properties of the technique when implemented on a phased array for estimation of maximum velocities in cardiac jet flow.

## 1.4 Thesis outline

The contributions of this thesis are summarized in Section 1.6, discussed in 1.7, and presented in Chapters 2-4. The following section provides the unfamiliar reader with a short introduction to some key concepts and conventional methods relevant for this work, including PW Doppler, clutter rejection and blood flow signal modeling.

## 1.5 Background

### 1.5.1 Pulsed Wave (PW) Doppler

In PW Doppler imaging, the volume of interest is insonated with several pulses in rapid succession, to obtain the signal from moving scatterers over time. The received signal from a single pulse is referred to as the *fast time signal*, whereas the signal from a fixed sample volume over successive pulses is called the *slow-time signal*. The velocity estimation in PW Doppler is based on a narrowband approximation, in which the transmitted pulse is assumed to be infinitely long and sinusoidal. In this case, the

resulting RF signal from a scatterer moving with constant velocity is also sinusoidal, with frequency given by the pulse frequency  $f_p$  and the axial velocity  $v_a$ :

$$s(r, k) = A \cos(2\pi f_d t_k + 4\pi f_p r/c + \phi). \quad (1.1)$$

where  $r$  is axial position,  $k$  is the slow-time index,  $t_k = k/\text{PRF}$  and PRF is the slow-time sampling frequency, or *pulse repetition frequency*. The frequency shift  $f_d$  is given by:

$$f_d = \frac{2v_a f_p}{c}. \quad (1.2)$$

Here  $c$  is the speed of sound. After IQ-demodulation, this becomes a complex single frequency signal:

$$s_{IQ}(r, k) = A e^{2\pi i f_d t_k + i\phi} \quad (1.3)$$

If the sample volume contains several scatterers with different velocities, the signal contribution from the scatterers will be uncorrelated, and the frequency content of the total signal will reflect the velocity distribution of the scatterers. The velocity distribution, or the velocity spectrum, may then be estimated as the discrete Fourier transform of a segment of the slow-time signal.

$$\hat{P}(f_d) = \left| \sum_{k=0}^N s_{IQ}(r, k) e^{-2\pi i f_d t_k} \right|^2 \quad (1.4)$$

The estimated velocity spectra are displayed as vertical lines in a *spectral display*, and the development of the velocity spectra over time is visualized along the horizontal direction, as shown in the right panel of Fig. 1.1. The measurable velocity span is determined by the pulse repetition frequency, and the resolution of the spectrum is determined by the number of slow-time samples  $N$ .

The velocity spectrum estimator used in conventional PW Doppler has several limitations. First and foremost, it only estimates the velocity components along the direction of the transmitted beam. To obtain the true velocity distribution, the beam-to-flow angle  $\theta$  must be estimated manually by the operator, using a simultaneous anatomical image or color Doppler image. The velocity spectrum is then scaled by an angle correction factor of  $1/\cos\theta$ . Because the angle correction factor tends to infinity when  $\theta$  approaches  $90^\circ$ , the velocity spectrum is very sensitive to errors in the angle estimate for high beam-to-flow angles. The use of PW Doppler is therefore not recommended for beam-to-flow angles above  $60^\circ$  [29, 30].

Another limitation of PW Doppler is that the observation time of each scatterer is finite, invalidating the narrowband assumption of (1.1)-(1.3). A scatterer moving with constant velocity through the sample volume will produce a spectrum with bandwidth inversely proportional to the transit time, commonly referred to as the *transit time effect*. Because the transit time is again inversely proportional to the velocity of the scatterer, this effect causes the same fractional broadening for all velocities [46]. Considering that each frequency component in the pulse contributes to the frequency content of the signal, the expression (1.3) becomes an integral:

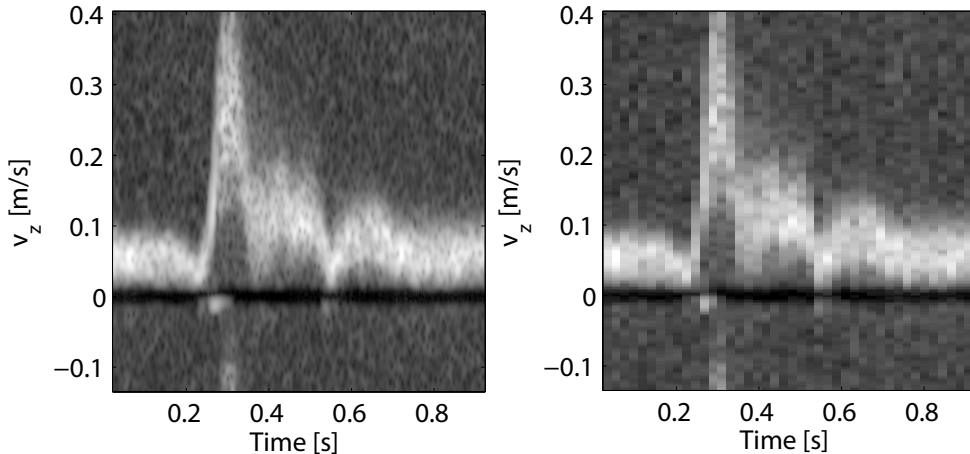


**Figure 1.2:** Left: example of a PW Doppler spectrum using overlapping temporal windows. Right: PW Doppler spectrum generated from the same data without using overlapping windows.

$$s_{IQ}(r, k) = \int_{f_p} A(f_p) e^{2\pi i f_d t_k + i\phi_r} df_p, \quad (1.5)$$

Because  $f_d$  and  $f_p$  only differ by a constant scaling factor, as described in (1.2), the relation (1.5) implies that the frequency content of  $S_{IQ}$  is essentially the same as that of the transmitted pulse with a scaling of the frequency axis. Consequently, the fractional broadening of the spectrum (1.4) is equal to the fractional bandwidth of the pulse. However, this is only true if the transit time is limited by axial resolution, because the signal model only included movement in the axial direction. If the transit time is limited by the lateral resolution or out-of-plane flow, the fractional broadening will be larger than the fractional bandwidth of the pulse. The spectral broadening due to the transit time effect causes overestimation of maximum velocities. It is also more severe for high beam-to-flow angles, as the Doppler shift decreases and the fractional broadening increases.

A final limitation of conventional PW Doppler is the high variance of the Fourier based spectrum estimator in (1.4). Each power estimate in the frequency spectrum is a random variable, and the underlying probability density function is a chi-squared distribution with two degrees of freedom. In this distribution, the standard deviation is equal to the expected mean value. This is an intrinsic property of the estimator and not dependent on spatial resolution or the number of slow-time samples used for spectrum estimation. The variance may, however, be reduced by spatial or temporal averaging of the estimated spectra. Temporal averaging of spectral estimates from overlapping windows is used in many applications and is commonly referred to as Welch's method [47]. In practice, this problem may be partially resolved by allowing overlap of the

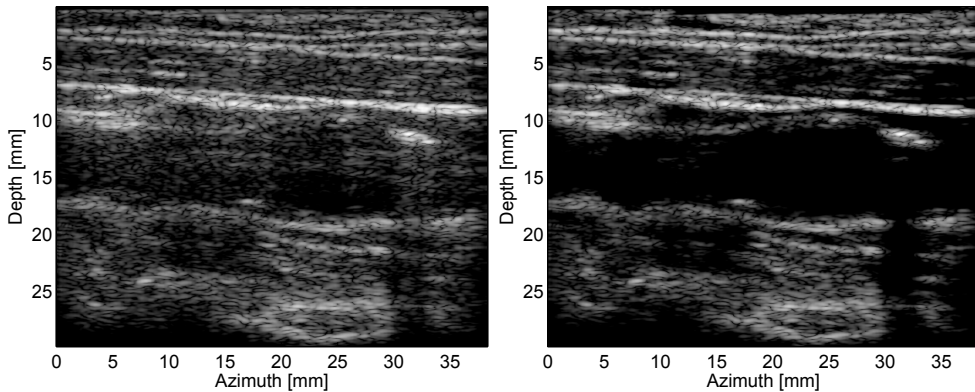


**Figure 1.3:** Left: B-mode image with clutter signal in the lumen due to reverberations. Right: Image generated from the same data after applying a reverberation suppression technique. Adapted from [49].

temporal windows used for spectral estimation, synthesizing a high temporal resolution in the spectral display. Temporal averaging may then be performed visually by the observer, as illustrated in Fig. 1.2.

### 1.5.2 Clutter rejection

The blood signal, which is the signal of interest in Doppler measurements, is typically 40-60 dB weaker than the signal from surrounding tissue [48]. Due to multiple reflections in tissue layers near the probe, multiple copies of the tissue signal, or reverberations, may occur after the direct echo, interfering with the blood signal. An example of reverberations in the lumen of the carotid artery is shown in Fig. 1.3. This unwanted signal contribution from tissue is commonly referred to as *clutter*.

The velocities in tissue are typically much lower than blood velocities, and the two signal components can in some cases be distinguished in the frequency domain. However, in many cases sidelobes from stationary or slowly moving tissue obscure the blood signal in the spectral display. Sidelobes appear because the signal used to generate the spectrum is only observed over a limited time, which corresponds to applying a rectangular window function to the slow-time signal. This causes spectral broadening and the occurrence of sidelobes in the frequency domain. The use of window functions before spectral estimation attenuates the sidelobes from tissue, but this only solves the problem if the sidelobes of the clutter fall below the thermal noise floor. The angle dependency of velocity measurements in ultrasound imaging also results in challenges for clutter rejection. In peripheral vessels such as the carotid artery, it may be difficult to separate the blood and tissue signal, because the movement of the vessel wall is aligned with the beam axis, whereas the blood flow is close to perpendicular to it. In these cases, the tissue velocities in the axial direction may be as high or even higher than the axial blood velocities. This is another reason why a beam-to-flow

angle smaller than  $60^\circ$  is recommended in these cases.

The clutter signal may be attenuated by applying high pass, or *clutter filters*, to the slow-time signal. A filter is usually characterized by its *amplitude response*, which is the attenuation as a function of input frequency. The *stopband* of a filter consist of the frequencies that are not allowed to pass. The required stopband attenuation may vary with the application. Similarly, the *passband* of a filter consist of frequencies that are allowed to pass through the filter without attenuation. Between the stopband and the passband is the *transition band*. Desired filter properties in Doppler ultrasound include a high stopband attenuation to suppress the strong clutter signal, and a narrow transition band to avoid attenuation of the frequencies of interest. In general, there is a tradeoff between these properties and the length of the impulse response of the filter.

### Linear time-invariant filters

A filter is *linear* if its output is obtained by a linear operation on its input. A filter is *causal* if its output is dependent on current and past inputs or outputs, but not future inputs or outputs. Finally, a filter is said to be *time-invariant* if a time shift in the input  $x$  implies the same time shift in the output  $y$ . A general causal linear time-invariant filter has the form:

$$\sum_{m=0}^{M-1} a(m)y(n-m) = \sum_{k=0}^K b(k)x(n-k). \quad (1.6)$$

If a filter is linear and time-invariant, the output  $y$  can be described as a convolution between the input  $x$  and the *filter impulse response*  $h$ :

$$y(n) = (h * x)(n) \quad (1.7)$$

The frequency response  $H$  of the filter may then be obtained as the Fourier transform of  $h$ , and filtering is equivalent to a multiplication in the Fourier domain:

$$Y(f) = H(f)X(f) \quad (1.8)$$

Thus, if  $X(f)$  is zero for some frequency  $f$ ,  $Y(f)$  will also be zero. In other words, no new frequency components are introduced in the signal by applying the filter. This is usually a desired filter property, especially when spectral analysis is to be performed on the filter output.

In addition to the amplitude response, linear time-invariant filters also have a *phase response*. The most ideal phase response is a *zero phase* filter, meaning that the phase of all input frequencies are unaltered after filtering. Thus a waveform with frequency content in the passband will not be distorted nor delayed by the filter. Unfortunately, the impulse response of a zero phase filter must be symmetric around zero. Such filters are not suited for real time implementation as they are not causal. However, applying a suitable time shift to a zero phase filter produces a causal filter which imposes a time shift on waveforms in the passband, but leave them undistorted. The time shift

corresponds to a linear phase variation in the frequency domain, and such filters are referred to as *linear phase* filters. Filters which are neither zero phase nor linear phase are referred to *non-linear phase* filters. Because they have no restrictions on the phase of the output, it is usually possible to achieve a desired amplitude response with shorter impulse response for non-linear phase filters than for linear phase filters.

### FIR filters

If  $a(0) \neq 0$  and  $a(m) = 0$  for  $m \geq 1$  in (1.6), the result is a Finite Impulse Response (FIR) filter, termed finite because each output is a weighted sum of a finite number of current or past inputs. The output of a FIR filter is a convolution between the input signal  $x$  and the impulse response  $h$  with  $h(k) = b(k)$ , see (1.6):

$$y(n) = \sum_{k=0}^K h(k)x(n-k) \quad (1.9)$$

The length of the impulse response  $K$  is referred to as the *order* of the FIR filter. Because all filter registers must be filled before the output is valid ( $n \geq K - 1$ ), an input signal of length  $N$  will result in an output signal with length  $N - K + 1$ . These lost samples due to *filter initialization* cause challenges when the acquired Doppler data contains interruptions, as further discussed in Chapter 2.

### IIR filters

If  $a(0) \neq 0$  and also  $a(m) \neq 0$  for some  $m \geq 1$  in (1.6), we get an Infinite Impulse Response (IIR) filter. Compared to FIR filters, for which the output is dependent on past and current inputs, the output of an IIR filter is also dependent on past outputs. Most analog filters based on resistors, inductors and capacitors employ feedback and are thus IIR filters.

In the case of IIR filters, the filter order is the length of  $a$  or  $b$  in (1.6), whichever is longer. The recursive formulation yields impulse responses that continue indefinitely. However, in practice the impulse responses are essentially zero after a finite number of samples and may be truncated, after which the filter is essentially a FIR filter. The resulting impulse responses may be quite long, however, and similar to FIR filters, the output samples are not valid during initialization of a truncated IIR filter. An alternative is to use a filter initialization technique, in which essentially a synthetic signal is appended to the start of the input signal to initialize the filter. For *step initialization*, the input signal is assumed to be equal to the first sample before the signal onset. More sophisticated techniques include projection initialization [50] and exponential initialization [51]. When using initialization techniques with IIR filters, we differentiate between the steady state frequency response, which is valid for infinitely long signals, and the transient frequency response, which is dependent on the length of the signal and the filter initialization technique.

### Polynomial regression filters

The last category of filters discussed in this section is the polynomial regression filters. Polynomial regression clutter filters essentially attenuate the clutter signal by approximating it with a low order polynomial, and subtracting the polynomial from the Doppler signal. For these filters, the filter order is defined as the order of the polynomial used for clutter estimation. A more detailed description of polynomial regression filters is included in chapter 2, but some of its properties are discussed here. Polynomial regression filters are well suited for short signals because no samples are lost due to filter initialization, and they have been shown to yield amplitude responses with narrow transition bands on short signal segments [52].

Unlike FIR and IIR filters, polynomial regression filters can not be represented on the form (1.6). Instead, the weighting of the slow-time samples changes over time, and such filters are therefore *time variant*. Polynomial regression filtering can therefore not be described as a multiplication in the Fourier domain like in (1.8), and frequency components may occur in the output signal that were not present in the input signal. A more quantitative analysis of the filter response of polynomial regression filters may be found in [52].

### Discussion

In general, it is possible to achieve a specified filter response using a lower filter order with an IIR filter than a FIR filter, making them potentially less computationally intensive and less memory demanding. A disadvantage of IIR filters is that they are never linear phase filters, although some IIR filters like the Bessel filters have approximately linear phase. Also, in their digital implementation, IIR filters are more prone to numerical instability as errors may propagate through the feedback loop. The main advantages of FIR filters are that they are easy to design and implement. It is for example easy to design a linear phase FIR filter, as the only requirement is that the impulse response is symmetric. The main disadvantage of FIR filters is the high memory demand and higher computational cost.

In PW Doppler and color Doppler imaging, the estimated power spectrum is not affected by the phase response of the slow-time clutter filter, making it possible to perform clutter filtering with non-linear phase FIR filters as well as IIR filters. The primary considerations when choosing clutter filters for Doppler are thus the properties of the amplitude response, or more precisely, sufficient stopband attenuation and a narrow transition band. For PW Doppler with a continuous stream of Doppler data, FIR and IIR filters are usually preferred because they are time invariant. Of these alternatives, IIR filters should be less computationally expensive because a lower filter order is achievable. However, FIR filters are easier to design and also less prone to numerical instability.

The use of polynomial regression filters for PW Doppler is not very common, but they are of interest when the slow-time signal used for PW Doppler is interrupted to acquire B-mode images, as will be further discussed in Chapter 2. The primary disadvantage of regression filters is that they are time variant, and this may lead to artifacts in the resulting frequency spectra, as will also be shown in Chapter 2.

### 1.5.3 Blood flow modeling

In ultrasound models of scattering from blood, the red blood cells are typically assumed to be independent scatterers. Red blood cells are small ( $< 10 \mu\text{m}$  diameter) compared to typical wavelengths in ultrasound ( $150 - 750 \mu\text{m}$ ). They are also densely packed and strongly interacting, so that concerning wave propagation, blood can be regarded as a continuum [53].

The scattering properties of blood are determined by spatial fluctuations in the cell concentration  $n(r, t)$ . The correlation length of  $n$  is so small compared to typical ultrasound wavelengths that it can be considered to be spatially uncorrelated, or  $\delta$ -correlated in space. This simplifies modeling of the backscattered signal as its spectral properties are the same as for noninteracting scatterers. Therefore, we will in the following describe the scattering from blood through a scatterer density function  $n_s$ .

The backscattered signal from the flow field will, however, be spatially correlated due to the spatial correlation of the transmitted pulse. If  $p$  denotes the point spread function, the backscattered signal from pulse  $k$  becomes:

$$x(\vec{r}, k) = \int_{r_1} p(r_1) n_s(\vec{r} - r_1, k) d^3 r_1, \quad (1.10)$$

Note that  $n_s$  is a discrete function of its second argument, we have thus assumed that changes in  $n(r, k)$  during the pulse propagation time are negligible. In the following,  $n_s(r, k)$  will be treated as a random variable. Each  $\hat{x}(r, k)$  is then a weighted average of random variables with near-zero correlation length, and can thus be approximated as a Gaussian random variable by the central limit theorem. The time series  $\hat{x}$  then becomes what is known as a *Gaussian process*. Note that the central limit theorem may also be used to argue that  $n_s(r, t)$  itself is a Gaussian process.

Even if the values in a Gaussian process are random, they may be correlated. If the slow-time covariance function  $C(k, l)$  is only dependent on the lag  $m = k - l$ , and the expected mean value does not vary with time, the Gaussian process is said to be *wide-sense stationary*. The Wiener-Khinchin theorem then states that the spectral power density function of the Gaussian process is equal to the temporal Fourier transform of its autocorrelation function  $R_x$ .

$$R_x(\rho, m) = \int_{\vec{r}} \sum_k x(\vec{r} + \vec{\rho}, m + k) x(\vec{r}, k), \quad (1.11)$$

$$G_x(f) = \sum_m R(0, m) e^{2\pi i f m \Delta t}. \quad (1.12)$$

It now remains to find the autocorrelation function of the slow-time signal  $x$ . Let  $\vec{v}'(\vec{r}, t)$  be the velocity field of the blood scatterers. Then

$$n^{\vec{v}}(\vec{r}, t) = \begin{cases} n_s(\vec{r}, t), & \text{if } v'(\vec{r}, t) = \vec{v} \\ 0, & \text{otherwise} \end{cases} \quad (1.13)$$

represents the blood scatterers moving with velocity  $\vec{v}$ . Because the spatial correlation length of  $n^{\vec{v}}$  is zero, its autocorrelation function can be expressed on the form:

$$n_2^{\vec{v}}(\vec{\rho}, m) = a\delta(\vec{\rho} - m\Delta t\vec{v}), \quad (1.14)$$

where the subscript is short notation for the autocorrelation operator. The autocorrelation function of the corresponding slow-time signal  $x^v$  then becomes:

$$\begin{aligned} \hat{x}_2^v(\vec{\rho}, m) &= \int_{\vec{r}_1} \int_{\vec{r}_2} \int_{\vec{r}_3} \sum_k p(\vec{r}_1)n(\vec{\rho} + \vec{r}_3 - \vec{r}_1, m + k)p(\vec{r}_2)n(\vec{r}_3 - \vec{r}_2, k) d^3\vec{r}_3 d^3\vec{r}_2 d^3\vec{r}_1 \\ &= a \int_{\vec{r}_1} \int_{\vec{r}_2} p(\vec{r}_1)p(\vec{r}_2)\delta(\vec{\rho} - \vec{r}_1 + \vec{r}_2 - m\Delta t\vec{v}) d^3\vec{r}_2 d^3\vec{r}_1 \\ &= a \int_{\vec{r}_2} p(\vec{\rho} + \vec{r}_2 - m\Delta t\vec{v})p(\vec{r}_2) d^3\vec{r}_2 = ap_2(\vec{\rho} - m\Delta t\vec{v}). \end{aligned} \quad (1.15)$$

Because the blood flow is spatially uncorrelated, the autocorrelation of the total signal  $x$  may be obtained by adding the contribution from all velocities:

$$\hat{x}_2(\rho, m) = \int_v ap_2(\rho - m\Delta t\vec{v}). \quad (1.16)$$

## 1.6 Summary of contributions

### 1.6.1 Evaluation of the use of sparse sequences for clinical applications (Chapter 2)

In conventional PW Doppler/B-mode duplex ultrasound, the Doppler signal is interrupted regularly to allow for the acquisition of B-mode image segments. This leads to several gaps in the Doppler data and in the corresponding spectral display. In this context, several sparse sequence methods have been proposed in which the Doppler signal is frequently interrupted by short B-mode acquisitions, and the PW Doppler spectra are generated from observation windows containing missing samples.

In this work we show that sparse sequence methods have two significant weaknesses. Firstly, in many applications, the backscattered echoes from preceding pulses are not sufficiently attenuated before the onset of the next pulse. In Doppler sequences without interruptions this is not a problem, as the interfering signal becomes stationary after a few samples and is removed by the clutter filter. However, after every B-mode interruption a transient signal contribution is introduced in the slow-time signal, with length equal to the reverberation time of a single Doppler pulse. This introduces broadband noise into the slow-time signal, and we show an example where the amplitude of this noise is 30 dB above the noise level. This reverberation noise can only be removed by discarding the samples containing the transient signal before clutter filtering. In a cardiac example we measured reverberation times exceeding 400  $\mu\text{m}$ , corresponding to 2-4 lost samples after every B-mode interruption with typical PRF values. For vascular imaging we found that typically one sample needs to be discarded after every interruption.

Secondly, the non-uniform sampling pattern of the Doppler data makes it necessary to regression filters for clutter removal, but we show that non-uniform sampling patterns degrade the filter response of polynomial regression filters and produces artifacts in the resulting velocity spectra. Using three example sequences, we show that artifacts that may occur include multiple copies of the spectra, spectral broadening and increased noise floor, depending on the sampling pattern used.

We also evaluated the use of sparse sequences for mean velocity estimation in color Doppler Imaging (CDI). For two of the example sequences, the bias in the mean estimate due to clutter rejection is smaller than 1.3 % of the Nyquist limit for all velocities. An *in vitro* flow example was shown the use of a sparse sequence resulted in an improved filter amplitude response and reduction in the bias due to signal loss in the transient band. Additionally, an *in vivo* example of blood flow with low axial velocity from the carotid artery is shown, where the use of a sparse sequence significantly reduced signal dropout in the lumen.

*This work is described in the paper: “Effects of reverberations and clutter filtering in pulsed Doppler using sparse sequences”, which has been accepted for publication in IEEE Transactions on Ultrasonics, Ferroelectrics and Frequency Control in revised form.*

### 1.6.2 2-D Tracking Doppler (Chapters 3 and 4)

Pulsed wave (PW) Doppler is an important tool in cardiovascular diagnostics. However, errors are frequently introduced in the estimates because of spectral broadening and incorrect choice of the beam-to-flow angle. Errors from both effects become worse with larger beam-to-flow angles.

The aim of this work is to evaluate the potential use of the recently proposed 2-D tracking Doppler technique [45] for reducing such errors. The behavior of the method was investigated using simulations and *in vitro* recordings. Using the signal model, it was shown that the Doppler spectra have lowest bandwidth and maximum power when the tracking angle is equal to the beam-to-flow angle. The findings motivated two velocity calibration methods, using either the minimum full width at half maximum (FWHM) or the maximum power of the 2-D tracking Doppler spectra to predict the Doppler angle. The techniques were tested using *in vitro* recordings of flow in a straight tube, at beam-to-flow angles of 63°, 73° and 83°. The results indicated that velocity calibration errors may be lower for the FWHM method than for PW Doppler with manual angle correction, especially for large beam-to-flow angles. With an *in vivo* example, it was demonstrated that applying the 2-D tracking Doppler technique in patients with carotid stenosis is feasible.

The properties of the 2D tracking Doppler method were also investigated for cardiac jet flow velocity estimation using phased array probes. A new signal model was developed to include the effects of a spatially variant point spread function. The simulation software Field II [54] was used to calculate point spread functions along flow lines. The expected velocity spectra were then calculated separately for each flow line and then summed incoherently. The results were validated using an *in vitro*

measurement

Using the signal model, it was shown that the spectral broadening of tracking Doppler is significantly lower than that of PW Doppler also in the case of cardiac imaging. In fact, for beam-to-flow angles up to 60 deg the spectral broadening of tracking Doppler was comparable to that of CW Doppler with a 0 deg beam-to-flow angle. The dependency of spectral broadening and spectral amplitude on the tracking angle was investigated in a simulation model of a straight tube with parabolic flow and a beam-to-flow angle of 71°. It was shown that the maximal spectral amplitude was found at the correct beam-to-flow angle, and the minimal spectral broadening was observed when the beam-to-flow angle was about 69°.

The correctness of the signal model and the results was validated using an *in vitro* measurement of a straight tube phantom, and an *in vivo* example was presented showing the feasibility of using tracking Doppler for maximum jet velocity estimation in an aortic insufficiency.

*This work is described in the papers:*

“Investigations of Spectral Resolution and Angle Dependency in a 2-D Tracking Doppler Method”, *which was a joint work with Tonje Fredriksen, and was published in IEEE Transactions on Ultrasonics, Ferroelectrics and Frequency Control, vol. 61, no. 7, pp. 1161–1170, 2014.*

“2-D Tracking Doppler for Cardiac Jet Flow Velocity Estimation”, *which has been submitted to IEEE Transactions on Ultrasonics, Ferroelectrics and Frequency Control.*

## 1.7 Discussion

In this thesis, several methods have been evaluated concerning two fundamental challenges of PW Doppler imaging: the duplex challenge and spectral broadening. The properties of the methods have largely been described using mathematical models of the received ultrasound signal. Simulation tools and *in vitro* measurements have been used to verify the conclusions and the correctness of the models, and *in vivo* measurements have been used to investigate the feasibility of using the methods in clinical applications.

### 1.7.1 The use of sparse sequences for duplex imaging

The feasibility of using sparse sequences for duplex imaging was investigated using methods in which velocity spectra are estimated without requiring uniformly sampled Doppler data [22–25]. Using these techniques, slow-time Doppler data with interleaved B-mode transmissions can be used to provide separate and interleaved B-mode and Doppler images without reduction in velocity range. In this work we focus on two fundamental problems which are common to all the proposed methods when applied to spectral Doppler, as they occur due to the use of a non-uniform sampling pattern.

First, it was shown that long reverberation times can introduce substantial signal dependent noise in acquisitions with frequent B-mode interruptions. The reverberation

noise occurs after each transition between B-mode and Doppler, and the duration of the noise is equal to the reverberation time of a single pulse, measured in number of slow-time samples. These samples must be discarded before clutter filtering to remove the noise, but in sparse sequences this may cause the loss of many samples due to the frequent interruptions. An *in vivo* example is shown where the reverberation noise has amplitude 30 dB higher than the noise floor and is also coherent, and would thus introduce strong coherent noise in the power spectrum estimates. This justifies that the noise should be removed before spectrum estimation.

The results showed that the reverberation problem is significantly more severe for cardiac applications than for vascular applications due to the low center frequency ( $\sim 2$  MHz). A reverberation time of more than  $400\ \mu\text{s}$  was measured in a healthy volunteer, which would correspond to 2-4 slow-time samples when using typical PRF values for cardiac imaging. This severely limits the use of sparse sequences in cardiac applications. For instance, in a sequence with one interruption for every 10 Doppler transmissions, 20-40 % of the Doppler data would be lost due to reverberation noise. In vascular imaging the center frequency is higher ( $\sim 5$  MHz) and thus the problem is less severe, but the presented results indicate that one sample still needs to be discarded after every B-mode interruption for PRF values of about 10 kHz or higher. In this case, the loss of samples might not be a critical problem, but may influence the choice of duplex sequence. Because the number of lost samples essentially scales with the number of interruptions, it might be preferable to use fewer and longer interruptions, an approach that is more similar to sequences used in conventional packet-based acquisition.

The reverberation problem is not specific to duplex imaging, but is relevant in all applications involving transitions between different pulses. One example is Doppler sequences using interleaved beams, where the first samples in each packet should be discarded to avoid reverberation noise. Another example is triplex imaging, where color Doppler, PW Doppler and B-mode images are displayed simultaneously. In this case, the reverberation problem is relevant because of the frequent transition between the imaging modalities. Notably, the reverberation problem also influences techniques where pulses are transmitted with unequally spaced intervals to overcome the Nyquist limit [55–58]. In this case, long reverberation times would lead to a non-stationary reverberant clutter signal due to the variations in pulse repetition time.

Another challenge when using sparse sequences is that they require the use of regression filters for clutter rejection due to the non-uniform sampling pattern. We show that the filter response of polynomial regression filters depends strongly on the sampling pattern of the slow-time data, and that some sampling patterns lead to distinct artifacts in the resulting velocity spectra. It is seen that using random sampling patterns result in an increased noise floor, whereas using non-random sampling patterns result in coherent noise. This may be explained by considering the clutter filtering of non-uniform data as a multiplication with a characteristic function (1 at sampled data, 0 otherwise) before filtering. The frequency response of the filter is therefore related to the Fourier transform of the characteristic function. The severity of the artifacts presented shows that this effect should be accounted for before applying clutter filters to non-uniformly sampled data.

For color Doppler imaging, we show that the use of sparse sequences for mean velocity estimation is possible without significant reverberation effects and without notable bias due to clutter filtering. It is also shown that sparse sequences offer a potential advantage compared to conventional packet-based CDI, because clutter filtering across several consecutive packets results in filters with a narrower transition band. Given the same required stopband attenuation, this approach both reduces overestimation due to loss of low frequency components and reduces the amount of signal dropouts compared to conventional packet-based imaging.

In summary, we have shown that the use of sparse sequences in cardiac applications is severely limited by the effects of long reverberation times. In vascular applications using a linear probe the reverberation problem should be considered, but might not be critical. However, the use of polynomial regression filters on non-uniformly sampled data may also introduce significant artifacts in the velocity spectra, depending on the sampling pattern. The presence of signal dependent noise in the spectra makes it less likely that sparse sequence spectral estimation methods will be used in clinical practice unless they can avoid clutter filtering of the signal. However, the clutter filtering artifacts have less impact on color Doppler images, and the use of sparse sequences in this modality might have some advantages over conventional packet-based imaging.

### 1.7.2 2-D Tracking Doppler

The 2-D tracking Doppler technique is a recently proposed method for generation of velocity spectra. In this method, the spectral power estimate for a given velocity is obtained by summation along straight lines in space and slow-time to increase transit time and thus reduce spectral broadening. In [45], properties of the technique were investigated when implemented on a linear array probe. Both simulations, *in vitro* and *in vivo* results indicated that the method reduced spectral broadening compared with conventional PW Doppler, especially for large beam-to-flow angles.

For all results presented in [45] the tracking angle coincided with the beam-to-flow angle. In clinical settings, determining the beam-to-flow angle is sometimes challenging as the flow field may be complex and not parallel to the vessel walls. Estimating the flow angle accurately is especially important for near transversal flow, as the angle correction factor tends to infinity as the beam-to-flow angle approaches  $90^\circ$ . We therefore extended the signal model to investigate the 2-D tracking Doppler spectra when the tracking angle differs from the beam-to-flow angle. It was shown that the expectation value of the spectra have lowest bandwidth and maximum power when the tracking angle is equal to the beam-to-flow angle.

The angle dependency of the method was studied through repeated measurements of *in vitro* flow, using the minimum FWHM and the maximum power as indicators of the correct beam-to-flow angle. The estimated angles using the minimum FWHM as indicator had a bias of less than 4 % for all the investigated beam-to-flow angles. The velocity calibration errors when using the minimum FWHM criterion were compared with expected velocity when using manual angle correction. Whereas the velocity errors of manual angle correction increase rapidly for large beam-to-flow angles, the estimated velocity calibration errors of the 2-D tracking Doppler method had

a standard deviation of less than 6% for all the investigated angles (63°, 73° and 83°).

Application of the tracking Doppler technique to cardiac applications presented several potential challenges. Compared with applications using a linear probe, a cardiac probe has smaller aperture and the region of interest is deeper, leading to higher F-numbers for receive focusing. The degraded resolution may affect the behavior of the method for erroneous tracking angles. In addition, the smaller width of plane waves emitted from a cardiac probe may limit the size of the tracking region for high velocities. The simulation results showed, however, that the tracking Doppler technique has the potential to resolve both the angle dependency and spectral broadening problems also when implemented on a phased array probe. A relative spectral broadening of 5% for a beam-to-flow angle of 80° may be good enough for use in clinical applications. Thus, the primary source of velocity estimation error is likely to be errors in angle correction.

The dependence of the maximal amplitude and spectral broadening on tracking angle when using a phased array was investigated using a model of a straight tube phantom. Similarly to the results in Chapter 3, the maximal spectral amplitude was found when the tracking angle coincided with the flow angle. The minimal spectral broadening was observed at a tracking angle slightly smaller than the true flow angle. A comparison of the angle dependency results from the two papers (Fig. 3.4 and Fig. 4.9) shows that the sensitivity of the parameters to the tracking angle is much greater when using a linear probe than when using a phased array. A probable explanation for this is that the improved resolution when using the linear array also results in less correlated signals between tracking lines with different angles. This would make automatic angle correction more difficult in cardiac applications than in vascular applications.

Several factors may limit the performance of the tracking Doppler technique *in vivo* compared to *in vitro* or in simulations. For example, the flow field may not be constant along the tracking line, or it may be out-of-plane, curved, accelerated or turbulent. All these effects would increase spectral broadening. Also, if the sample volume contains flow lines with beam-to-flow angle smaller than the tracking angle, this may lead to an overestimation of maximum velocities. It should be noted, however, that all of these effects would also limit the quality of conventional PW Doppler in a similar way.

Automatic angle detection may also be more challenging *in vivo*, for several reasons. Several flow lines may be present with different beam-to-flow angles. If the flow is non-uniform, curved or out-of-plane, the estimated angle may be dependent on the geometry of the vessel. Also the direction of the flow may change during the heart cycle due to movement of the heart valves and walls, limiting the use of temporal averaging. The severity of most of these problems can be reduced by increasing spatial resolution, but this again might require increased caution by the operator when selecting the tracking region.

A natural improvement of the 2-D tracking Doppler technique would be to use 3-D probes to allow tracking also in the elevation direction. Also, the use of diverging waves from phased array probes might have potential and should be investigated. More ambitious extensions of the method may include automatic detection of jets, and detection and tracking of curved flow fields. The primary challenges expected for these potential extensions are increased computational workload and, for cardiac

applications, the limited spatial resolution of the system.

The combination of increased spectral resolution and more robust velocity calibration for large beam-to-flow angles may give both challenges and opportunities in blood flow imaging. Most importantly, the increased robustness for large beam-to-flow angles may facilitate reliable velocity estimation for angles above  $60^\circ$ . This can improve blood velocity estimation in regions with near-transversal flow, for instance in vascular imaging or when imaging the heart from a parasternal view. However, as the 2-D tracking method produces narrower spectra, and hence might give lower maximum velocity estimates than conventional approaches, introducing the method in the clinics would necessitate a revision of thresholds used in clinical guidelines.

## 1.8 Concluding remarks

Methods concerning two fundamental challenges of pulsed wave Doppler have been evaluated using mathematical models of the received ultrasound signal.

It has been shown that long reverberation times may introduce significant signal dependent noise when using sparse sequences for velocity estimation. Based on the high reverberation noise power and the long reverberation times seen in our cardiac example, we conclude that the use of sparse sequences is not recommended for cardiac applications.

In vascular imaging, the reverberation problem may be resolved by discarding one sample after every B-mode interruption. However, regular time-invariant filters cannot be applied to sparse signals, and the use of polynomial regression filters was shown to produce different artifacts in the velocity spectra depending on the applied sampling pattern.

Properties of the 2-D tracking Doppler method have been investigated both for use in vascular applications, and for cardiac applications. All results indicate that 2-D tracking significantly reduces spectral broadening compared with PW Doppler, especially for high beam-to-flow angles. In the cardiac study, the spectral broadening of tracking Doppler was substantially lower than that of PW Doppler, reducing spectral broadening by factor of six or more for all investigated beam-to-flow angles. For beam-to-flow angles below  $60^\circ$ , the spectral broadening of tracking Doppler spectra was comparable to that of CW Doppler with flow in the beam direction.

The dependency of 2-D tracking Doppler spectra on the tracking angle was also investigated. In all results, the maximal spectral amplitude was found when the tracking angle coincided with the beam-to-flow angle. The spectral broadening measures were also minimal close to the true tracking angles, but the angle would have been slightly underestimated in the cardiac case, if used as a criterion. A comparison of the two modalities reveals that the tracking Doppler technique is less sensitive to changes in tracking angle in cardiac applications than in vascular imaging. This makes automatic as well as manual angle correction more difficult in cardiac applications.

## 1.9 List of publications

Papers included in the thesis:

1. **Jørgen Avdal**, Lasse Løvstakken and Hans Torp: “Effects of reverberations and clutter filtering on pulsed Doppler using sparse sequences”, *accepted for publication in IEEE Transactions on Ultrasonics, Ferroelectrics and Frequency control in revised form*.
2. Tonje Fredriksen, **Jørgen Avdal**, Ingvild Kinn Ekroll, Torbjørn Dahl, Lasse Løvstakken and Hans Torp: “Investigations of Spectral Resolution and Angle Dependency in a 2-D Tracking Doppler Method”, *published in IEEE Transactions on Ultrasonics, Ferroelectrics and Frequency Control, vol. 61, no. 7, pp. 1161-1170, 2014*.
3. **Jørgen Avdal**, Ingvild Kinn Ekroll, Thomas Skaug, Lasse Løvstakken and Hans Torp: “2-D tracking Doppler for Cardiac Jet Flow Estimation”, *submitted to IEEE Transactions on Ultrasonics, Ferroelectrics and Frequency control*.

Additional conference presentations, posters and proceedings:

1. **Jørgen Avdal**, Anders Kristoffersen, Asta Håberg and Pål Erik Goa: “Functional MRI employing Compressed Sensing and separation of signal and noise in k-space”, poster at *The 20th Annual Meeting of ISMRM, Melbourne, Australia, 2012*.
2. **Jørgen Avdal**, Lasse Løvstakken, Solveig Fadnes, Ingvild Ekroll and Hans Torp: “2-D Tracking Doppler for Cardiac Jet Flow Velocity Estimation”, poster and proceeding at *The 2014 International IEEE ultrasonics symposium*.



# References

- [1] R. Aaslid, T.-M. Markwalder, and H. Nornes, “Noninvasive transcranial doppler ultrasound recording of flow velocity in basal cerebral arteries,” *Journal of neurosurgery*, vol. 57, no. 6, pp. 769–774, 1982.
- [2] D. Maulik and I. Zalud, *Doppler ultrasound in obstetrics and gynecology*. Springer, 2005.
- [3] J. A. Levy and V. E. Noble, “Bedside ultrasound in pediatric emergency medicine,” *Pediatrics*, vol. 121, no. 5, pp. e1404–e1412, 2008.
- [4] L. S. Cohen, P. F. Escobar, C. Scharm, B. Glimco, and D. A. Fishman, “Three-dimensional power doppler ultrasound improves the diagnostic accuracy for ovarian cancer prediction,” *Gynecologic oncology*, vol. 82, no. 1, pp. 40–48, 2001.
- [5] B. Sigel, “A brief history of doppler ultrasound in the diagnosis of peripheral vascular disease,” *Ultrasound in medicine & biology*, vol. 24, no. 2, pp. 169–176, 1998.
- [6] S. Satomura, “Ultrasonic doppler method for the inspection of cardiac functions,” *The Journal of the Acoustical Society of America*, vol. 29, no. 11, pp. 1181–1185, 1957.
- [7] S. Satomura, “Study of the flow patterns in peripheral arteries by ultrasonics,” *J. Acoust. Soc. Japan*, vol. 15, pp. 151–155, 1959.
- [8] D. L. Franklin, W. Schlegel, and R. F. Rushmer, “Blood flow measured by doppler frequency shift of back-scattered ultrasound,” *Science*, vol. 134, no. 3478, pp. 564–565, 1961.
- [9] P. N. T. Wells, “Physical principles of ultrasonic diagnosis,” 1969.
- [10] D. J. Mozersky, D. E. Hokanson, D. W. Baker, D. S. Sumner, and D. E. Strandness, “Ultrasonic arteriography,” *Archives of Surgery*, vol. 103, no. 6, pp. 663–667, 1971.
- [11] D. G. McDonald and G. R. Leopold, “Ultrasound b-scanning in the differentiation of baker’s cyst and thrombophlebitis,” *The British journal of radiology*, vol. 45, no. 538, pp. 729–732, 1972.

- 
- [12] F. E. Barber, D. W. Baker, A. W. Nation, D. E. Strandness, and J. M. Reid, "Ultrasonic duplex echo-doppler scanner," *Biomedical Engineering, IEEE Transactions on*, no. 2, pp. 109–113, 1974.
- [13] K. Kristoffersen and B. Angelsen, "A time-shared ultrasound Doppler measurement and 2-D imaging system," *Biomedical Engineering, IEEE Transactions on*, vol. 35, no. 5, pp. 285–295, 1988.
- [14] H. Klebæk, J. A. Jensen, and L. K. Hansen, "Neural network for sonogram gap filling," in *Ultrasonics Symposium, 1995. Proceedings., 1995 IEEE*, vol. 2, pp. 1553–1556, IEEE, 1995.
- [15] G. Montaldo, M. Tanter, J. Bercoff, N. Benech, and M. Fink, "Coherent plane-wave compounding for very high frame rate ultrasonography and transient elastography," *Ultrasonics, Ferroelectrics and Frequency Control, IEEE Transactions on*, vol. 56, no. 3, pp. 489–506, 2009.
- [16] J. Bercoff, G. Montaldo, T. Loupas, D. Savery, F. Meziere, M. Fink, and M. Tanter, "Ultrafast compound doppler imaging: providing full blood flow characterization," *Ultrasonics, Ferroelectrics and Frequency Control, IEEE Transactions on*, vol. 58, no. 1, pp. 134–147, 2011.
- [17] N. Oddershede and J. A. Jensen, "Effects influencing focusing in synthetic aperture vector flow imaging," *Ultrasonics, Ferroelectrics and Frequency Control, IEEE Transactions on*, vol. 54, no. 9, pp. 1811–1825, 2007.
- [18] B. Denarie, T. A. Tangen, I. K. Ekroll, N. Rolim, H. Torp, T. Bjastad, and L. Lovstakken, "Coherent plane wave compounding for very high frame rate ultrasonography of rapidly moving targets," *Medical Imaging, IEEE Transactions on*, vol. 32, no. 7, pp. 1265–1276, 2013.
- [19] F. Gran, A. Jakobsson, and J. A. Jensen, "Adaptive spectral doppler estimation," *Ultrasonics, Ferroelectrics and Frequency Control, IEEE Transactions on*, vol. 56, no. 4, pp. 700–714, 2009.
- [20] I. K. Ekroll, H. Torp, and L. Lovstakken, "Spectral doppler estimation utilizing 2-d spatial information and adaptive signal processing," *Ultrasonics, Ferroelectrics and Frequency Control, IEEE Transactions on*, vol. 59, no. 6, pp. 1182–1192, 2012.
- [21] S. Ricci, "Adaptive spectral estimators for fast flow-profile detection.," *IEEE transactions on ultrasonics, ferroelectrics, and frequency control*, vol. 60, no. 2, pp. 421–427, 2013.
- [22] E. Gudmundson, A. Jakobsson, J. A. Jensen, and P. Stoica, "Blood velocity estimation using ultrasound and spectral iterative adaptive approaches," *Signal Processing*, vol. 91, no. 5, pp. 1275–1283, 2011.

- [23] J. A. Jensen, "Spectral velocity estimation in ultrasound using sparse data sets," *The Journal of the Acoustical Society of America*, vol. 120, p. 211, 2006.
- [24] S. Mollenbach and J. A. Jensen, "Duplex scanning using sparse data sequences," in *Ultrasonics Symposium, 2008. IUS 2008. IEEE*, pp. 5–8, IEEE, 2008.
- [25] J. Richey, D. Friboulet, A. Bernard, O. Bernard, and H. Liebgott, "Blood Velocity Estimation Using Compressive Sensing,," *IEEE transactions on medical imaging*, 2013.
- [26] L. Hatle, A. Brubakk, A. Tromsdal, and B. Angelsen, "Noninvasive assessment of pressure drop in mitral stenosis by doppler ultrasound,," *British heart journal*, vol. 40, no. 2, pp. 131–140, 1978.
- [27] L. Hatle, B. Angelsen, and A. Tromsdal, "Noninvasive assessment of atrioventricular pressure half-time by doppler ultrasound,," *Circulation*, vol. 60, no. 5, pp. 1096–1104, 1979.
- [28] S. Samstad, L. Hegrenaes, T. Skjaerpe, and L. Hatle, "Half time of the diastolic aortoventricular pressure difference by continuous wave doppler ultrasound: a measure of the severity of aortic regurgitation?,," *British heart journal*, vol. 61, no. 4, pp. 336–343, 1989.
- [29] C. Oates, A. Naylor, T. Hartshorne, S. Charles, T. Fail, K. Humphries, M. Aslam, and P. Khodabakhsh, "Joint recommendations for reporting carotid ultrasound investigations in the united kingdom,," *European Journal of Vascular and Endovascular Surgery*, vol. 37, no. 3, pp. 251–261, 2009.
- [30] P. R. Hoskins, K. Martin, and A. Thrush, *Diagnostic ultrasound: physics and equipment*, ch. 9. Cambridge University Press, 2010.
- [31] H. Baumgartner, J. Hung, J. Bermejo, J. B. Chambers, A. Evangelista, B. P. Griffin, B. Iung, C. M. Otto, P. A. Pellikka, and M. Quiñones, "Echocardiographic assessment of valve stenosis: Eae/ase recommendations for clinical practice,," *European Journal of Echocardiography*, 2008.
- [32] B. Dunmire, K. Beach, K. Labs, M. Plett, and D. Strandness Jr, "Cross-beam vector doppler ultrasound for angle-independent velocity measurements,," *Ultrasound in medicine & biology*, vol. 26, no. 8, pp. 1213–1235, 2000.
- [33] L. Bohs, B. Geiman, M. Anderson, S. Gebhart, and G. Trahey, "Speckle tracking for multi-dimensional flow estimation,," *Ultrasonics*, vol. 38, no. 1, pp. 369–375, 2000.
- [34] J. Kortbek and J. A. Jensen, "Estimation of velocity vector angles using the directional cross-correlation method,," *Ultrasonics, Ferroelectrics and Frequency Control, IEEE Transactions on*, vol. 53, no. 11, pp. 2036–2049, 2006.

- 
- [35] J. A. Jensen and N. Oddershede, "Estimation of velocity vectors in synthetic aperture ultrasound imaging," *Medical Imaging, IEEE Transactions on*, vol. 25, no. 12, pp. 1637–1644, 2006.
- [36] A. Swillens, P. Segers, H. Torp, and L. Løvstakken, "Two-dimensional blood velocity estimation with ultrasound: speckle tracking versus crossed-beam vector doppler based on flow simulations in a carotid bifurcation model," *Ultrasonics, Ferroelectrics and Frequency Control, IEEE Transactions on*, vol. 57, no. 2, pp. 327–339, 2010.
- [37] P. Tortoli, G. Bambi, and S. Ricci, "Accurate doppler angle estimation for vector flow measurements," *Ultrasonics, Ferroelectrics and Frequency Control, IEEE Transactions on*, vol. 53, no. 8, pp. 1425–1431, 2006.
- [38] P. Tortoli, G. Guidi, and C. Atzeni, "A review of experimental transverse doppler studies," *Ultrasonics, Ferroelectrics and Frequency Control, IEEE Transactions on*, vol. 41, no. 1, pp. 84–89, 1994.
- [39] P. Tortoli, G. Guidi, L. Mantovani, and V. L. Newhouse, "Velocity magnitude estimation with linear arrays using doppler bandwidth," *Ultrasonics*, vol. 39, no. 3, pp. 157–161, 2001.
- [40] J. A. Jensen, "Transverse spectral velocity estimation," *Ultrasonics, Ferroelectrics, and Frequency Control, IEEE Transactions on*, vol. 61, no. 11, pp. 1815–1823, 2014.
- [41] T. Loupas and R. W. Gill, "Multifrequency doppler: improving the quality of spectral estimation by making full use of the information present in the backscattered rf echoes," *Ultrasonics, Ferroelectrics and Frequency Control, IEEE Transactions on*, vol. 41, no. 4, pp. 522–531, 1994.
- [42] H. Torp and K. Kristoffersen, "Velocity matched spectrum analysis: A new method for suppressing velocity ambiguity in pulsed-wave doppler," *Ultrasound in medicine & biology*, vol. 21, no. 7, pp. 937–944, 1995.
- [43] B.-F. Osmanski, J. Bercoff, G. Montaldo, T. Loupas, M. Fink, and M. Tanter, "Cancellation of doppler intrinsic spectral broadening using ultrafast doppler imaging," *Ultrasonics, Ferroelectrics, and Frequency Control, IEEE Transactions on*, vol. 61, no. 8, pp. 1396–1408, 2014.
- [44] S. Ricci, R. Matera, and P. Tortoli, "An improved doppler model for obtaining accurate maximum blood velocities," *Ultrasonics*, 2014.
- [45] T. D. Fredriksen, I. K. Ekroll, L. Lovstakken, and H. Torp, "2-D Tracking Doppler: A new method to limit spectral broadening in pulsed wave doppler," *Ultrasonics, Ferroelectrics and Frequency Control, IEEE Transactions on*, vol. 60, no. 9, pp. 1896–905, 2013.

- [46] V. Newhouse and J. Reid, "Invariance of doppler bandwidth with flow axis displacement," in *Ultrasonics Symposium, 1990. Proceedings., IEEE 1990*, pp. 1533–1536, IEEE, 1990.
- [47] P. D. Welch, "The use of fast fourier transform for the estimation of power spectra: a method based on time averaging over short, modified periodograms," *IEEE Transactions on audio and electroacoustics*, vol. 15, no. 2, pp. 70–73, 1967.
- [48] D. H. Evans and W. N. McDicken, *Doppler ultrasound: physics, instrumentation, and signal processing*, vol. 2. Wiley Chichester, 2000.
- [49] J. M. Rau, S.-E. Måsøy, R. Hansen, B. Angelsen, and T. A. Tangen, "Methods for reverberation suppression utilizing dual frequency band imaging," *The Journal of the Acoustical Society of America*, vol. 134, no. 3, pp. 2313–2325, 2013.
- [50] E. S. Chornoboy, "Initialization for improved iir filter performance," *Signal Processing, IEEE Transactions on*, vol. 40, no. 3, pp. 543–550, 1992.
- [51] R. Peterson, L. Atlas, and K. Beach, "A comparison of iir initialization techniques for improved color doppler wall filter performance," in *Ultrasonics Symposium, 1994. Proceedings., 1994 IEEE*, vol. 3, pp. 1705–1708, IEEE, 1994.
- [52] H. Torp, "Clutter rejection filters in color flow imaging: A theoretical approach," *Ultrasonics, Ferroelectrics and Frequency Control, IEEE Transactions on*, vol. 44, no. 2, pp. 417–424, 1997.
- [53] B. Angelsen, "A theoretical study of the scattering of ultrasound from blood," *Biomedical Engineering, IEEE Transactions on*, no. 2, pp. 61–67, 1980.
- [54] J. A. Jensen, "Simulation of advanced ultrasound systems using Field II," in *Biomedical Imaging: Nano to Macro, 2004. IEEE International Symposium on*, pp. 636–639, IEEE, 2004.
- [55] V. Newhouse, P. LeCong, E. Furgason, and C. Ho, "On increasing the range of pulsed doppler systems for blood flow measurement," *Ultrasound in medicine & biology*, vol. 6, no. 3, pp. 233–237, 1980.
- [56] H. Nishiyama and K. Katakura, "Non-equally-spaced pulse transmission for non-aliasing ultrasonic pulsed doppler measurement," *Journal of the Acoustical Society of Japan. E*, vol. 13, no. 4, pp. 215–222, 1992.
- [57] G. E. C. Nogueira, A. Ferreira, and J. T. Vidal, "A nonuniform sampled coherent pulsed doppler ultrasonic velocimeter with increased velocity range," *Ultrasonics, Ferroelectrics and Frequency Control, IEEE Transactions on*, vol. 46, no. 2, pp. 452–456, 1999.
- [58] D. Posada, B. Chayer, G. Cloutier, and D. Garcia, "Nyquist velocity extension in ultrafast color doppler," in *Ultrasonics Symposium (IUS), 2014 IEEE International*, pp. 2261–2264, IEEE, 2014.



## Chapter 2

# Effects of reverberations and clutter filtering in pulsed Doppler using sparse sequences

Jorgen Avdal<sup>1</sup>, Hans Torp<sup>1</sup>, and Lasse Løvstakken<sup>1</sup>

<sup>1</sup> MI Lab and Dept. of Circulation and Medical Imaging, NTNU, Norway

Duplex ultrasound is a modality where an ultrasound system is used for simultaneous acquisition of both B-mode images and velocity (Doppler) data. Conventional duplex sequences interleave packets of B-mode and Doppler transmissions, producing undesirable gaps during B-mode interruptions. In recent years, several techniques have been proposed for avoiding such gaps by using sparse sequences, where velocity spectra are generated from non-uniformly sampled Doppler data containing frequent B-mode interruptions. In this work, two negative effects are discussed that may influence velocity estimation when using non-uniformly sampled sequences. Firstly, it is shown that long reverberation times lead to discontinuities in the signal from stationary clutter after each B-mode interruption. Secondly, using frequency analysis, it is shown that clutter filtering of non-uniformly sampled data may introduce artifacts in the velocity spectrum, and also lead to significant bias in mean velocity estimates. Methods are presented for quantification of these effects, and utilized to analyze three types of sparse duplex sequences for blood velocity estimation. In particular, it is argued that the use of such sequences in cardiac applications is not recommended due to long reverberation time. Additionally, it is found that the use of regression filters to filter non-uniformly sampled data may produce significant artifacts in Pulsed Wave Doppler spectra, but is less significant for Color Doppler Imaging applications. In vitro and in vivo examples are included showing the presence and magnitude of these problems in clinically relevant applications.

## 2.1 Introduction

Doppler ultrasound is a non-invasive technique for velocity estimation of moving tissue and blood. By insonating the volume of interest with several pulses in rapid succession, it is possible to follow moving scatterers over time. The velocity distribution can then be estimated by Fourier analysis, as done in pulsed wave (PW) Doppler, or the mean

velocity may be estimated by correlation techniques [1], as done in Color Doppler imaging (CDI).

In addition to Doppler measurements, simultaneous B-mode images are desired for visualization of anatomical structures. However, whereas low center frequency and long pulse length are preferred in Doppler imaging to increase the Nyquist velocity limit and penetration depth, high center frequency and short pulse length are preferred in B-mode imaging for increased resolution. Therefore, separate pulses are typically used for the two modalities. A recently proposed method in which B-mode and Doppler images may be generated from the same data, is coherent spatial compounding for ultrafast imaging using plane or diverging waves [2–4]. In this method, spatial resolution is improved by compounding images from multiple angles, and the Doppler pulse repetition frequency (PRF) is reduced according to the number of different angles used in the compounding process. However, approximately 10 compounding angles are necessary to achieve image quality comparable to B-mode [3], in which case the Doppler PRF would be too low for applications with high velocity flow. For example in assessment of severe stenosis in the carotid artery, velocities in the range 3-7 m/s have been reported [5], and thus aliasing may already occur when using the maximal PRF. This motivates the use of separate B-mode transmissions also when using coherent compounding.

In conventional duplex imaging the Doppler acquisition is interrupted regularly to acquire segments of B-mode images [6]. Early attempts included alternating between B-mode and Doppler transmissions [7]. This produces a continuous stream of both Doppler and B-mode data, but effectively halves the PRF of the Doppler acquisition and introduces non-stationary clutter from the B-mode echoes. Another alternative is time-sharing between Doppler and B-mode acquisitions, where the two modalities are acquired separately in relatively short (10-50 ms) disjoint time periods [8]. This restores the full PRF of the Doppler signal, but the signal is lost during B-mode interruptions. Techniques have also been proposed to reduce the number of B-mode transmissions, thus reducing the number and the duration of interruptions in the sequence. However, as long as the Doppler signal is not continuous, it is not possible to use overlapping windows for PW Doppler without introducing gaps in the spectral display. Even small interruptions in the Doppler signal cause potentially large gaps in the velocity estimates, depending on the length of the observation window and the impulse response of the clutter filter. Techniques have in this context been proposed to estimate the missing signal segments. [9, 10].

In recent years, methods have been proposed for spectral estimation from non-uniformly sampled data, where gaps between the Doppler samples are used for B-mode transmissions. Using these methods, in this work referred to as *sparse sequence* methods, both maximal PRF and a continuous stream of Doppler data are achieved. In [11], the autocorrelation function was estimated directly from the sparse Doppler data, and further Fourier transformed to produce the Doppler spectrum display. In [12], a method was suggested for spectral estimation from gapped velocity data, based on the PG-APES (Periodically Gapped Amplitude and Phase Estimation) method [13]. In [14], the Blood Iterative Adaptive Approach (BIAA) and Blood Sparse Learning via Iterative Minimization (BSLIM) methods are proposed. These are iterative methods

for estimation of velocity spectra without restrictions on the sampling pattern, and have been further developed for ultrasound Doppler applications in the works [15] and [16]. In other approaches, the missing data are estimated, allowing velocity estimation to be performed on a full data set. In [17], the missing samples were reconstructed using a filter bank technique. Recently, a compressive sensing technique was proposed [18], reconstructing the missing data based on the assumption that the data has a sparse representation in a given basis.

The above methods have primarily been tested on fully sampled data which have been synthetically undersampled in post-processing. One potential challenge when these methods are implemented on an ultrasound system, is that long reverberation times may lead to interference between subsequent pulses. If echoes from one insonation are not sufficiently attenuated before the onset of the next pulse, they will interfere with direct echoes from the region of interest. In uniformly sampled Doppler sequences without B-mode interruptions this is usually not a problem, as the signal interference becomes stationary after a few samples and is removed by the clutter filter. In a duplex sequence, however, a discontinuity in the clutter signal is introduced every time an acquisition switches from B-mode to Doppler. Due to frequent B-mode interruptions, this problem is particularly relevant for sparse sequences.

Another challenge for the sparse duplex methods is that the contribution from stationary tissue, or clutter, needs to be removed before velocity estimation. Multiple reflections, particularly in near field layers, produces clutter which reduces image contrast and has been found to be a dominating source of image degradation in fundamental ultrasound imaging [19], [20]. If not removed, clutter can severely compromise velocity measurements. In CDI, remaining clutter might lead to severe underestimation of velocities. In PW Doppler, the clutter signal may obscure blood velocities due to spectral leakage, or due to clutter from non-stationary tissue [21].

Clutter rejection is typically performed using highpass FIR-filters or IIR-filters, or polynomial regression filters for shorter segments. For sparse duplex sequences with missing samples, applying FIR or IIR-filters is not straightforward as they require uniform sampling. Polynomial regression filters do not have this limitation and were the preferred choice for clutter removal in [11] and [14]. The use of regression filters, however, may introduce frequencies in the output that are not present in the input signal [22], and thus degrade the quality of spectra used for clinical diagnosis. In addition, further degradation of the filter response may be expected when applying a regression filter to non-uniformly sampled data.

The aims of this work are to describe and quantify the problems caused by long reverberation time and regression filtering of non-uniformly sampled data, and reassess the feasibility of using sparse Doppler sequences in cardiac and carotid applications. The outline of the paper is detailed in the following. In section 2.2, methods are developed for quantifying the impact of reverberation time and clutter filtering on Doppler velocity estimates when using sparse duplex sequences. These methods are applied in sections 2.3 and 2.4 to investigate the feasibility of utilizing sparse sequences for cardiac and carotid PW Doppler and CDI. The results are discussed in section 2.5 and section 2.6 contains concluding remarks.

## 2.2 Theory

In this section a brief introduction to reverberation time and polynomial regression filters are provided. Further, methods for estimation of reverberation times and quantification of clutter filtering effects on velocity estimation are presented.

### 2.2.1 Reverberation time

In an ultrasound scan, signal from tissue deeper than  $c\text{PRT}/2$  will lead to interference between subsequent transmissions if not sufficiently attenuated. Here  $c$  is the speed of sound and  $\text{PRT} = 1/\text{PRF}$  is the pulse repetition time of the sequence. Combined with multiple reflections in the tissue, this may lead to a reverberation time much longer than the pulse repetition time. Note that whereas the term reverberations is associated with multiple reflections from the body wall close to the transducer, a signal may also be reverberant due to reflections from deep tissue structures. The signals from preceding transmissions are attenuated due to propagation in tissue, but also due to defocusing, because of a mismatch between the focus depth and the time-of-flight of the signal. However, such reverberant signals may interfere with velocity estimation as long as they are above the thermal noise floor.

In the following, a model is presented describing the impact of long reverberation time on duplex sequences. The received signal  $C$  from a single pulse transmission can be written

$$C(t) = \sum_{m=1}^M C_m(t + \tau(m, t)), \quad (2.1)$$

where  $C_m$  is the signal from channel  $m$ ,  $t$  is the time after pulse excitation and  $\tau(m, t)$  is the delay on channel  $m$  at depth  $ct/2$ . Let  $t_R$  (reverberation time) be the time from pulse excitation until  $C$  drops below the noise floor. If the signal is not allowed to settle before the next excitation ( $\text{PRT} < t_R$ ), echoes from several transmissions will arrive simultaneously at the transducer. To describe the total signal  $S$ , it will then be necessary to include the contributions from preceding pulses. If it is assumed that the relative motion between the probe and the reflecting tissue structures can be neglected, so that  $C(t)$  is constant from pulse to pulse, and beamforming is performed with fixed focus on receive, as used in PW Doppler, the signal  $S$  becomes:

$$S(t) = \sum_{n=0}^{\infty} C(t + n\text{PRT}), \quad (2.2)$$

After a number of PRTs, namely  $N = \lceil t_R/\text{PRT} \rceil$ , the clutter signal will drop below the noise floor. Now, if the insonation starts at  $k = 0$ , the received signal after pulse  $k$  can be approximated:

$$S_k(t) \approx \begin{cases} \sum_{n=0}^k C(t + n\text{PRT}) + r_k(t), & k < N \\ \sum_{n=0}^{N-1} C(t + n\text{PRT}) + r_k(t), & k \geq N \end{cases} \quad (2.3)$$

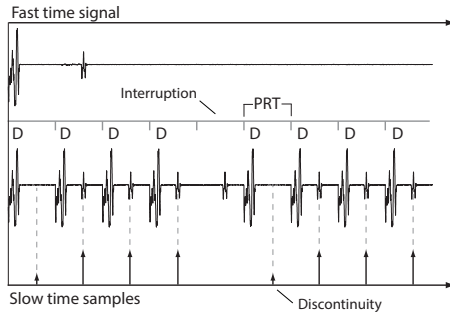


**Figure 2.1:** Illustration of the problem caused by long reverberation time. A received signal with a late echo is measured with low PRF (top). When transmitting with high PRF (middle), the late echo influences subsequent measurements, but the signal becomes stationary after two samples. However, after an interruption due to one or more B-mode transmissions, a discontinuity occurs in the slow time signal (bottom).

where  $r_k$  represents thermal noise. As can be seen, the clutter signal becomes stationary after  $N$  consecutive pulses.

Now, if the pulse at  $k = k_1$  is left out, corresponding for instance to a B-mode interruption in a duplex sequence, this introduces a non-stationary response in the  $N - 1$  slow-time samples  $k_1 + 1 \leq k < N + k_1$ . This is illustrated in Fig. 2.1 for the case  $N = 2$ . The discontinuity in the Doppler signal after the B-mode interruption introduces high frequency noise into the slow time signal, which is not removed by the clutter filter. Note that no actual B-mode firing is necessary for reverberation noise to occur, the omission of Doppler firings alone is sufficient.

The power of the reverberation noise due to one missing Doppler transmission in the subsequent signal is obtained by summation of the contributions from  $n \geq 1$  in (2.2):

$$P_1(t) = \sum_{n=1}^{N-1} |C(t + n\text{PRT})|^2. \quad (2.4)$$

For interruptions of more than one sample, the reverberation noise power would be at least  $P_1(t)$ . Thus, if assuming that no B-mode interruptions are within  $N$  samples of each other, a lower bound for the reverberation noise power in the signal is given by:

$$P(t) \geq r_B \sum_{n=1}^{N-1} |C(t + n\text{PRT})|^2, \quad (2.5)$$

where  $r_B$  is the density of B-mode interruptions (not transmissions). Equality is achieved if each interruption is exactly one transmission or if  $N \leq 2$ .

Based on the theory presented above, the following method is used for estimation of reverberation time.

- Measure the received signal  $C$  from a Doppler pulse with low PRF, that is, with  $\text{PRT} \gg t_R$ .
- Estimate the reverberation time  $t_R$  until  $C$  drops below the noise floor.
- Calculate  $N = \lceil t_R/\text{PRT} \rceil$ .

The reverberation effects can be eliminated by discarding  $N - 1$  samples after every B-mode interruption before clutter rejection. In a sequence with many interruptions this may severely reduce the number of available Doppler samples. Therefore, knowledge of the reverberation time and amplitude should influence the choice of duplex sequence for a given PRF. In general, the PRF of the Doppler transmission may differ from that of B-mode transmissions, but some velocity estimation methods put restrictions on this. For example, the approach suggested in [11] requires the duration of the B-mode interruptions to be a multiple of the Doppler PRT.

## 2.2.2 Clutter filtering of sparse sequences

A brief introduction to regression filters is given below. For more background, the reader is referred to [22] and [23].

Polynomial regression filtering attenuates the signal from slowly moving tissue, assuming that it may be approximated by a low order polynomial. A least-squares polynomial fit of the data is found and then subtracted from the signal. Regression filtering may be implemented by constructing an orthogonal basis of polynomials with increasing polynomial order, finding the projections of the signal onto the  $p + 1$  polynomials with lowest order, and subtracting these from the signal. The quantity  $p$  is the order of the filter.

Polynomial regression filters are not time-invariant [22]. Because of this, defining a frequency response is not straightforward. For real valued signals, an average over all possible phases is necessary to achieve a well-defined frequency response. However, if the input is a complex harmonic signal  $x_\omega$ , the amplitude of the filtered signal  $y_\omega$  is unaffected by a phase shift in  $x_\omega$ , as this is equivalent to multiplication with a constant phase factor. It is then possible to define the frequency response  $P$  by [22]:

$$x_\omega(k) = e^{ik\omega}; \quad k = 1, 2, \dots, K \quad (2.6)$$

$$y_\omega(k) = \sum_{n=1}^K a(k, n)x_\omega(n) \quad (2.7)$$

$$P(\omega) = \frac{1}{K} \sum_{k=1}^K |y_\omega(k)|^2 \quad (2.8)$$

where  $A = \{a(k, n)\}$  is the filter matrix.

Regression filters perform better than FIR or IIR filters for short Doppler segments, as they can produce filter responses with narrower transition bands. For longer signals,

FIR and IIR filters are normally preferred as they are time-invariant. For sparse signals, however, filtering using FIR and IIR filters is not straightforward due to non-uniform sampling. Because a least squares polynomial fit can be estimated regardless of sampling pattern, polynomial regression filters have been preferred in these cases.

Regression filters are applied to sparse data by first utilizing the Gram-Schmitt orthogonalization algorithm to create a modified set of Legendre polynomials  $P_n$ , using the inner product:

$$\langle U, V \rangle = \sum_{s \in I} U(s)V(s)' \quad (2.9)$$

where  $I$  denotes the indices of Doppler samples. Filtering is then implemented by projecting the signal onto the polynomials (using the same inner product) and subtracting the lower order components. Using this method, the estimated clutter signal is essentially a least squares polynomial fit of the measured Doppler data, using  $P_n$ ,  $n = 0 \dots p$  as regressors.

The following frequency analysis is proposed for quantifying the impact of clutter filters on a velocity estimation scheme, where the scheme to be evaluated includes sampling sequence, clutter filtering, and algorithms for spectral and mean velocity estimation.

- Construct single frequency signals  $x_\omega(k) = e^{ik\omega}$ , with  $-\pi \leq \omega < \pi$ .
- Sample according to chosen sampling sequence. To account for reverberation effects, discard  $N - 1$  samples after every B-mode interruption.
- Perform clutter filtering (2.7) and calculate the amplitude response (2.8).
- Calculate the mean frequency estimate  $\hat{\omega}$  and the frequency bias  $\hat{\omega} - \omega$  from each  $y_\omega$ .
- Calculate the frequency spectrum from each  $y_\omega$ .

This form of frequency analysis was used in [22], and is here expanded to include sparse signals.

## 2.3 Materials and methods

The methods described in 2.2.1 and 2.2.2 were utilized to evaluate the use of sparse sequences in two clinical applications, cardiac PW Doppler and CDI/PW Doppler in the carotid artery using plane waves [24], [25], [26]. These are both applications where pathology typically requires measurement of high velocities and therefore a high PRF, e.g. in the presence of stenosis, where blood velocities can be 4 m/s or more [5], [27]. As simultaneous high quality B-mode images are also desirable for navigation and anatomical assessment, some sort of interleaving of B-mode and Doppler firings is necessary.

To support the theoretical analysis, *in vivo* Doppler data were acquired for experimental validation. The presence and impact of reverberations are shown both

in the cardiac and carotid applications, and it is shown that the cardiac application is very susceptible to reverberation problems due to the lower transmit frequency. Clutter filtering problems are therefore exemplified using data acquired from the carotid artery, for three different types of sparse sequences. Finally, a sequence was implemented on a research system to illustrate that sparse Doppler sequences containing B-mode interruptions may be used for CDI with only minor impact from reverberations and clutter filtering effects, as long as these problems are considered during sequence design. The sequence was evaluated both *in vitro* and *in vivo*.

In the following, the sequence setup and the post-processing necessary to perform the analysis and experimental validation are presented.

### 2.3.1 Data acquisition and processing

All *in vivo* and *in vitro* data were acquired using a Sonix MDP research system (Ultrasonix, Richmond, BC, Canada), with a Sonix DAQ for channel data acquisition. Sequence programming was performed using the development toolkit Texo which allows for the use of custom sequences. For B-mode, focused line acquisition was utilized to ensure high quality tissue images for all applications. For velocity estimation in vascular imaging, single plane waves were utilized on transmit and parallel beamforming on receive, achieving the highest Doppler PRF and also allowing simultaneous mean velocity estimation and retrospective PW Doppler at every image point in the field of view. For the cardiac PW Doppler example, fixed focus was utilized on both transmit and receive.

Channel data were sampled with frequency 40 MHz. IQ demodulation, receive filtering and beamforming were then performed offline. For receive beamforming, dynamic focus was used for B-mode images and CDI, whereas PW Doppler and signals acquired with low PRF for estimation of reverberation effects were beamformed with fixed focus in the sample volume. No apodization was used on transmit or receive. Using the notation from (2.1), the delays for beam  $B$  at depth  $ct/2$  are given by

$$\tau_B(m, t) = \sqrt{(p(m - B)/c)^2 + t^2} - t, \quad (2.10)$$

where  $c = 1540$  m/s is the speed of sound,  $p$  is the pitch of the transducer, and  $m$  is the channel index. The setup parameters are given in Table 2.1. All data were acquired from healthy volunteers.

### 2.3.2 Reverberation quantification

The method for reverberation quantification described in 2.2.1 required a Doppler transmission with low PRF to estimate the received signal  $C$  in (2.1). In addition, a Doppler sequence with missing transmissions was acquired to illustrate the resulting reverberation noise in the slow time signal. A three-part sequence was implemented on the scanner to ensure that the data were acquired from the same spatial region: Focused B-mode transmissions for navigation, followed by a Doppler transmission with PRF 1 kHz, and finally a Doppler sequence of 400 transmissions, alternating between a sequence with every 5th transmission missing, and Doppler without interruptions every

**Table 2.1:** In vivo imaging parameters

Parameter	B-mode	Doppler	Cardiac
Probe	L9-4/38	L9-4/38	SA4-2/24
Probe type	Linear	Linear	Phased
Elements used on transmit	128	128	64
Pitch [ $\mu\text{m}$ ]	304	304	254
TxFrequency $f_0$ [MHz]	6.7	5	2
PRF [kHz]	12	0.6-12	1-10
Cycles @ $f_0$	1.5	2.5	5
Receive $F\#$	1.4	2.3	3.7
Transmit $F\#$	2.2	$\infty$	3.7

100 transmissions. Every fifth sample was discarded from the uninterrupted Doppler data in post-processing, to ensure that the only difference between the packets was the missing transmissions. Clutter filtering was then performed on the sparse data as described in 2.2.2, using a polynomial filter with observation window 100 and order 15. For simplicity, no B-mode pulses were fired during the interruptions, as the lack of Doppler transmissions alone causes reverberation noise (as explained in 2.2.1).

### 2.3.3 Quantification of clutter filtering effects

The effect of clutter filtering on sparsely sampled Doppler data was quantified for the power spectral estimation scheme proposed in [11]. For PW Doppler, first the autocorrelation function  $R(m)$  was estimated from the slow time signal  $y(k)$ :

$$\hat{R}(m) = \frac{1}{N_m} \sum_{k \in I_m} y(k-m)^* y(k). \quad (2.11)$$

The sum was taken over the  $N_m$  indices  $I_m$  such that both  $k-m$  and  $k$  correspond to Doppler transmissions for  $k \in I_m$ . The power spectrum estimate was then calculated as the Fourier transform of  $\hat{R}(m)$ :

$$\hat{S}(f) = \sum_{m=-N}^{N-1} w(m) \hat{R}(m) e^{-2\pi i f t_m}, \quad (2.12)$$

where  $w$  is a window function and  $t_m = m/\text{PRF}$ . For CDI, the normalized mean frequency was estimated by:

$$f_d = \angle \hat{R}(1) / 2\pi. \quad (2.13)$$

The frequency spectrum and the mean frequency was converted to velocities using the relation:

**Table 2.2:** Sequence setup

Tag	Description	Sequence	Period	% B-mode
A	Short period	v v v v b v v v v b ..	5	20
B	Packet	v x 39 b x 11 ..	50	22
C	Random	v v v b v b b v v v ..	256	23

v=velocity sample, b = B-mode sample

$$v = \frac{c \text{ PRF}}{2f_0} f_d, \quad (2.14)$$

where  $c$  is the speed of sound,  $f_0$  is the center frequency and PRF is the pulse repetition frequency of the measurement sequence.

When choosing sequences for the analysis of clutter filtering effects, sequences containing approximately 20% B-mode samples were chosen to maintain a decent B-mode frame rate when using focused beams (approximately 19 frames per second using a PRF of 12 kHz and 128 transmissions per B-mode frame). The sequences are described in Table 2.2. Sequence A has short period, and is comparable to the sequences used in [11]. Sequence B is a packet acquisition with short and frequent B-mode interruptions, an attempt at a sequence without long interruptions and without losing too many Doppler samples due to transitions between the different modes. Sequence C is a random acquisition with period 256, comparable to the sequence used in [18].

In order to compare the analysis to *in vivo* results, a slow time signal was extracted from a recording in the carotid artery, acquired using an uninterrupted plane wave Doppler sequence with a PRF of 4 kHz. The data were synthetically undersampled in post processing to emulate the sequences A-C.

### 2.3.4 In vivo and in vitro color Doppler

As will be shown in the results section, the use of sparse sequences might not be suited for cardiac applications due to reverberation problems, and might also result in significant artifacts in PW Doppler spectra due to clutter filtering problems. However, it is also shown that it is possible to use such sequences for CDI in the carotid artery with only minor impact from these problems. Therefore, two sequences based on sequence B were implemented on the scanner for *in vitro* and *in vivo* validation. For *in vivo* validation, each packet consisted of 39 single plane wave transmissions with PRF 6 kHz used for Doppler followed by 22 focused B-mode transmissions with PRF 12 kHz. One Doppler sample was discarded after each interruption to avoid reverberation noise from B-mode transmissions. Clutter filtering was performed using a regression filter of order 10 with observation window spanning four packets. For comparison, the same data were filtered using a regression filter of order 4 spanning a single packet, with no B-mode interruptions. To enable quantification of low Doppler shifts, filter orders were

chosen to be as low as possible without passing the signal from moving tissue. Color Doppler images were then produced using the mean velocity estimates in (2.13) and (2.14). To make the visualization less dependent on segmentation threshold values, segmentation was only performed on B-mode amplitude. The chosen parameters resulted in about 30 independent velocity estimates per second.

For *in vitro* validation, an uninterrupted Doppler sequence with a PRF of 6 kHz was used, using single plane waves transmitted from a linear probe. The uninterrupted Doppler data were used to provide a ground truth velocity measurement, using 200 samples, before undersampling the data synthetically and applying the two filters used for the *in vivo* recording.

## 2.4 Results

### 2.4.1 In vivo reverberation quantification

Figure 2.2 shows how the use of sparse sequences in cardiac PW Doppler introduces reverberation noise into the slow time signal. Using a Doppler PRF of 10 kHz, and with every fifth Doppler pulse missing, the power of the reverberation noise was 29-30 dB, as shown in panel C. The reverberation time of almost 500 s seen in panel B means that reverberant noise will influence the received signal from the next four transmissions.

The power of the noise in panel C was compared to the theoretical noise power estimate in 2.2.1. By inserting the received signal of panel B into (2.5) with  $N = 4$  and  $r_B = 0.2$  (one interruption per five samples), the reverberation noise power is estimated to be 28 dB.

For comparison, a corresponding measurement of the reverberation time when using a linear probe and plane waves with transmit frequency 5 MHz is shown in Figure 2.3. The sample volume was positioned at depth 13 mm. In this case, the reverberation time was approximately 100 s, meaning that for a PRF between 10 kHz and 20 kHz it would be sufficient to discard one sample after every B-mode interruption.

### 2.4.2 Impact of clutter filtering on the velocity spectrum

The left column of Fig. 2.4 shows the resulting frequency responses when a polynomial regression clutter filter is applied to data sampled with the sparse sequences A-C in Table 2.2. One sample was discarded after every B-mode interruption before filtering. As is observed, clutter filtering results in different artifacts for the different sparse sequences. When using sequence A, where the sampling pattern is periodic with short period (5 samples), the filtering produces copies of the signal distributed throughout the velocity spectrum. For the packet-like acquisition B, the effect of filtering is an increase in sidelobe level. Filtering data acquired using the random sequence C distributes energy throughout the spectrum, producing an artificial noise floor which in this case reduces the dynamic range to about 25 dB.

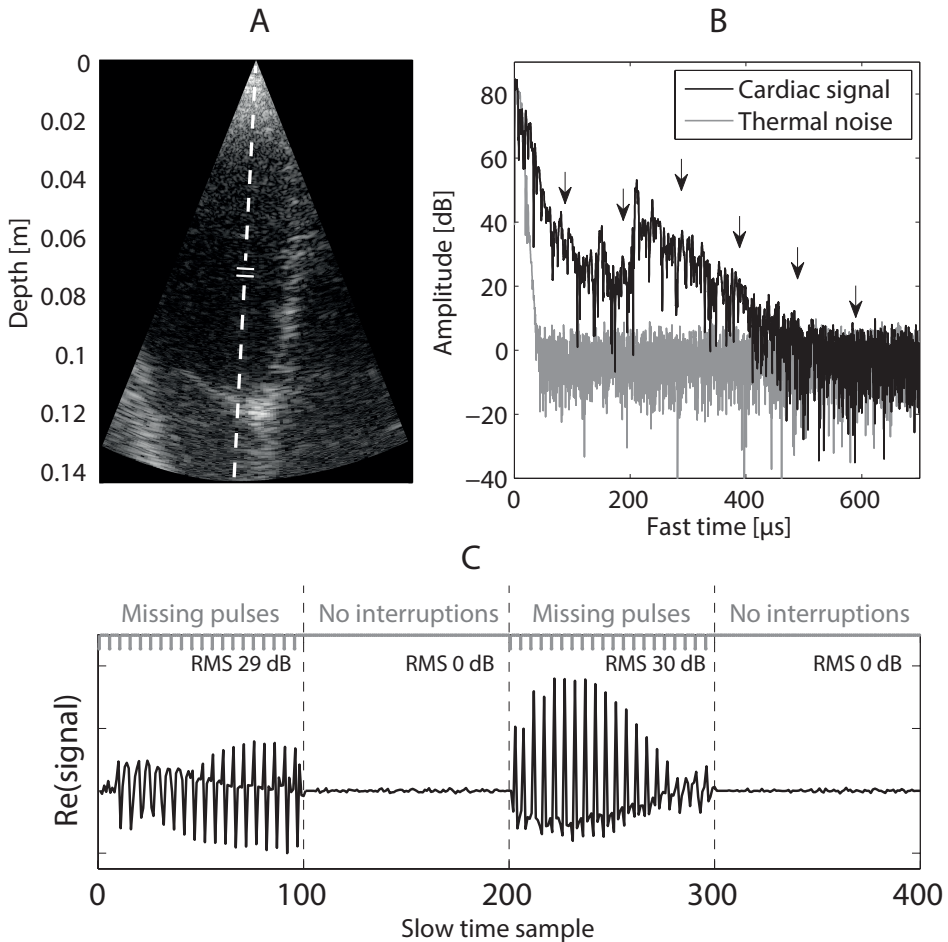


**Figure 2.2:** Illustration of noise due to reverberations in a cardiac measurement. (A) B-mode image showing the sample volume and the corresponding beam. (B) The received signal. Arrows indicate parts of the signal that will contribute to the slow time signal when sampling with PRF 10 kHz. (C) Slow time signal, with reverberation noise occurring after each interruption in the Doppler signal.

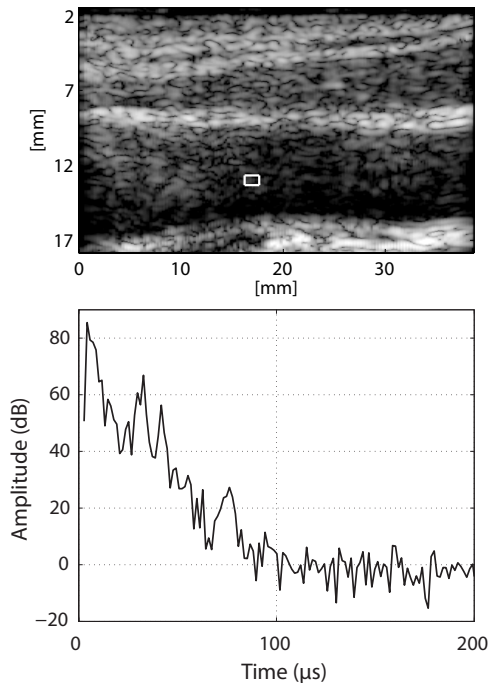


**Figure 2.3:** Amplitude of the signal  $C(t)$  from a plane wave transmission using a linear probe, at depth 13 mm in the carotid artery, illustrated in the upper panel. The transmit frequency is 5 MHz. The data are normalized so that the thermal noise level is at 0 dB.

The right column of Fig. 2.4 shows how these artifacts influence PW Doppler spectra from the carotid artery. When using sequence A, the aliasing-like artifacts severely compromises the quality of the spectrum. For sequences B and C the clutter filtering results in increased sidelobes and noise floor, respectively, but the contour of the spectrum is still resolvable.

### 2.4.3 Impact of clutter filtering on the mean frequency estimate

Fig. 2.5 shows the amplitude responses and bias in the mean frequency estimator as function of input frequency when clutter filtering data sampled with the sequences A-C. One sample was discarded after every B-mode interruption before filtering. As shown, the amplitude responses are not significantly affected by sparse sampling. When using sequence A, large bias (up to 17% of the Nyquist limit) is observed in bands around frequencies corresponding to the repetition frequency of the sampling pattern. For sequences B and C, however, the bias is smaller than 1.3 % of the Nyquist

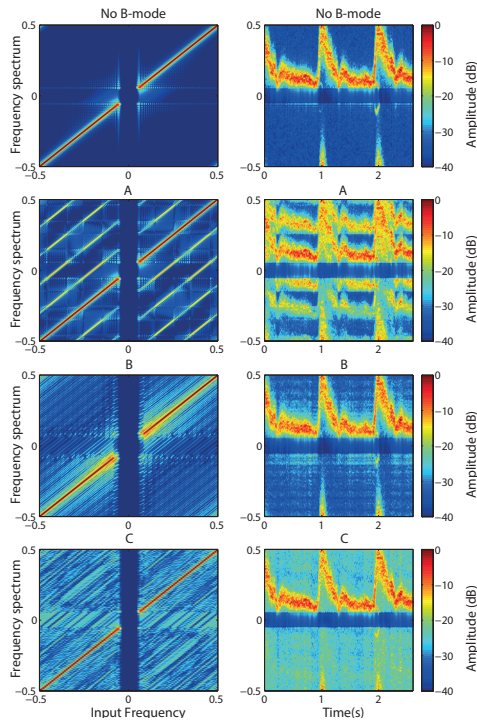


**Figure 2.4:** Filter responses for sequences A-C (Table 2.2) are shown in the left panels. The packet size was 100 samples and the polynomial filter had order 15. A hanning window was used as window function. Corresponding spectrograms when the sampling schemes are applied to a fully sampled *in vivo* data set are shown in the right panels.

limit for all frequencies.

#### 2.4.4 Experimental validation of Color Doppler Imaging sequence

Based on the small velocity bias found for sequence B, it was chosen for the implementation of a CDI sequence on the research system. Two clutter filters were compared, a regression filter with observation window spanning four packets, and a conventional regression filter with observation window spanning a single packet, without B-mode interruptions. The two filters have equal stopband (-70 dB), but the filter spanning four packets has narrower transition band, as shown in Fig. 2.6.

The results from the *in vitro* recording are shown in Fig. 2.6. A Doppler acquisition without interruptions and a 4th order Butterworth clutter filter were used to provide ground truth velocity estimates. The data were then undersampled using sequence B, and one sample was discarded after every B-mode interruption before applying the two

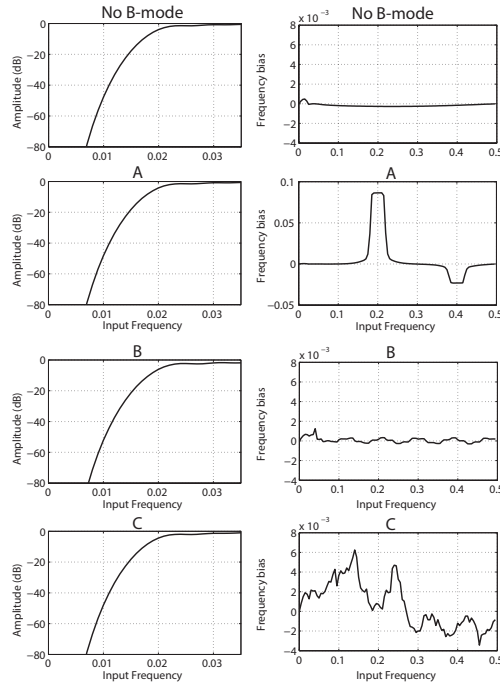


**Figure 2.5:** The amplitude response (left) and frequency bias of the autocorrelation estimate (right) when using sequences A-C (Table 2.2) with an observation window of 200 samples and polynomial order 10 for the regression filter. For the amplitude responses in the left column the attenuation was less than 2 dB for all frequencies above 0.03. Note that the frequency bias when using sequence A is presented with a different scale on the y-axis.

regression filters. The amplitude responses of the filters used are shown in the lower left panel. As the clutter-to-blood signal ratio was lower in the phantom than *in vivo*, the filter used for ground truth estimates had lower cutoff frequency than the evaluated filters, in order to minimize signal loss from low velocity flow. As is seen, filtering using single packets in this case causes overestimation of flow velocities, as lower frequency components in the signal are attenuated by the filter. The overestimation becomes more severe for the lower velocities along the walls. Increasing the length of the observation window by clutter filtering across four packets largely removes the overestimation except for the lowest velocities.

*In vivo* color Doppler images using the same filters are shown in Fig. 2.7. In the left panels the sparse regression filter was applied to an observation window of four packets, whereas in the right panels, using the same observation window, the four packets were filtered separately before averaging the autocorrelation estimates. To make the visualization less dependent on threshold parameters, segmentation was only

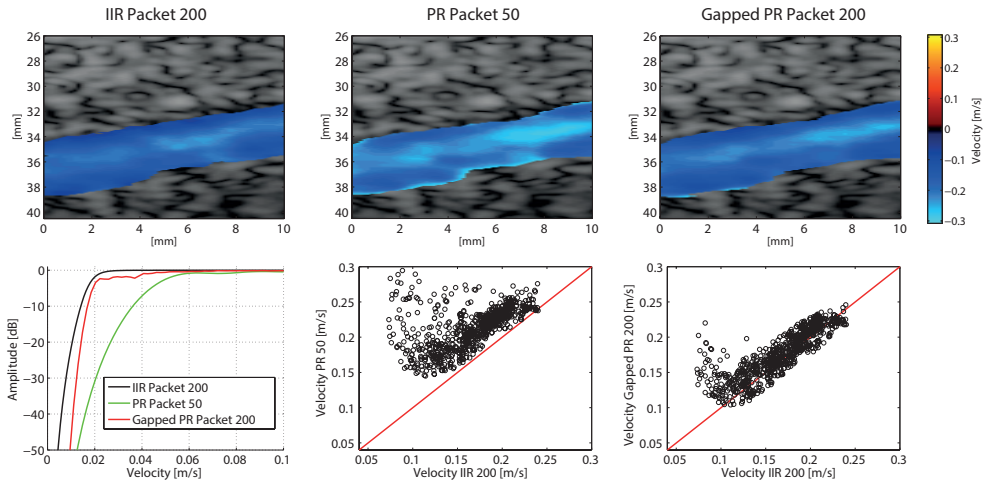


**Figure 2.6:** Results from in vitro color Doppler imaging. The three CDI images are produced using the same observation window of length 200 samples, but filtered using three different clutter filters. The IIR filter is applied to fully sampled data and used as ground truth velocities. The data were then synthetically undersampled using sequence B and filtered using a conventional polynomial regression filter with packet size 50, and a regression filter with packet size 200 containing B-mode interruptions. When using the conventional filter, autocorrelation estimates were averaged over the 4 packets. The amplitude responses of the filters and scatter plots showing all velocity measurements in the ROI are shown in the lower panels.

performed on B-mode amplitude, so that high frequency noise appears in the dropout regions where the Doppler results would normally be removed during segmentation. Visual inspection shows that clutter filtering across several packets reduces the amount of dropouts and thus increases the measurable velocity span.

## 2.5 Discussion

This work has investigated the feasibility of using sparse sequences for Doppler imaging. Sparse imaging techniques are of interest in ultrasound imaging, as they have the potential to provide separate and interleaved B-mode and Doppler without reduction in velocity range. However, in this work it was shown that long reverberation times can introduce substantial signal dependent noise in acquisitions with frequent B-mode interruptions. It was also shown that clutter rejection on sparsely sampled data introduces artifacts in the velocity spectra, and may also lead to significant bias in the mean velocity estimates. Methods have been proposed for quantification of these effects. These methods have been used to evaluate the feasibility of using sparse sequences for PW Doppler and CDI in cardiac and vascular imaging.

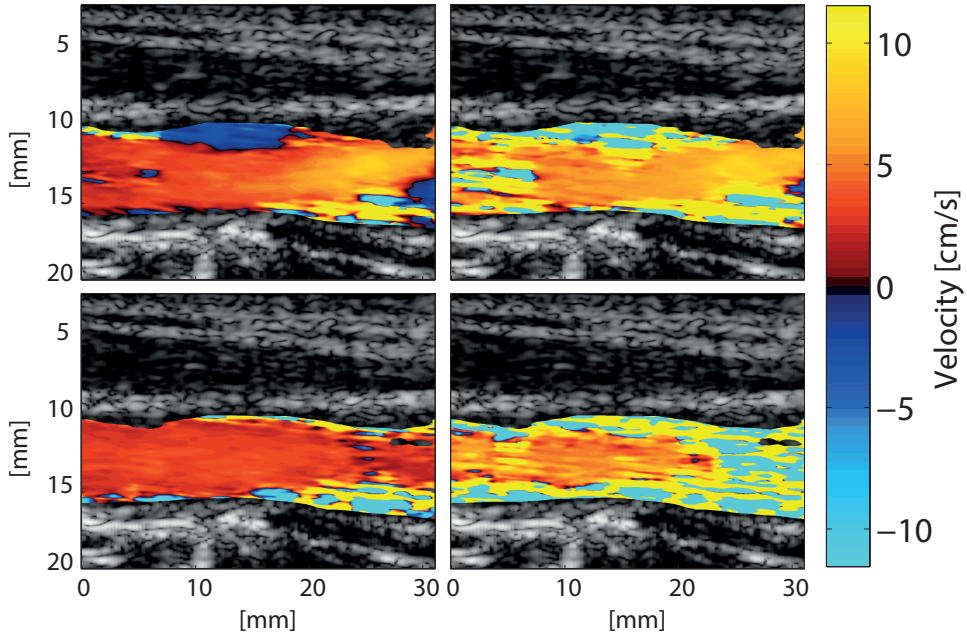


**Figure 2.7:** In vivo mean velocity estimates of flow with low axial velocity, based on sequence B. The two images on the left show the results when clutter filtering is performed with observation windows spanning four packets. The images on the right show the corresponding results when packets in the same observation windows are filtered separately and the autocorrelation estimate is averaged over the four packets. The images are only segmented using B-mode amplitude, so that high frequency noise appears where the signal falls below the noise floor.

For the investigated examples, the analysis showed that reverberation effects should be considered. In the cardiac example shown in Fig. 2.2, unless 2-4 Doppler samples are discarded after every B-mode interruption, reverberant echoes will produce significant noise when using PRF values relevant for clinical practice. Additionally, since the distribution of B-mode interruptions in the sequence is not random, the noise appears structured and may be interpreted as a false flow signal. As it will be necessary to discard several samples after every interruption, sequences with frequent and short interruptions will be less efficient and have lower SNR in the Doppler signal. This puts strong limitations on the use of sparse sequences for cardiac applications. When using a 5 MHz linear probe for imaging of the carotid artery, the problem is less severe due to the higher center frequency, but it is still necessary to discard one sample after every interruption for PRF values of about 10 kHz or higher. Of the sequences types evaluated in this work, packet-like sequences like sequence B is least affected by long reverberation times. Due to the frequent B-mode interruptions sequences like

A and C will be less robust against transient effects in general and especially with reverberation times spanning several PRTs. Note that long reverberation time is a potential problem not just in duplex imaging, but in all applications using interleaving. For example in beam interleaved Doppler sequences, the first samples in each packet should be discarded to avoid reverberation noise.

For PW Doppler, the main motivation for the use of sparse sequences is to avoid gaps in the spectral display during B-mode interruptions and maintain the maximal PRF for high velocity estimation. Another advantage is increased flexibility in choosing observation windows for velocity estimation, without compromising the frame rate of the B-mode images. A long observation window can be utilized to achieve a sharper filter response for the removal of stationary tissue. It also improves the resolution of the velocity spectrum estimates, and allows for better quantification of low velocities. In addition, overlapping windows may be used to increase the line density in the spectral display, or Welch's method may be applied for improved velocity spectrum estimation.

However, due to the non-uniform sampling pattern the use of sparse sequences also requires polynomial regression filters for clutter removal. The results presented in Fig. 2.4 show that these filters applied to sparsely sampled data may introduce artifacts in the velocity spectrum. When using sequence A, strong aliasing artifacts appeared that made it difficult to delineate the contour of the spectrum. The use of sequence B resulted in an increased sidelobe level that may lead to an apparent broadening of the spectrum and overestimation of maximal velocities. When using the random sequence C, an increased noise floor was observed. Assuming sufficiently attenuated clutter, the amplitude of the noise due to clutter filtering scales with blood signal strength, and therefore reduces the dynamic range of the blood signal. Even though the observed artifacts are specific to the sequences used, the severity of the artifacts shows that this effect should be accounted for before applying clutter filters to non-uniformly sampled data.

Another notable disadvantage in using sparse sequences for spectral velocity estimation is related to the use of regression filters in general. When using FIR or IIR filters before velocity spectrum estimation, a sufficient criterion for clutter filtering is that the sidelobes of the clutter are sufficiently attenuated. Regression filters, however, are not time-invariant, and therefore stronger stopband attenuation is required as residual clutter may be distributed throughout the velocity spectrum.

For the CDI case, however, the results in Fig. 2.5 show that the use of sparse sequences for mean velocity estimation is possible without significant reverberation effects and without notable bias due to clutter filtering. Whereas the strong biases observed when using sequence A would not be acceptable for most applications, the biases when using sequence B and C are both below 1.3% of Nyquist for all input frequencies. Of these two sequences, sequence B provides the best SNR because fewer samples need to be discarded due to reverberation effects.

The main difference between conventional CDI and a sparse sequence implementation using sequence B is that in the latter case, the observation window of the clutter filter spans several packets rather than just one packet. The potential advantage of this approach is shown in the Color Doppler results in section 2.4.4. The sharper filter

response achieved by clutter filtering across several consecutive packets both reduces overestimation due to clutter filtering (Fig. 2.6), and reduces the amount of signal dropouts (Fig. 2.7) given the same required stopband attenuation. This gave a fairly good representation of the blood flow even for the diastolic flow in the *in vivo* example, where the axial blood velocities were as low as 1-4 % of the Nyquist velocity.

The example sequences in this paper used about 20% B-mode transmissions, so that a decent frame rate could be achieved using conventional focused B-mode transmissions. As stated in the introduction, techniques have been proposed for reducing the number of B-mode firings. Reducing the number of B-mode interruptions will reduce the number of samples that need to be discarded due to long reverberation time, as argued in 2.2.1, and should also reduce the severity of the regression filter artifacts shown in Fig. 2.4. However, these effects will still be significant and should be considered when using sparse sequences for velocity estimation.

## 2.6 Conclusion

It has been shown that long reverberation times may introduce significant signal dependent noise when using sparse sequences for velocity estimation, with imaging parameters relevant for clinical use. The problem is particularly severe for cardiac applications where a reverberation time of 500 s was observed. Additionally, clutter filtering of sparsely sampled data produces artifacts in the velocity spectra and may introduce significant bias in mean velocity estimates. The results show that these challenges should be considered when designing and utilizing sparse duplex sequences, and general methods have been proposed for quantification of these effects. However, it was possible to design a sequence where these effects had only marginal impact on mean velocity estimation, and it was shown that a Color Doppler Imaging scheme based on this sequence could improve conventional packet based acquisition by reducing bias in the velocity estimate and increasing the measurable velocity span.



# References

- [1] C. Kasai, K. Namekawa, A. Koyano, and R. Omoto, “Real-time two-dimensional blood flow imaging using an autocorrelation technique,” *IEEE Trans. Sonics Ultrason*, vol. 32, no. 3, pp. 458–464, 1985.
- [2] G. Montaldo, M. Tanter, J. Bercoff, N. Benech, and M. Fink, “Coherent plane-wave compounding for very high frame rate ultrasonography and transient elastography,” *Ultrasonics, Ferroelectrics and Frequency Control, IEEE Transactions on*, vol. 56, no. 3, pp. 489–506, 2009.
- [3] J. Bercoff, G. Montaldo, T. Loupas, D. Savery, F. Meziere, M. Fink, and M. Tanter, “Ultrafast compound Doppler imaging: providing full blood flow characterization,” *Ultrasonics, Ferroelectrics and Frequency Control, IEEE Transactions on*, vol. 58, no. 1, pp. 134–147, 2011.
- [4] B.-F. Osmanski, M. Pernot, G. Montaldo, A. Bel, E. Messas, and M. Tanter, “Ultrafast Doppler imaging of blood flow dynamics in the myocardium,” *Medical Imaging, IEEE Transactions on*, vol. 31, no. 8, pp. 1661–1668, 2012.
- [5] G.-M. von Reutern, M.-W. Goertler, N. M. Bornstein, M. Del Sette, D. H. Evans, A. Hetzel, M. Kaps, F. Perren, A. Razumovsky, T. Shiogai, *et al.*, “Grading carotid stenosis using ultrasonic methods,” *Stroke*, vol. 43, no. 3, pp. 916–921, 2012.
- [6] F. E. Barber, D. W. Baker, A. W. Nation, D. E. Strandness, and J. M. Reid, “Ultrasonic duplex echo-Doppler scanner,” *Biomedical Engineering, IEEE Transactions on*, no. 2, pp. 109–113, 1974.
- [7] D. Phillips, J. Powers, M. Eyer, W. Blackshear Jr, K. Bodily, D. Strandness Jr, and D. Baker, “Detection of peripheral vascular disease using the duplex scanner III,” *Ultrasound in medicine & biology*, vol. 6, no. 3, pp. 205–218, 1980.
- [8] B. A. Angelsen and K. Kristoffersen, “Combination of ultrasonic 2D-echo amplitude imaging and Doppler measurements,” in *Cardiac Doppler Diagnosis*, pp. 33–42, Springer, 1985.
- [9] K. Kristoffersen and B. Angelsen, “A time-shared ultrasound Doppler measurement and 2-D imaging system,” *Biomedical Engineering, IEEE Transactions on*, vol. 35, no. 5, pp. 285–295, 1988.

- 
- [10] H. Klebæk, J. A. Jensen, and L. K. Hansen, “Neural network for sonogram gap filling,” in *Ultrasonics Symposium, 1995. Proceedings., 1995 IEEE*, vol. 2, pp. 1553–1556, IEEE, 1995.
- [11] J. A. Jensen, “Spectral velocity estimation in ultrasound using sparse data sets,” *The Journal of the Acoustical Society of America*, vol. 120, p. 211, 2006.
- [12] P. Liu and D. Liu, “Periodically gapped data spectral velocity estimation in medical ultrasound using spatial and temporal dimensions,” in *Acoustics, Speech and Signal Processing, 2009. ICASSP 2009. IEEE International Conference on*, pp. 437–440, IEEE, 2009.
- [13] E. G. Larsson and J. Li, “Spectral analysis of periodically gapped data,” *Aerospace and Electronic Systems, IEEE Transactions on*, vol. 39, no. 3, pp. 1089–1097, 2003.
- [14] E. Gudmundson, A. Jakobsson, J. A. Jensen, and P. Stoica, “Blood velocity estimation using ultrasound and spectral iterative adaptive approaches,” *Signal Processing*, vol. 91, no. 5, pp. 1275–1283, 2011.
- [15] A. Jakobsson, G.-O. Glentis, and E. Gudmundson, “Computationally Efficient Time-Recursive IAA-Based Blood Velocity Estimation,” *Signal Processing, IEEE Transactions on*, vol. 60, no. 7, pp. 3853–3858, 2012.
- [16] E. Gudmundson, A. Jakobsson, and G. Fredrik, “Overcoming the Nyquist limit in blood flow velocity estimation,” in *2012 IEEE International Ultrasonics Symposium (IUS’12), Proceedings of*, IEEE, 2012.
- [17] S. Mollenbach and J. A. Jensen, “Duplex scanning using sparse data sequences,” in *Ultrasonics Symposium, 2008. IUS 2008. IEEE*, pp. 5–8, IEEE, 2008.
- [18] J. Richy, D. Friboulet, A. Bernard, O. Bernard, and H. Liebgott, “Blood Velocity Estimation Using Compressive Sensing,” *IEEE transactions on medical imaging*, 2013.
- [19] M. A. Lediju, M. J. Pihl, J. J. Dahl, and G. E. Trahey, “Quantitative assessment of the magnitude, impact and spatial extent of ultrasonic clutter,” *Ultrasonic imaging*, vol. 30, no. 3, pp. 151–168, 2008.
- [20] G. F. Pinton, G. E. Trahey, and J. J. Dahl, “Sources of image degradation in fundamental and harmonic ultrasound imaging using nonlinear, full-wave simulations,” *Ultrasonics, Ferroelectrics and Frequency Control, IEEE Transactions on*, vol. 58, no. 4, pp. 754–765, 2011.
- [21] M. A. Lediju, B. C. Byram, and G. E. Trahey, “Sources and characterization of clutter in cardiac B-mode images,” in *Ultrasonics Symposium (IUS), 2009 IEEE International*, pp. 1419–1422, IEEE, 2009.

- [22] H. Torp, “Clutter rejection filters in color flow imaging: A theoretical approach,” *Ultrasonics, Ferroelectrics and Frequency Control, IEEE Transactions on*, vol. 44, no. 2, pp. 417–424, 1997.
- [23] S. Bjaerum, H. Torp, and K. Kristoffersen, “Clutter filter design for ultrasound color flow imaging,” *Ultrasonics, Ferroelectrics and Frequency Control, IEEE Transactions on*, vol. 49, no. 2, pp. 204–216, 2002.
- [24] J. Udesen, F. Gran, K. L. Hansen, J. A. Jensen, C. Thomsen, and M. B. Nielsen, “High frame-rate blood vector velocity imaging using plane waves: simulations and preliminary experiments,” *Ultrasonics, Ferroelectrics and Frequency Control, IEEE Transactions on*, vol. 55, no. 8, pp. 1729–1743, 2008.
- [25] I. K. Ekroll, A. Swillens, P. Segers, T. Dahl, H. Torp, and L. Lovstakken, “Simultaneous quantification of flow and tissue velocities based on multi-angle plane wave imaging,” *Ultrasonics, Ferroelectrics and Frequency Control, IEEE Transactions on*, vol. 60, no. 4, pp. 727–738, 2013.
- [26] I. K. Ekroll, T. Dahl, H. Torp, and L. Løvstakken, “Combined Vector Velocity and Spectral Doppler Imaging for Improved Imaging of Complex Blood Flow in the Carotid Arteries,” *Ultrasound in medicine & biology*, 2014.
- [27] H. Baumgartner, J. Hung, J. Bermejo, J. B. Chambers, A. Evangelista, B. P. Griffin, B. Iung, C. M. Otto, P. A. Pellikka, and M. Quiñones, “Echocardiographic assessment of valve stenosis: EAE/ASE recommendations for clinical practice,” *European Journal of Echocardiography*, 2008.



## Chapter 3

# Investigations of Spectral Resolution and Angle Dependency in a 2-D Tracking Doppler Method

Tonje D. Fredriksen<sup>1</sup>, Jørgen Avdal<sup>1</sup>, Ingvild K. Ekroll<sup>1,2</sup>, Torbjørn Dahl<sup>1,2</sup>, Lasse Løvstakken<sup>1</sup>, and Hans Torp<sup>1</sup>

<sup>1</sup> MI Lab and Dept. of Circulation and Medical Imaging, NTNU, Norway

<sup>2</sup> St. Olav's University Hospital, Trondheim, Norway

An important source of error in velocity measurements from conventional pulsed wave (PW) Doppler is the angle used for velocity calibration. Because there are great uncertainties and interobserver variability in the methods used for Doppler angle correction in the clinic today, it is desirable to develop new and more robust methods.

In this work, we have investigated how a previously presented method, 2-D tracking Doppler, depends on the tracking angle. A signal model was further developed to include tracking along any angle, providing velocity spectra which showed good agreement with both experimental data and simulations. The full-width at half-maximum (FWHM) bandwidth and the peak value of predicted power spectra were calculated for varying tracking angles. It was shown that the spectra have lowest bandwidth and maximum power when the tracking angle is equal to the beam-to-flow angle. This may facilitate new techniques for velocity calibration, e.g., by manually adjusting the tracking angle, while observing the effect on the spectral display. An *in vitro* study was performed in which the Doppler angles were predicted by the minimum FWHM and the maximum power of the 2-D tracking Doppler spectra for 3 different flow angles. The estimated Doppler angles had an overall error of  $0.24^\circ \pm 0.75^\circ$  when using the minimum FWHM. With an *in vivo* example, it was demonstrated that the 2-D tracking Doppler method is suited for measurements in a patient with carotid stenosis.

### 3.1 Introduction

Blood velocity measurements are essential in cardiovascular diagnostics. Increased flow velocities or abnormal flow patterns can indicate disease and a possible need for surgery. Ultrasound imaging is the primary instrument for cardiovascular diagnostics

as the measurements can be done noninvasively and in real-time. High velocity flow is found, for instance, at stenotic regions. The degree of stenosis is normally assessed by using pulsed wave (PW) Doppler to estimate the maximum velocities. With PW Doppler the complete spectrum of velocities are estimated; typically displayed as a 2-D sonogram with velocity along the y-axis and time along the x-axis. PW Doppler analysis of the Doppler signal is usually performed using the fast Fourier transform (FFT) on short data segments in time, acquired from a single sample point in space. For high velocities and large beam-to-flow angles, the blood will pass rapidly through the sample volume, resulting in a short observation time and a broadening of the estimated velocity spectrum. The loss in frequency resolution may give severe overestimation of blood velocities and a risk of misdiagnosis.

Approaches for increasing the transit time include methods that utilize the full 2-D Fourier transform of the signal in the fast- and slow-time directions. Reduced spectral broadening has been shown by several authors [1–4], but only for flow in the axial direction. In [5] we presented a method called 2-D tracking Doppler, which tracks the scatterers along the direction of the flow. The method is based on the principles described in [4], but is adapted for situations with any beam-to-flow angle. By using plane transmit waves and parallel receive beams, it is possible to have instantaneous acquisition of multiple image lines in a 2-D region. By tracking the scatterers along the direction of the flow within this region, the transit time is increased, giving a higher spectral velocity resolution. The method was in [5] tested both *in vitro* and *in vivo* on a carotid artery of a healthy volunteer. The results showed that the 2-D tracking Doppler method could be used to increase the velocity resolution in PW Doppler, especially for large beam-to-flow angles.

In addition to a limited transit time, the greatest source of error in PW Doppler velocity estimation is the angle used for calibrating the spectra. Conventional Doppler techniques can only measure the axial component of blood flow. The blood velocity is estimated by multiplying the measured velocity with an angle correction factor of  $1/\cos\theta$ , where  $\theta$  is the estimated beam-to-flow angle. As the angle correction factor tends to infinity as  $\theta$  approaches  $90^\circ$ , the velocity estimates are very sensitive to angle estimation errors for large beam-to-flow angles. Therefore, clinical guidelines [6] discourage the use of Doppler angles above  $60^\circ$ .

Several techniques have been suggested to overcome the angle dependence in Doppler ultrasound. Cross-beam vector Doppler has been one of the main approaches to 2-D flow imaging since the onset of the idea in the 1970s. Using triangulation, the 1-D velocity estimates from two different angles of insonation can be used to reconstruct a 2-D velocity vector [7]. An alternative dual-beam method has been introduced by Tortoli and colleagues [8], [9], characterized by the different role played by each beam. One of the beams acts as reference, being devoted to estimate only the flow direction. Through the inspection of the spectrum from the reference beam, a  $90^\circ$  beam-to-flow angle is sought. Such spectra, from transverse flow, are expected to be centered on the zero frequency, and even small deviations from the desired  $90^\circ$  orientation cause noticeable losses of spectral symmetry. However, local secondary flow oscillations, which are often found at atherosclerotic regions [10], may restrict the applicability of the method.

Another approach has been described by J. Jensen and colleagues [11], [12], in which both the velocity magnitude and angle is determined using a crosscorrelation technique. The angle is found from beamforming directional signals in a number of directions and then selecting the angle with the highest normalized correlation. This method has some similarities with the presented method in that minimum spectral bandwidth corresponds to the maximum correlation. However, it only estimates the mean velocity, whereas the 2-D tracking Doppler method produces a full Doppler spectrum display. Mean velocity estimates may have a bias caused by clutter filtering or spatial averaging and they do not provide the peak velocity, as used in e.g., stenosis classification.

Techniques for Doppler angle estimation based on the transit time spectrum broadening effect has been presented by several authors [13–18]. Because the Doppler bandwidth is inversely proportional to the transit time of a scatterer crossing the ultrasound beam, the Doppler angle can be estimated from the resulting Doppler bandwidth. Many promising results have been shown *in vitro*, but the methods have not yet reached clinical practice.

The 2-D tracking Doppler method generates velocity spectra with increased velocity resolution, especially at large beam-to-flow angles. In this work, it is demonstrated that the spectra broaden when the incorrect tracking angle is chosen, compared with spectra with the correct tracking angle. The angle dependency of the 2-D tracking Doppler method will be investigated using simulations and *in vitro* and *in vivo* experiments. Two methods for velocity calibration are proposed; using the Doppler angle given by the minimum spectral broadening or the maximum power. In Section 3.2.1, a brief description of the 2-D tracking Doppler algorithm is given. In Section 3.2.2, the signal model presented in [5] is extended to include incorrect selection of the tracking angle. The experimental work is described in Section 3.3. 2-D tracking Doppler spectra from varying Doppler angles will be presented in Section 3.4, and compared with a conventional PW Doppler method. In Section 3.5, the results are discussed.

## 3.2 Theory

Two spectral Doppler methods have been applied in this work; the 2-D tracking Doppler method and the more conventional Welch's method. The 2-D tracking Doppler algorithm was described in [5], but will also be summarized in Section 3.2.1.

A signal model was presented in [5] where statistically expected 2-D tracking Doppler spectra were calculated for tracking angles equal to the beam-to-flow angles. In Section 3.2.2, this model will be extended to include tracking along any angle, which allows for investigation of the influence of incorrect tracking angle on the 2-D tracking Doppler estimates.

### 3.2.1 The 2-D Tracking Doppler Algorithm

The 2-D tracking Doppler algorithm requires simultaneous acquisition of Doppler signals from a 2-D spatial region. The complex pre-envelope of the received signal is denoted by  $u(x, z, k)$ , and the in-phase and quadrature demodulated (IQ) signal is denoted by  $u_{IQ}(x, z, k)$ , where  $x$  and  $z$  are the spatial coordinates in the azimuth and axial direction, respectively, and  $k$  is the slow time index. Post-processing of the data is performed in two steps:

1. The beamformed signal is resampled along a tracking line, using 2-D spline interpolation.
2. The resampled data are processed using the velocity matched spectrum algorithm, first presented in [4] and later applied in [5].

For a chosen tracking angle,  $\theta$ , the resampled signal can be written as

$$u_{\theta}(r, k) = u(r \sin \theta + x_0, r \cos \theta + z_0, k) , \quad (3.1)$$

$$u_{IQ,\theta}(r, k) = u_{IQ}(r \sin \theta + x_0, r \cos \theta + z_0, k) , \quad (3.2)$$

where  $r$  is the position along the line through the sample volume point  $[x_0, z_0]$ . The resampled signal as a function of slow-time was described in [5] as an M-mode matrix. M-mode usually refers to data from one scan line as a function of time (slow time), but is in this context extended to include any straight line in space and slow time.

The signal from scatterers moving with constant velocity will form straight lines in the M-mode matrix, where the slope of each line corresponds to a particular velocity. A velocity spectrum can then be generated by summing the signal along lines with varying slopes.

$$\begin{aligned} \hat{p}(v) &= \left| \sum_k w(k) u_{\theta}(r_0 + kvT, k_0 + k) \right|^2 \\ &= \left| \sum_k w(k) u_{IQ,\theta}(r_0 + kvT, k_0 + k) e^{i\omega_d k \Delta t} \right|^2 , \end{aligned} \quad (3.3)$$

$$\Delta t = \frac{2vT}{c} \cos \theta , \quad (3.4)$$

where  $v$  is a velocity,  $r_0$  and  $k_0$  are the center positions in range and time,  $\omega_d$  is the angular demodulation frequency,  $T$  is the pulse repetition time, and  $w$  is a smooth window function which is zero outside the range  $k \in [-N/2, N/2 - 1]$ , where  $N$  is the window length in number of samples. Because  $u_{IQ}$  is complex demodulated, a phase correction factor must be included to account for axial motion.

Using the same formulation as in (3.3), an expression for a conventional, Fourier-based estimate of the power spectrum in a point  $r_0$  can be written as

$$\begin{aligned}\hat{p}_{conv}(v) &= \left| \sum_k w(k) u_\theta(r_0, k_0 + k) e^{i\omega_0 k \Delta t} \right|^2 \\ &= \left| \sum_k w(k) u_{IQ,\theta}(r_0, k_0 + k) e^{i\omega_0 k \Delta t} \right|^2,\end{aligned}\quad (3.5)$$

where  $\omega_0$  is the center frequency of the received signal, which may differ slightly from the demodulation frequency,  $\omega_d$ .

Note that  $\hat{p}(v)$  and  $\hat{p}_{conv}(v)$  also are functions of  $r_0$  and  $k$ . However, these variables were omitted for clarity.

### 3.2.2 Signal Model

In [5], the statistical expectation values of the power spectra were calculated for tracking angles equal to the beam-to-flow angles. We will now extend the model to include tracking along any angle, by introducing a 2-D point spread function. All motion is assumed to be in the imaging plane. The calculated statistical expectation value of the power spectra will henceforth be referred to as the expected velocity spectra.

The complex pre-envelope of the received signal,  $s(x, z, k)$  was in [5] sampled along an oblique line to produce a signal  $s_\theta(r, k)$ . By adding noise with power  $N_0$ , a clutter filter  $h(k)$  and a bandpass filter  $b(r)$  a signal corresponding to  $u_\theta(r, k)$  was constructed. The expected power spectrum for the 2-D tracking Doppler method was shown to be

$$\begin{aligned}\langle \hat{p}(v) \rangle &= \sum_{k,n} w_2(k) R_{s_\theta}(kvT, k-n) h_2(n) \\ &\quad + \sum_k w_2(k) N_0 b_2(kvT) h_2(k),\end{aligned}\quad (3.6)$$

where  $\langle \rangle$  is the expectation value operator, the subscript  $_2$  is a shorthand notation for the autocorrelator operator, and  $R_{s_\theta}$  is the autocorrelation of  $s_\theta$ .

In the subsequent formulations in [5],  $\theta = \theta_0$  was assumed, where the beam-to-tracking angle is denoted  $\theta$  and the beam-to-flow angle  $\theta_0$ . However, by introducing the 2-D point spread function,  $f(\vec{r})$ , the signal can be evaluated along any tracking angle.

If the blood velocity field is uniform with velocity  $v_0$  at an angle  $\theta_0$  and the velocity component in the elevation direction is zero, the autocorrelation of the signal can be written in terms of the autocorrelation of the point spread function:

$$R_{s_\theta}(\rho, m; \vec{v}_0) = f_2(\rho \vec{e}_\theta - m \vec{v}_0 T), \quad (3.7)$$

$$\vec{v}_0 = v_0 \cdot \vec{e}_{\theta_0} , \quad (3.8)$$

where  $\vec{e}_\theta$  and  $\vec{e}_{\theta_0}$  are unit vectors in the  $\theta$  and  $\theta_0$  directions respectively. Inserting (3.7) into (3.6), we obtain the expected power spectrum for the 2-D tracking Doppler method, given the true velocity  $\vec{v}_0$ :

$$\begin{aligned} \langle \hat{p}_\theta(v | \vec{v}_0) \rangle &= \sum_{k,n} w_2(k) f_2(k\vec{v}T - (k-n)\vec{v}_0T) h_2(n) \\ &+ \sum_k w_2(k) N_0 b_2(kvT) h_2(k) , \end{aligned} \quad (3.9)$$

$$\vec{v} = v \cdot \vec{e}_\theta \quad (3.10)$$

The geometry of a situation in which  $\theta \neq \theta_0$  is shown in Fig. 3.1. The velocity is  $v_0$  and the beam-to-flow angle is  $\theta_0$ . By choosing a different tracking angle,  $\theta$ , the point spread function is evaluated at a distance  $\vec{r} = k\vec{v}T - k\vec{v}_0T$  from its center. Assuming an ideal plane wave, where the phase fronts extend in the lateral direction, the estimated velocity spectrum in direction  $\theta$  will have maximum power when

$$v \cos \theta = v_0 \cos \theta_0 = v_z . \quad (3.11)$$

In [5], an expression for the expected power for the conventional PW Doppler spectra was found by using the same signal model, but only considering samples originating from a fixed position in space:

$$\begin{aligned} \langle \hat{p}_{conv}(v) \rangle &= \sum_{k,n} w_2(k) R_{s_\theta}(0, k-n) h_2(n) e^{-i\omega_0 k \Delta t} \\ &+ \sum_k w_2(k) N_0 b_2(0) h_2(k) e^{-i\omega_0 k \Delta t} . \end{aligned} \quad (3.12)$$

Inserting (3.7) into (3.12) we get the expected power spectrum for the conventional PW Doppler method, given the true velocity  $\vec{v}_0$ :

$$\begin{aligned} \langle \hat{p}_{conv}(v | \vec{v}_0) \rangle &= \sum_{k,n} w_2(k) f_2(-(k-n)\vec{v}_0T) h_2(n) e^{-i\omega_0 k \Delta t} \\ &+ \sum_k w_2(k) N_0 b_2(0) h_2(k) e^{-i\omega_0 k \Delta t} . \end{aligned} \quad (3.13)$$

### 3.3 Methods

Velocity spectra were generated by applying the 2-D tracking Doppler algorithm to data from simulations and *in vitro* and *in vivo* recordings. Spectra from one or more

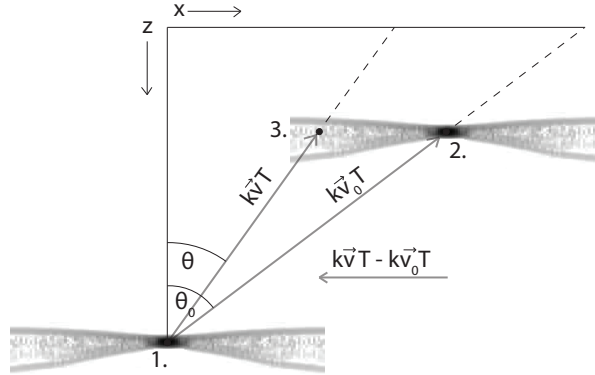


**Figure 3.1:** Geometric considerations and explanation of the behavior of the 2-D tracking Doppler method when the angle of the tracking trajectory is chosen incorrectly. The diagram shows a point spread function moving from one location to another in the imaging plane. The beam-to-flow angle is  $\theta_0$  and the chosen angle for the tracking trajectory is  $\theta$ . During  $k$  pulse repetition periods, the scatterers move a distance  $kv_0T$  from point 1 to point 2. When evaluating the signal along a line with angle  $\theta$ , the maximum correlation is found at point 3. Because of the widened correlation area in the side lobes of the point spread function, the velocity spectrum will broaden. Underestimations of the traveling distance, and hence underestimations of the velocity, will be the result for this scenario. The opposite is true for  $\theta > \theta_0$ .

tracking angles were generated from a region of interest (ROI). The ROI was chosen as large as possible while ensuring that the flow inside was moving approximately along straight lines with uniform velocities. The tracking length,  $L$ , was limited by the size of the ROI for high velocities. For low velocities,  $L$  was limited by the temporal window length,  $N_w$ , and given by the formula  $L = v \cdot N_w \cdot PRT$ , where  $v$  is the velocity and  $PRT$  is the pulse repetition time.

For comparison, velocity spectra were also generated by a conventional PW Doppler method, using (3.13) for the signal model and (3.5) for the *in vitro* and *in vivo* experiments. The same data were used for both spectral estimation techniques, using only a single sample from the tracking line for the conventional method. The same temporal window length was used in the two approaches, and no spatial averaging was performed following any of the two spectral estimation techniques.

### 3.3.1 Field II Simulations

To validate the new signal model derived in 3.2.2, comparisons were done with the widely used ultrasound simulation program Field II [19], which utilizes an approximate form of the time-domain impulse response function. The blood flow was modeled as a collection of random point scatterers in a simple cylindrical volume with a constant, uniform velocity of 1 m/s at a beam-to-flow angle of  $50^\circ$ . The acquisition and post-

processing parameters were the same as listed in Table 3.1, but with a PRF of 6 kHz.

2-D tracking Doppler spectra were generated by extracting signals from tracking trajectories angled at  $20^\circ$ ,  $50^\circ$  and  $70^\circ$  in the cylindrical phantom, and utilizing (3.3) and (3.5). The resulting spectra were qualitatively compared with spectra obtained using (3.9) and (3.13).

### 3.3.2 Application of the Signal Model

2-D tracking Doppler spectra were generated for different combinations of the beam-to-flow angle,  $\theta_0$ , and the tracking angle,  $\theta$ , using the signal model (3.9) and the parameters given in Table 3.1. The spectra were plotted and qualitatively compared with spectra generated from *in vitro* recordings.

To investigate how the spectral width and the maximum power in the 2-D tracking Doppler spectra vary with tracking angle, the signal model (3.9) was used to calculate the expected Doppler power spectra for  $\theta_0 = 73^\circ$  and  $\theta$  ranging from  $65^\circ$  to  $77^\circ$ . The full-width at half-maximum (FWHM) of the spectral main lobes were estimated and compared with the FWHM when  $\theta = \theta_0$ , to obtain the relative spectral broadening. To be able to compare the FWHM value for different tracking angles, (3.11) was used to estimate the axial velocity components,  $v_z$ , of the flow. The spectral broadening and the maximum power were visualized as functions of the velocity calibration error, allowing the bias and sensitivity of angle correction based on either parameter to be evaluated.

### 3.3.3 *In Vitro* Recordings

To investigate the performance of the 2-D tracking Doppler method for arbitrary tracking angles, recordings were done using a flow phantom for which the correct beam-to-flow angle was easy to identify. The flow phantom consisted of a silicon tube with an inner diameter of 6 mm, coupled to a flow loop driven by the PhysioPulse 100 Flow System (Shelley Medical Image Technologies, London, ON, Canada), giving a slowly pulsating flow. However, only a short time period with approximately constant flow velocities was used for the recording. The tube was partly surrounded by a stiff silicon layer, creating an imaging distance of approximately 3.7 cm and a beam-to-flow angle of  $73^\circ$ . The phantom was filled with a blood-mimicking fluid that has been tested and described by Ramnarine *et al.* [20].

A longitudinal cross section of the tube was imaged using a SonixMDP ultrasound scanner with a 5 MHz linear probe and a SonixDAQ for channel data acquisition (Ultrasonix, Richmond, BC, Canada). The acquisition consisted of continuous plane wave transmissions and the RF channel data was beamformed and complex demodulated offline using Matlab (The MathWorks Inc., Natick, MA). The acquisition setup and post-processing parameters are listed in Table 3.1.

A region of interest (ROI) with center in the middle of the tube was chosen from a B-mode image. Signals from lines of varying slopes centered in the middle of the ROI were extracted and processed using the algorithm given in Section 3.2.1. Both velocity-time spectra and power-velocity plots were used to investigate properties of the

2-D tracking Doppler method. The power-velocity plots were generated by averaging spectral estimates from 100 temporal segments of length 120 with an overlap of 119.

### 3.3.4 Velocity Calibration Analysis

Repeated measurements of *in vitro* flow were performed using the setup described in Section 3.3.3, with beam-to-flow angles of 63°, 73° and 83°. For each measurement, different directions were tracked with an angular step of 0.2° for the recordings with beam-to-flow angles of 63° or 73°, and an angular step of 0.1° for the recordings with a beam-to-flow angle of 83°. The flow angle was then automatically estimated in two different ways: by minimizing the FWHM, or by maximizing the peak value in the corresponding 2-D tracking Doppler spectrum. The velocity calibration percentage errors,  $e_{pct}$ , of the resulting angles,  $\theta$ , were calculated using the formula

$$e_{pct} = \frac{1/\cos\theta - 1/\cos\theta_0}{1/\cos\theta_0} \cdot 100, \quad (3.14)$$

where  $\theta_0$  was measured from B-mode images of the tubes. Both methods for velocity calibration were evaluated by estimating the mean and the standard deviation of 10 independent angle estimates for each of the three beam-to flow angles.

The velocity calibration errors resulting from the minimum FWHM estimates were plotted and compared with the velocity calibration errors expected when using manual angle correction, e.g., from the B-mode or color flow image. To illustrate the potential error which can occur when performing manual angle correction, it was assumed that the Doppler angle can be estimated within  $\pm 3^\circ$ .

### 3.3.5 *In Vivo* Recordings

The 2-D tracking Doppler method was tested in a patient with a moderate carotid stenosis. The study was approved by The Regional Committee for Medical and Health Research Ethics (REC) in Trondheim, Norway. A color flow image of the artery, recorded with a high-end ultrasound scanner, Vivid E9 (GE Vingmed Ultrasound, Horten, Norway), is shown in Fig. 3.2. Narrowing of the artery, resulting from plaque formation, is causing a high-velocity jet to be formed.

Recordings for the 2-D tracking Doppler method were done in the same way as for the *in vitro* recordings, using the SonixMDP ultrasound scanner with a SonixDAQ for channel data acquisition. The region of interest (ROI) was placed in the stenotic part of the carotid bifurcation. The beam-to-flow angle was estimated, by visual inspection of color flow images, to be approximately 50°. However, it may have varied to some extent during the heart cycle. The acquisition setup and post-processing parameters are listed in Table 3.1.

The tracking line was probed to find the point that maximized the SNR for the conventional PW Doppler method, and a point close to the beginning of the line was selected.

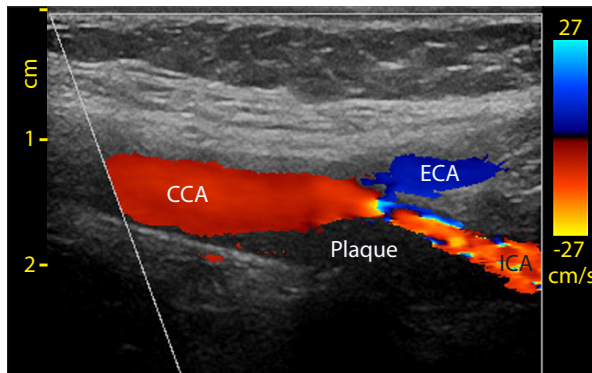


**Figure 3.2:** A color flow image overlaid on a B-mode image of a carotid artery with moderate carotid stenosis. The image shows the common carotid artery (CCA) bifurcation which divides into the external carotid artery (ECA) and the internal carotid artery (ICA). Plaque formation causes a high velocity jet to be formed, depicted in orange color in the lower right of the image. The recording was done using a high-end Vivid E9 ultrasound scanner.

**Table 3.1:** Parameters

Acquisition setup		Post-processing parameters		
Parameter	Value	Parameter	<i>In vivo</i> value	<i>In vitro</i> value
Tx center frequency	5 MHz	Tracking length	1 cm	1.5 cm
Pulse periods	2.5	Window	Hamming	Hamming
PRF	8 kHz	Window length	80 samples	120 samples
F-number	1.4	HP-filter	FIR, order 50	FIR, order 50
		HP-filter cutoff	400 Hz	400 Hz

## 3.4 Results

### 3.4.1 Validation of Signal Model

In Fig. 3.3, 2-D tracking Doppler spectra generated from Doppler signals simulated using Field II, and 2-D tracking Doppler spectra predicted by the signal model are shown. The results show good agreement between the spectra from the two models.

### 3.4.2 Investigations of the Tracking Angle Sensitivity

Fig. 3.4 shows relative broadening and maximum power in Doppler power spectra, predicted using the signal model (3.9). The black line (left y-axis) shows relative broadening of the 2-D tracking Doppler spectra and the gray dashed line (right y-axis) shows the maximum power, plotted with respect to the velocity calibration percentage

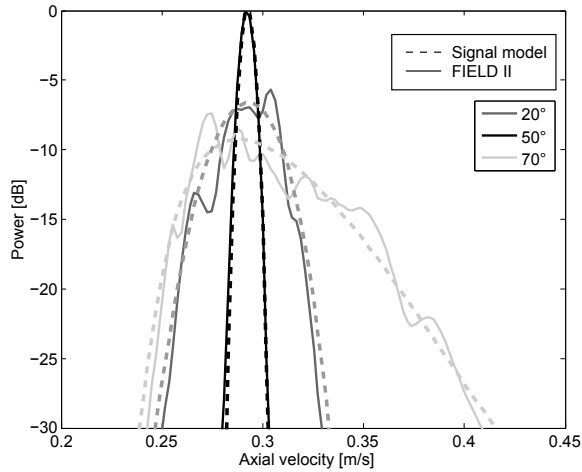


**Figure 3.3:** 2-D tracking Doppler spectra generated for validation of the signal model (dashed lines) with the Field II software (solid lines).

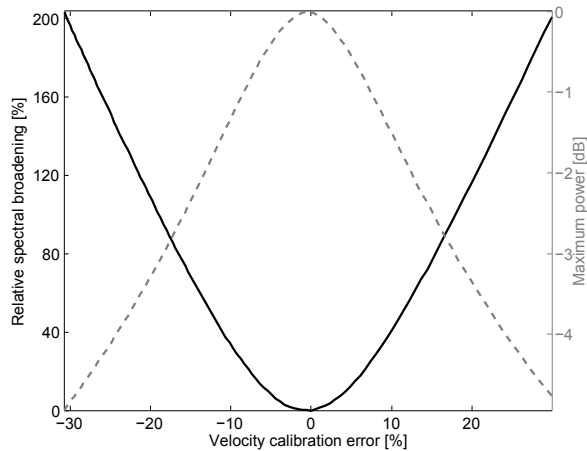


**Figure 3.4:** Relative broadening (solid line) and maximum power (dashed line) plotted with respect to the velocity calibration error. The FWHM of the spectral main lobe of predicted velocity spectra were estimated for varying  $\theta$  and compared with the FWHM when  $\theta = \theta_0$ . The FWHM is at its minimum and the maximum power is at the maximum when the tracking angle is equal to the beam-to-flow angle.

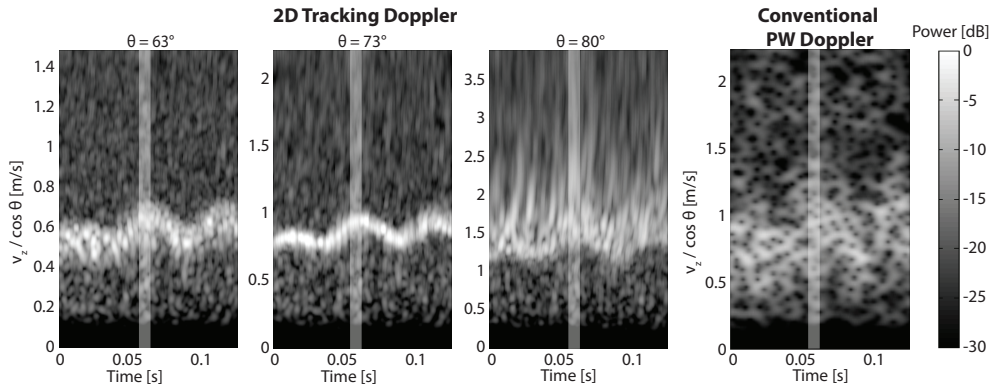


**Figure 3.5:** Velocity spectra generated from an *in vitro* recording of flow in a straight tube. The three left spectra are generated using the 2-D tracking Doppler method with three different tracking angles,  $\theta$ . The rightmost spectrum is generated using a conventional PW Doppler method. The velocity axes are scaled using the limits  $v_{min} = 0$  and  $v_{max} = v_{Nyq} / \cos \theta$ , to make the spectra comparable for different tracking angles. The dynamic range in decibels is given by the color bar. The white transparent lines mark the time period used when generating the power-velocity plots in Figs. 3.6 and 3.7(a).

error (3.14). The plot shows that the velocity resolution is highest and the peak power is largest for  $\theta = \theta_0$ .

In Fig. 3.5, velocity spectra generated from an *in vitro* recording of flow in a straight tube are shown. The 2-D tracking Doppler spectrum with the correct tracking trajectory angle ( $\theta = \theta_0 = 73^\circ$ ) seems to provide the highest contrast and velocity resolution. From this spectrum, it is observed that the flow has a slightly oscillating character around a center velocity of approximately 0.9 m/s. Broadening of the spectra is observed when using incorrect tracking angles. This is most evident for the spectrum with the largest tracking angle.

Figs. 3.6 and 3.7 show power-velocity plots from the *in vitro* recording, at times marked with vertical lines in Fig. 3.5, compared to those predicted using (3.9) and (3.13).

In Fig. 3.6, 2-D tracking Doppler spectra with  $\theta = \theta_0 = 73^\circ$  are compared with conventional PW Doppler spectra. The predicted spectra correspond well to the *in vitro* spectra, with some differences due to estimator variance. In addition to an improved velocity resolution, due to the more narrow spectral peaks, the 2-D tracking Doppler spectra have a signal-noise-ratio (SNR) that is about 9 dB higher than the conventional PW Doppler spectra.

In Fig. 3.7 a), 2-D tracking Doppler spectra generated from the *in vitro* recording using three different tracking trajectory angles are shown. Fig. 3.7 b), shows the corresponding velocity spectra predicted by (3.9). To be able to compare the spectra for different tracking angles, equation (3.11) was used to estimate the axial velocity

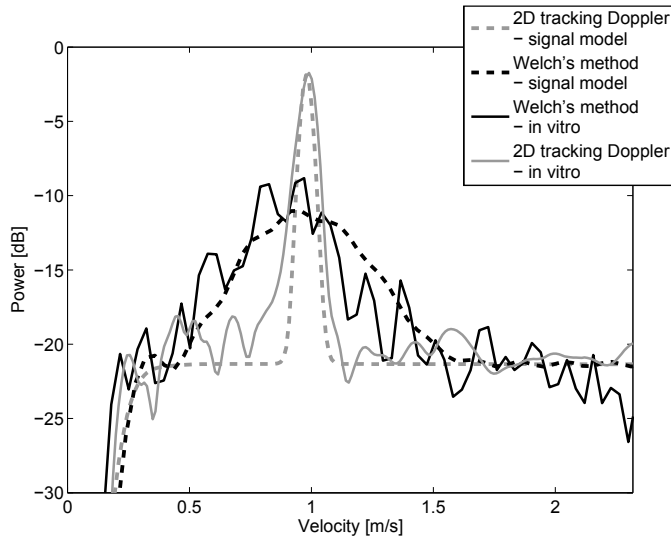


**Figure 3.6:** Velocity spectra generated from the *in vitro* recording and their corresponding predicted velocity spectra. Short time periods, marked with white vertical lines in Fig. 3.5, were averaged when generating the spectra. Only the 2-D tracking Doppler spectrum with  $\theta = \theta_0 = 73^\circ$  and the conventional spectrum are shown here. An increase in velocity resolution may be observed in the 2-D tracking Doppler spectra compared with the conventional PW Doppler spectra.

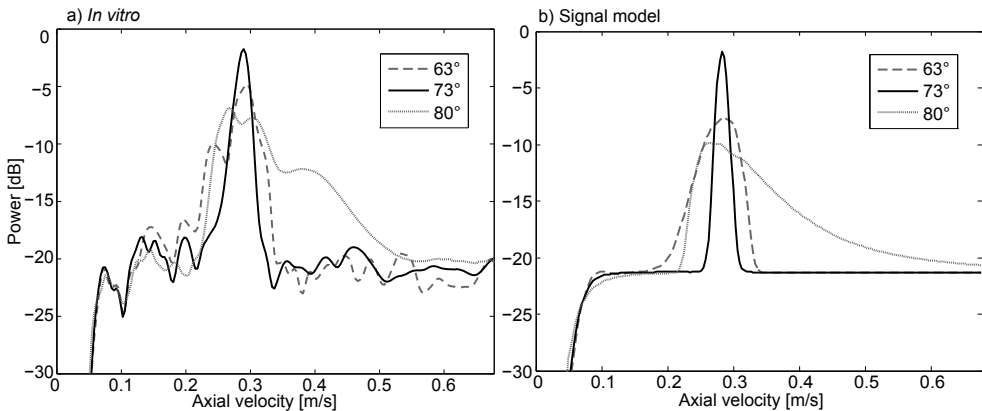


**Figure 3.7:** (a) Velocity spectra generated from the *in vitro* recording and (b) their corresponding predicted velocity spectra. Short time periods, marked with white transparent lines in Fig. 3.5, were averaged when generating the *in vitro* spectra. Eq. (3.11) was used to estimate the axial velocity component,  $v_z$ , of the flow. The highest velocity resolution is found when using the correct tracking angle.

component,  $v_z$ , of the flow. The spectra found using the correct tracking angle have the highest velocity resolution and the maximum power. The spectra with  $\theta = 63^\circ$  and  $\theta = 80^\circ$  seem to have a spectral leakage towards the low and the high velocity region respectively. The same trends are found in the predicted spectra as in the *in vitro* spectra, although the difference in maximum power is slightly larger in the predicted spectra.

### 3.4.3 Velocity Calibration

In Table 3.2, the mean values and the standard deviations of angle estimates using the minimum FWHM and the maximum power are given. The results show that the mean values of the angles estimated by the maximum power are closer to the angles measured from the B-mode images than the angles estimated by the minimum FWHM. However, the angles estimated by the minimum FWHM have lower standard deviations than the angles estimated by the maximum power.

**Table 3.2:** Results from the Velocity Calibration Analysis

	63°	73°	83°	Total error
Estimated angle by min. FWHM (°)	63.66 ± 1.05	72.78 ± 0.68	83.28 ± 0.35	0.24 ± 0.75
Velocity calibration error by min. FWHM (%)	2.46 ± 3.70	-1.1 ± 3.85	4.4 ± 5.61	1.92 ± 4.74
Estimated angle by max. power (°)	62.86 ± 2.06	73.10 ± 1.80	83.17 ± 0.37	0.04 ± 1.60
Velocity calibration error by max. power (%)	0.03 ± 7.07	1.55 ± 10.06	2.75 ± 5.63	1.44 ± 7.81

The circles in Fig. 3.8 give the velocity calibration errors in percent for 30 measurements when using the minimum FWHM for Doppler angle estimation. The two lines give the estimated maximum velocity calibration errors for the manual angle correction, given a  $\pm 3^\circ$  error in the chosen angle. For the investigated angles, the measured calibration errors for the 2-D tracking Doppler method are smaller than the maximum calibration errors for the conventional approach.

### 3.4.4 *In Vivo* Imaging

In Fig. 3.9, a conventional PW Doppler spectrum and two 2-D tracking Doppler spectra generated from an *in vivo* recording are shown. The recording was done on a patient with a moderate carotid stenosis. The 2-D tracking Doppler spectrum with

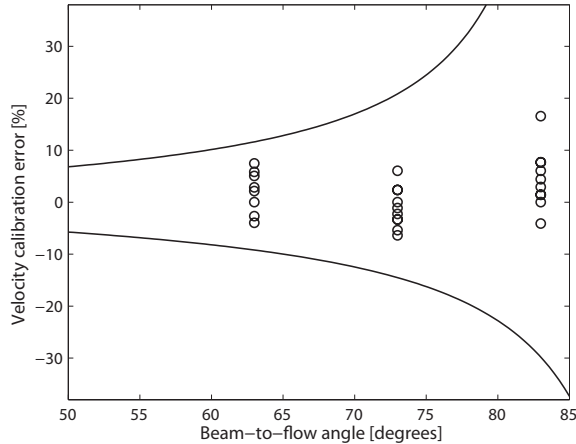


**Figure 3.8:** Experimental results using the 2-D tracking Doppler method for velocity calibration. The circles give the velocity calibration errors in percent for 30 measurements of *in vitro* flow. The Doppler angles used for velocity calibration were estimated by using the minimum FWHM of the velocity spectra. The two lines give the velocity calibration errors for the manual angle correction, given a  $\pm 3^\circ$  error in the chosen angle.

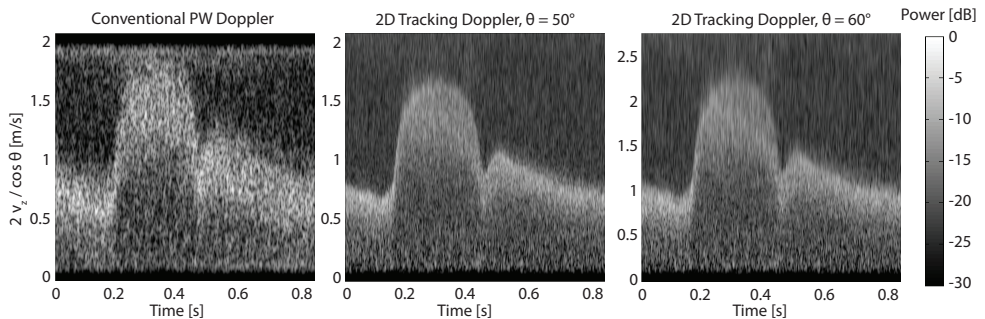


**Figure 3.9:** Velocity spectra generated from an *in vivo* recording of flow in a carotid artery at a stenotic region. The left spectrum is generated using a conventional PW Doppler method. The two rightmost spectra are generated by the 2-D tracking Doppler method, using tracking angles of  $50^\circ$  and  $60^\circ$ . The velocity axes are scaled using the limits  $v_{min} = 0$  and  $v_{max} = 2v_{Nyq} / \cos \theta$ , to make the spectra comparable for different tracking angles. A higher velocity resolution may be observed in the 2-D tracking Doppler spectrum with  $\theta = 50^\circ$ , compared with the 2-D tracking Doppler spectrum with  $\theta = 60^\circ$ . The dynamic range in decibels is given by the color bar.

$\theta = 50^\circ$  has a better velocity resolution than the 2-D tracking doppler spectrum with  $\theta = 60^\circ$ . By visual inspection, an estimate of the maximum velocity was found to be approximately 1.6 m/s when using the suggested spectral estimation technique, whereas an estimate of this parameter could not be extracted from the conventional PW Doppler spectrum.

### 3.5 Discussion

In this work, we have investigated properties of the 2-D tracking Doppler method when the tracking direction differs from the flow direction. A motivation for such a study is estimation of the beam-to-flow angle, which is essential for calibration of velocity spectra.

The 2-D tracking Doppler method was investigated for varying tracking angles using simulations, *in vitro* and *in vivo* experiments, focusing on situations with high beam-to-flow angles, where limitations in velocity estimation and calibration are most evident. It was shown that when applied to the same data, the 2-D tracking Doppler method reduced spectral broadening and increased the SNR compared with a conventional spectral estimation technique, and further, that it can give information about the beam-to-flow angle. The latter is possible because of relative broadening of the velocity spectrum at erroneous tracking angles.

An erroneous tracking trajectory results in summation of the signal along lines that extend through the side lobes of the point spread function, causing broadening of the velocity spectra. Spectral leakage toward the low- and the high-velocity region was observed for spectra with tracking angles that were too small or too large, respectively. This asymmetric behavior of the spectra may be due to the side lobes of the point spread function, because they are not symmetric around point 3 in Fig. 3.1.

The improved velocity resolution in the 2-D tracking Doppler spectra over conventional spectra is due to the increased transit time, especially at large beam-to-flow angles. When using a large tracking length in the 2-D tracking Doppler method, a long transit time is achieved and the transit time broadening is minimal. However, in complex flow fields, a shorter tracking distance is more appropriate, because the presence of velocity gradients will broaden the spectrum. A compromise in the tracking length must therefore be found. The suitable tracking length for the *in vivo* test case was based on apparent uniform flow in the color flow image, which was found to be approximately 1 cm. A longer tracking length was set for the more uniform *in vitro* flow. The temporal window length was reduced for high velocities because of the tracking distance limitation. Averaging in the flow direction could be done for low velocities, but at the cost of extra computational time. Because of the greater interest in high velocities for this examination, this was not deemed necessary.

Conventional power spectral estimation [(3.5) and (3.13)] was used as a reference in simulations, *in vitro* and *in vivo*. The poor spectral resolution of this approach, found especially in the *in vitro* comparison, is partly due to the large beam-to-flow angles. The effect is also enhanced by the short temporal excerpt of the flow, containing only small oscillations around the highest velocities of a sinusoidal waveform. These

oscillations were not resolvable by the conventional approach, resulting in a very poor representation of the power spectrum; however, the sinusoidal waveform would be recognizable in a longer temporal segment. The quality of the conventional spectra was also influenced by acquisition parameters, which were more suited for the tracking technique than regular spectral estimation. The short pulse length, which is preferable for tracking, limits the SNR, as will the use of unfocused transmit waves. However, the latter is required for tracking of lateral flow.

2-D tracking Doppler spectra were calculated for different tracking angles by using an extended version of the signal model applied in [5]. The predicted spectra showed good agreement with both the *in vitro* results and the spectra generated from the Field II simulated signal, although the signal model does not contain any restrictions on the size of the transmit aperture. An infinitely large plane wave is assumed and no edge effects are therefore present. Small differences between the spectra generated from the Field II simulated signal and the signal model may be observed in Fig. 3.3 because of estimator variance. It is assumed in the model that the blood flow is in the imaging plane. Presence of out-of-plane flow would shorten the effective tracking length and, hence, broaden the main lobe of the velocity spectrum.

The *in vitro* recordings were done on flow in a straight tube, where a near-parabolic flow profile was expected. The mid-point of the tracking trajectory was placed in the middle of the tube. An erroneous tracking angle was therefore expected to result in broadening toward lower velocities *in vitro*, compared with the spectra predicted using the signal model, for which an infinitely large blood vessel of uniform velocity was assumed. However, no significant difference between the *in vitro* spectra and the signal model spectra was found. This may be due to the short tracking lengths applied for the low velocities. Using the *in vitro* spectra generated with a tracking angle of  $63^\circ$  as an example, the radial distance,  $R$ , from the center of the tube can be calculated using the formula  $R = 0.5 \cdot N_w / PRF \cdot v \cdot \sin(10^\circ)$ . For  $v = 0.4$  m/s, this corresponds to a distance of 0.5 mm, which is much less than the tube radius.

Both the minimum FWHM and the maximum power of the spectra were investigated as candidates for Doppler angle estimation. Repeated measurements of *in vitro* flow were performed and the statistical analysis of the angle estimates (Table 3.2) showed that both methods could provide reliable estimates of the true flow angle, and could therefore be used for automatic angle correction of velocity spectra. However, the standard deviations of the velocity calibration errors were found to be larger for the maximum power method than the minimum FWHM. Also, if the technique is to be used as a guide for the examiner during an investigation, spectral broadening is the most attractive candidate because this may be easier to observe than changes in the SNR. The angles estimated by the minimum FWHM were somewhat biased for two of the investigated beam-to-flow angles. However, angles measured from B-mode images were used as a ground truth in the analysis. A possible inaccuracy in these measurements could explain the calculated bias in the angles estimated by the minimum FWHM.

In Fig. 3.8 the velocity calibration errors for the minimum spectral broadening method were compared with the velocity calibration errors for a conventional method. The results indicated that the 2-D tracking Doppler method gives better velocity

estimates than the conventional approach for large beam-to-flow angles, because all the velocity calibration errors for the 2-D tracking Doppler method were smaller than the velocity calibration errors resulting from a  $3^\circ$  erroneous Doppler angle. The validity of using  $\pm 3^\circ$  as a maximum angle error for the conventional approach can be investigated further in a more comprehensive study. In any case, the maximum velocity calibration errors of the conventional method increase rapidly for large beam-to-flow angles, whereas the estimated velocity calibration errors of the 2-D tracking Doppler method has a standard deviation of less than 6% for all the investigated angles. The increased robustness of the 2-D tracking Doppler method for large beam-to-flow angles may facilitate reliable velocity estimation for angles above  $60^\circ$ . This can improve blood velocity estimation in regions with near-transversal flow, for instance in vascular imaging or when imaging the heart from a parasternal view.

The results in Fig. 3.9 indicate that also *in vivo*, the 2-D tracking Doppler method gives better velocity resolution than the conventional PW Doppler method. The SNR is poor in all spectra, but the velocity-time waveform may be easier to delineate in the 2-D tracking Doppler spectra, because the clutter aliasing is overlapping with the high velocities in the conventional spectrum. This ability of the tracking technique to resolve the ambiguity problem, when the maximum velocity is beyond the Nyquist limit, has earlier been shown for blood flow in the axial direction [4]. The SNR is somewhat better in the conventional PW Doppler spectrum than in the 2-D tracking Doppler spectrum. This may be due to out-of-plane motion, because the sample point for the conventional PW Doppler method was placed near the source of the jet, and not in the middle of the tracking line. The 2-D tracking Doppler spectrum in Fig. 3.9 with  $\theta = 50^\circ$  has a better velocity resolution than the other spectra. In the 2-D tracking Doppler spectrum with  $\theta = 60^\circ$  the high velocities are blurred, suggesting that the tracking angle is incorrect.

Further studies will include a more comprehensive patient study for evaluation of the 2-D tracking Doppler method, with respect to both spectral estimation and calibration. As a ground truth for the beam-to-flow angle, the results could be compared with vector Doppler or speckle tracking estimates. A challenge *in vivo* is that spatial velocity gradients are expected to broaden the spectra, which may reduce the angle sensitivity of the technique. Also, the flow direction may vary through the heart cycle, and in regions of complex flow the accuracy of the angle estimation may be limited. However, in many applications the primary interest is the quantification of high velocity flow, for instance in cases of valvular insufficiency or in stenotic regions where flow of less complexity can be found, e.g., in the laminar vena contracta of the jet. In these situations, the 2-D tracking Doppler technique should be applicable, and might provide angle-corrected velocity spectra with significantly higher spectral resolution than the conventional approach.

## 3.6 Conclusion

We have investigated how the 2-D tracking Doppler method depends on the tracking angle. The results showed that the 2-D tracking Doppler method can provide PW

Doppler spectra with improved velocity resolution at large beam-to-flow angles, in addition to information about the Doppler angle. Using a signal model, it was shown that the spectra have lowest bandwidth and maximum power when the tracking angle is equal to the beam-to-flow angle. New techniques for velocity calibration were tested *in vitro*, showing improved performance for large beam-to-flow angles compared with a conventional technique. With an *in vivo* example, it was demonstrated that the method is suitable for vascular Doppler assessment.



# References

- [1] L. Wilson, “Description of broad-band pulsed doppler ultrasound processing using the two-dimensional fourier transform,” *Ultrasonic imaging*, vol. 13, no. 4, pp. 301–315, 1991.
- [2] P. M. Embree and W. T. Mayo, “Two dimensional processing of pulsed doppler signals,” June 5 1990. US Patent 4,930,513.
- [3] T. Loupas and R. W. Gill, “Multifrequency doppler: improving the quality of spectral estimation by making full use of the information present in the backscattered rf echoes,” *Ultrasonics, Ferroelectrics and Frequency Control, IEEE Transactions on*, vol. 41, no. 4, pp. 522–531, 1994.
- [4] H. Torp and K. Kristoffersen, “Velocity matched spectrum analysis: A new method for suppressing velocity ambiguity in pulsed-wave doppler,” *Ultrasound in medicine & biology*, vol. 21, no. 7, pp. 937–944, 1995.
- [5] T. D. Fredriksen, I. K. Ekroll, L. Lovstakken, and H. Torp, “2d tracking doppler: A new method to limit spectral broadening in pulsed wave doppler,” in *Ultrasonics Symposium (IUS), 2012 IEEE International*, pp. 334–337, IEEE, 2012.
- [6] C. Oates, A. Naylor, T. Hartshorne, S. Charles, T. Fail, K. Humphries, M. Aslam, and P. Khodabakhsh, “Joint recommendations for reporting carotid ultrasound investigations in the united kingdom,” *European Journal of Vascular and Endovascular Surgery*, vol. 37, no. 3, pp. 251–261, 2009.
- [7] B. Dunmire, K. Beach, K. Labs, M. Plett, and D. Strandness Jr, “Cross-beam vector doppler ultrasound for angle-independent velocity measurements,” *Ultrasound in medicine & biology*, vol. 26, no. 8, pp. 1213–1235, 2000.
- [8] P. Tortoli, G. Bambi, and S. Ricci, “Accurate doppler angle estimation for vector flow measurements,” *Ultrasonics, Ferroelectrics and Frequency Control, IEEE Transactions on*, vol. 53, no. 8, pp. 1425–1431, 2006.
- [9] S. Ricci, S. Diciotti, L. Francalanci, and P. Tortoli, “Accuracy and reproducibility of a novel dual-beam vector doppler method,” *Ultrasound in medicine & biology*, vol. 35, no. 5, pp. 829–838, 2009.

- 
- [10] J. M. Mari, M. Khoo, C. Riga, G. Coppola, C. Bicknell, and C. G. Caro, "Index proposal and basic estimator study for quantification of oscillation of the secondary flow pattern in tortuous vessels," *Ultrasonics*, vol. 52, no. 2, pp. 294–305, 2012.
- [11] J. Kortbek and J. A. Jensen, "Estimation of velocity vector angles using the directional cross-correlation method," *Ultrasonics, Ferroelectrics and Frequency Control, IEEE Transactions on*, vol. 53, no. 11, pp. 2036–2049, 2006.
- [12] J. A. Jensen and N. Oddershede, "Estimation of velocity vectors in synthetic aperture ultrasound imaging," *Medical Imaging, IEEE Transactions on*, vol. 25, no. 12, pp. 1637–1644, 2006.
- [13] V. L. Newhouse, E. Furgason, G. Johnson, and D. Wolf, "The dependence of ultrasound doppler bandwidth on beam geometry," *Sonics and Ultrasonics, IEEE Transactions on*, vol. 27, no. 2, pp. 50–59, 1980.
- [14] V. L. Newhouse, D. Censor, T. Vontz, J. A. Cisneros, and B. B. Goldberg, "Ultrasound doppler probing of flows transverse with respect to beam axis," *Biomedical Engineering, IEEE Transactions on*, no. 10, pp. 779–789, 1987.
- [15] V. Newhouse, K. Dickerson, D. Cathignol, and J.-Y. Chapelon, "Three-dimensional vector flow estimation using two transducers and spectral width," *Ultrasonics, Ferroelectrics and Frequency Control, IEEE Transactions on*, vol. 41, no. 1, pp. 90–95, 1994.
- [16] P. Tortoli, G. Guidi, and C. Atzeni, "A review of experimental transverse doppler studies," *Ultrasonics, Ferroelectrics and Frequency Control, IEEE Transactions on*, vol. 41, no. 1, pp. 84–89, 1994.
- [17] C.-K. Yeh and P.-C. Li, "Doppler angle estimation using ar modeling," *Ultrasonics, Ferroelectrics and Frequency Control, IEEE Transactions on*, vol. 49, no. 6, pp. 683–692, 2002.
- [18] P.-L. Lee, Y.-H. Chou, J.-C. Hsieh, and H. K. Chiang, "An improved spectral width doppler method for estimating doppler angles in flows with existence of velocity gradients," *Ultrasound in medicine & biology*, vol. 32, no. 8, pp. 1229–1245, 2006.
- [19] J. A. Jensen, "Field: A program for simulating ultrasound systems," in *10TH NORDIC/BALTIC CONFERENCE ON BIOMEDICAL IMAGING, VOL. 4, SUPPLEMENT 1, PART 1: 351–353*, Citeseer, 1996.
- [20] K. V. Ramnarine, D. K. Nassiri, P. R. Hoskins, and J. Lubbers, "Validation of a new blood-mimicking fluid for use in doppler flow test objects," *Ultrasound in medicine & biology*, vol. 24, no. 3, pp. 451–459, 1998.

## Chapter 4

# 2-D tracking Doppler for Cardiac Jet Flow Velocity Estimation

Jørgen Avdal<sup>1,2</sup>, Ingvild K. Ekroll<sup>2,3</sup>, Thomas Skaug<sup>2,4</sup>, Lasse Løvestakken<sup>1,2</sup>, and Hans Torp<sup>1,2</sup>

<sup>1</sup> MI Lab, <sup>2</sup> Dept. of Circulation and Medical Imaging, NTNU, Norway

<sup>3</sup> St. Olav's University Hospital, Trondheim, Norway

<sup>4</sup> Dept. of Cardiology, St. Olav's University Hospital, Trondheim, Norway

The maximum velocity of jet flow through an insufficient heart valve provides important information on the pressure gradient, and is usually measured by continuous wave Doppler. With this method, correct estimation of the maximum velocity relies on a small ( $< 20^\circ$ ) beam-to-flow angle. 2-D tracking Doppler is a recently proposed method which has been shown to produce robust estimates of blood velocities even at high ( $50^\circ$ - $80^\circ$ ) beam-to-flow angles, and can also partially suppress the effects of aliasing. The method reduces transit-time broadening by sampling and summing the received signal along the trajectory of the blood scatterers. In this study, the tracking Doppler technique is further investigated for use in cardiac applications using phased array plane wave imaging. A new simulation model is presented, accounting for spatial variations in the point spread function. Simulating flow with a maximum velocity of 4 m/s, and using a -6dB threshold, the spectral broadening when utilizing tracking Doppler is predicted to be less than 1 % for beam-to-flow angles between 0 and 60 deg, clearly outperforming PW Doppler and being comparable to CW Doppler with  $0^\circ$  beam-to-flow angle. Additionally, the maximum spectral amplitude was found when the tracking is performed in the flow direction, indicating the potential for automatic angle correction. A tracking Doppler sequence was implemented on a modified GE Vivid E9 scanner (GE Vingmed, Horten, Norway), and the model was validated using an *in vitro* measurement. Feasibility of using the method for determination of maximum flow velocity in an aortic insufficiency was shown.

### 4.1 Introduction

The maximum velocity in cardiac jet flow is an important parameter in the diagnosis of heart disease. Together with the simplified Bernoulli equation  $\Delta P = 4v^2$  [1], the maximum flow velocity provides an estimate of the peak pressure gradient across septal defects and stenotic or insufficient heart valves, and is for instance used to assess

the severity of valvular stenosis. Another example is the pulmonary artery systolic pressure, which may be estimated from the velocity of tricuspid regurgitations [2]. Delineation of the maximum velocity in the Doppler spectrum is used for estimation of the velocity-time integral (VTI). The VTI, measured at the mitral annulus or the left ventricular outflow tract, multiplied with the corresponding cross-sectional area provides an estimate of stroke volume [3]. Importantly, in aortic stenosis, the aortic valve area can be calculated based on the equation of continuity, using a VTI of the stenotic jet by CW Doppler together with stroke volume measurements [4]. Maximal velocities are also used for estimation of the pressure half-time (PHT). In mitral stenosis, the PHT can easily be measured from the apical window and is related to the mitral valve area [5]. In aortic regurgitation the aorto-ventricular PHT reflects both the degree of regurgitation and left ventricular end-diastolic pressure [6].

In severe aortic stenosis velocities may exceed 4 m/s [7] and in mitral and aortic regurgitation the velocities usually reach 4 - 6 m/s [8,9], which would lead to aliasing if measured by pulsed wave (PW) Doppler. The use of CW Doppler ensures that no such aliasing of the maximal velocities occur, but the modality has some limitations. For example, it has no spatial resolution. In addition, when using CW Doppler, a good spectral velocity estimate depends on a small beam-to-flow angle. Angle correction is not recommended due to difficulties in estimating the correct Doppler angle needed for velocity calibration. Larger beam-to-flow angles also lead to increased spectral broadening due to the decreased transit time, resulting in overestimation of the peak velocities. These imaging requirements may lead to prolonged examination times as it is difficult to locate a proper view in certain patients [10]. Especially for aortic stenosis it is recommended to use CW Doppler with multiple acoustic windows to detect the highest velocities. [7].

Compared to CW Doppler, PW Doppler is more susceptible to spectral broadening and aliasing problems, due to the smaller sample volume and the limited velocity range implied when using a pulsed sequence. However, some methods have been proposed with potential to reduce the severity of these problems. In the multifrequency Doppler technique [11], Doppler spectra are generated from several ultrasound frequencies transmitted simultaneously and then averaged to reduce the variance of the spectral estimates. In the velocity matched spectrum technique [12], the sample volume followed the scatterers in the axial direction over time, reducing spectral broadening for small beam-to-flow angles. It was also shown that the latter technique could reduce the effects of aliasing, and an example was shown in which velocities as high as 4.5 times the Nyquist limit were measured. An analysis in the 2-D Fourier domain shows that these two techniques share many of the same properties [13].

Two-dimensional (2-D) tracking Doppler is a recently proposed extension of the velocity matched spectrum technique, in which the observation window follows the trajectory of the blood scatterers in both axial and lateral directions to increase transit time and thus reduce spectral broadening. By using plane waves on transmit and parallel receive beams, the signal from a moving scatterer may be tracked by using spatial interpolation for each time instance. In [14] it was shown that the use of the method for spectral velocity estimation in the carotid artery resulted in a significant reduction in spectral broadening compared with conventional PW Doppler. In [15],

the dependency of the method on the tracking angle was investigated, and it was shown that the estimated velocity spectra had lowest bandwidth and highest amplitude when the tracking angle coincided with the beam-to-flow angle. These quantities could potentially be used for automatic angle correction. Also, because the tracking Doppler method acquires data from a large spatial region, color Doppler images may be generated from the same data.

The potential ability of the tracking Doppler method to accurately measure high velocities at a wide range of beam-to-flow angles motivates this study of the performance of the method for measurement of jet flow velocities in the heart. Adaptation of the tracking Doppler technique to cardiac applications, however, presents several potential challenges. Compared with velocity estimation in the carotid artery using a linear probe, a cardiac probe has smaller aperture and the region of interest is deeper. This leads to higher F-numbers for receive focusing, and thus decreased spatial resolution, which may affect the dependency of the tracking Doppler spectra on the tracking angle. Diffraction effects may lead to non-uniform beam profiles in depths of interest, which may cause spectral broadening or artifacts in the spectra. In addition, the smaller width of plane waves emitted from a cardiac probe potentially limits the size of the tracking region for high velocities.

The aim of this work is to investigate the properties of the 2-D tracking method using phased arrays for measurement of cardiac jet flow velocities with non-zero beam-to-flow angles, using a signal model and simulations as well as *in vitro* and *in vivo* measurements. Specifically, we want to quantify the spectral broadening properties for different beam-to-flow angles, and investigate the potential for automatic angle correction by quantifying the dependencies of the spectral bandwidth and amplitude on the tracking angle. The work is a continuation of [14] and [15], where these properties were quantified for vascular applications using a linear probe. A new model is presented in this work to allow for a spatially variant point spread function. The results are validated using an *in vitro* measurement, and feasibility of applying the 2-D tracking Doppler technique *in vivo* is shown by using it to measure the maximum blood velocity in an aortic insufficiency.

## 4.2 Methods

### 4.2.1 Doppler processing

For conventional PW Doppler, the axial velocities are estimated by performing a temporal Fourier transform of the ultrasound signal from a fixed spatial position [14].

$$\hat{p}^c(v) = \left| \sum_k w(k) S(\vec{r}_0, k_0 + k) e^{-2i\omega_0 k v_z \Delta t / c} \right|^2. \quad (4.1)$$

Here  $w$  is a window function,  $S(\vec{r}, k)$  is the IQ demodulated ultrasound signal,  $\vec{r}_0$  is spatial position,  $k$  is the slow-time index,  $\omega_0$  is the received signal center frequency,  $\Delta t$  is the pulse repetition time,  $c$  is the speed of sound,  $v_z = v \cos \alpha$ ,  $v$  is the velocity and

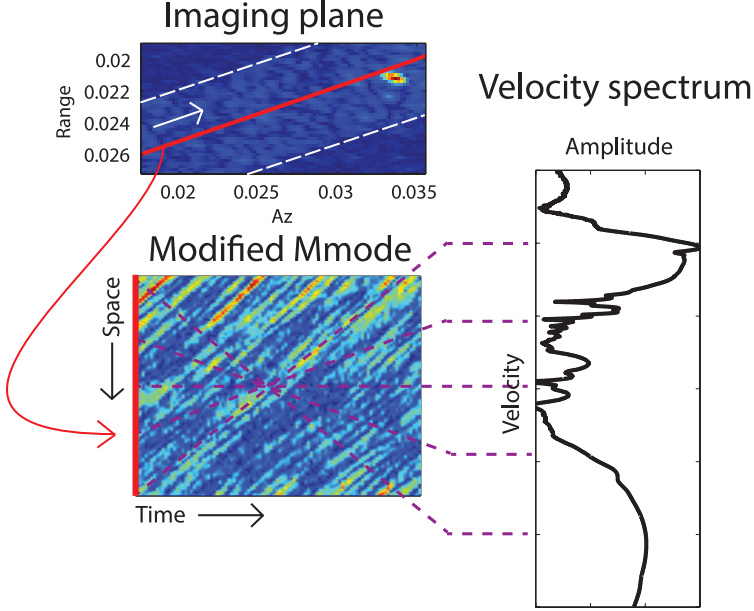


**Figure 4.1:** Illustration of the signal summation performed for generation of tracking Doppler spectra. For each slow-time frame, the signal is sampled from a spatial line, indicated in red. Then for each velocity, the spectral amplitude of that velocity is estimated by summation along skewed lines in the 2-D domain consisting of space and slow-time.

$\alpha$  is the assumed beam-to-flow angle. For 2-D tracking Doppler, the signal is summed along the assumed trajectory  $T$  of the scatterers [14]:

$$\hat{p}(v) = \left| \sum_k w(k) S(\vec{r}_0 + kv\Delta t \vec{e}_T, k_0 + k) e^{-2i\omega_0 kv_z \Delta t / c} \right|^2, \quad (4.2)$$

where  $\vec{e}_T$  is a unit vector in the tracking direction. The summation performed to produce tracking Doppler spectra is illustrated in Fig. 4.1. In the 2-D Fourier domain, this corresponds to summation along skewed lines, each with an angle corresponding to the velocity  $v$ , see Fig. 4.2. The figure also shows that, in comparison, conventional PW Doppler corresponds to projecting the Doppler signal in the 2D Fourier domain down on the Doppler frequency axis.

## 4.2.2 Signal model

In the signal model, it is assumed that the spatial correlation length of blood scatterers is much shorter than the wavelength of the transmitted signal [16]. Let  $h_F(\vec{r}, t)$  be the

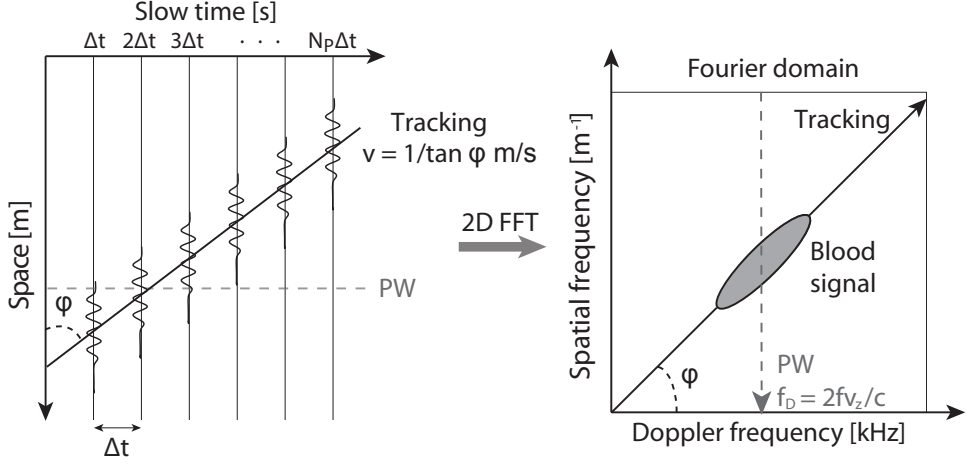


**Figure 4.2:** Comparison of PW Doppler and Tracking Doppler in spatial and Fourier domains. In tracking Doppler, the summation in space and slow-time corresponds to a summation along a skewed line through the origin in 2-D Fourier space, with tilt angle  $\varphi$  depending on the tracking velocity as shown. For PW Doppler, the signal contribution comes from a fixed spatial position, corresponding to a projection down on the Doppler frequency axis in 2-D Fourier space.

IQ demodulated signal from a single scatterer moving along a flow line  $F$ . The signal contribution  $S_F$  from  $F$  is obtained by summation of the signal from all scatterers along  $F$ :

$$S_F(\vec{r}, k) = \sum_n a_n h_F(\vec{r}, t_n + k\Delta t), \quad (4.3)$$

where  $a_n$  is an amplitude scaling factor and  $t_n$  is the time lag of scatterer number  $n$ . Because the scatterers in blood are  $\delta$ -correlated in space by assumption, the expected power spectrum when tracking along the line  $T$  from scatterers moving along  $F$  becomes:

$$\langle p_F(v) \rangle = \langle a \rangle \int_t \left| \sum_k w(k) h_F(\vec{r}_0 + kv\Delta t \vec{e}_T, t + k\Delta t) e^{-2i\omega_0 kv_z \Delta t/c} \right|^2 dt, \quad (4.4)$$

where  $\vec{r}_0$  is the center of the sample volume and  $a = \sum_n a_n^2$ . The corresponding expression for conventional PW Doppler is:

$$\langle p_F^c(v) \rangle = \langle a \rangle \int_t \left| \sum_k w(k) h_F(\vec{r}_0, t + k\Delta t) e^{-2i\omega_0 kv_z \Delta t/c} \right|^2 dt, \quad (4.5)$$

Again, based on the assumed  $\delta$ -correlation in space for blood scatterers, the expected total power spectrum is found by summing the power spectra from each flow line.

### 4.2.3 Simulations

The signals  $h_F$  were calculated using the simulation software Field II [17, 18]. For a flow line  $F$ , point spread functions  $f(\vec{r}|\vec{r}_n)$  were calculated for scatterers at spatial positions  $\vec{r}_n \in F$ , sufficiently dense to produce  $f(\vec{r}|\vec{r}_f)$  for a scatterer at any point  $r_f \in F$  by interpolation. The signal  $h_F$  could then be obtained for any velocity profile along  $F$ , using the relation:

$$h_F(\vec{r}, t) = f(\vec{r}|\vec{r}_f(t)), \quad (4.6)$$

where the velocity profile is given implicitly by  $\vec{r}_f(t)$ . The relation between the simulation model parameters is illustrated in Fig. 4.3.

The described model provides the statistically expected velocity spectrum rather than a realization of the signal. A good estimate of the spectrum could also be obtained by simulation of long ensembles with high scatterer density, but the chosen method was preferred as it is faster and also has no variance except due to numerical error.

For simulation of Doppler signals used for tracking Doppler and PW Doppler, plane waves were used on transmit. CW Doppler acquisition was simulated in Field II as a PW Doppler using half of the aperture on transmit and the other half on receive, using fixed focus, long pulse length and pulse repetition frequency (PRF) high enough to avoid aliasing, see Table 4.1 for details. The resulting signal then has spatial sensitivity and temporal frequency content similar to that of a CW Doppler signal after IQ demodulation.

### 4.2.4 Spectral broadening

The spectral broadening properties of the 2-D tracking Doppler method were quantified by simulating a typical flow pattern for a cardiac jet. The Computational Fluid Dynamics (CFD) simulation software ANSYS Fluent (ANSYS Inc, Canonsburg, PA, USA) was used to simulate a jet from a 5 mm opening. Two cylindrical chambers with diameter 20 cm and lengths 10 cm and 30 cm were connected by a cylindrical hole with diameter 5 mm and length 3 mm, and pressure was applied uniformly across the cross-section of the first chamber. The flow field and velocity profile are shown in Fig. 4.4. In this analysis, only the contribution from the central flow line was included.

The signals  $h_F$  were calculated, as described in 4.2.2, for the central flow line, with beam-to-flow angles between  $0^\circ$  and  $80^\circ$ . For each beam-to-flow angle, the expected power spectra for conventional PW Doppler, CW Doppler and tracking Doppler when tracking along  $F$  were calculated using (4.4) and (4.5). See Table 4.1 for simulation setup parameters. To estimate the spectral broadening properties, we used the half-power threshold, which is the velocity with power equal to half the maximum power in the descending slope located at the higher frequencies of the spectrum. This measure is used as an estimate for the maximal velocity in a method described by Ricci *et al* [19]. For our purposes we note that the value of the estimator increases with increasing

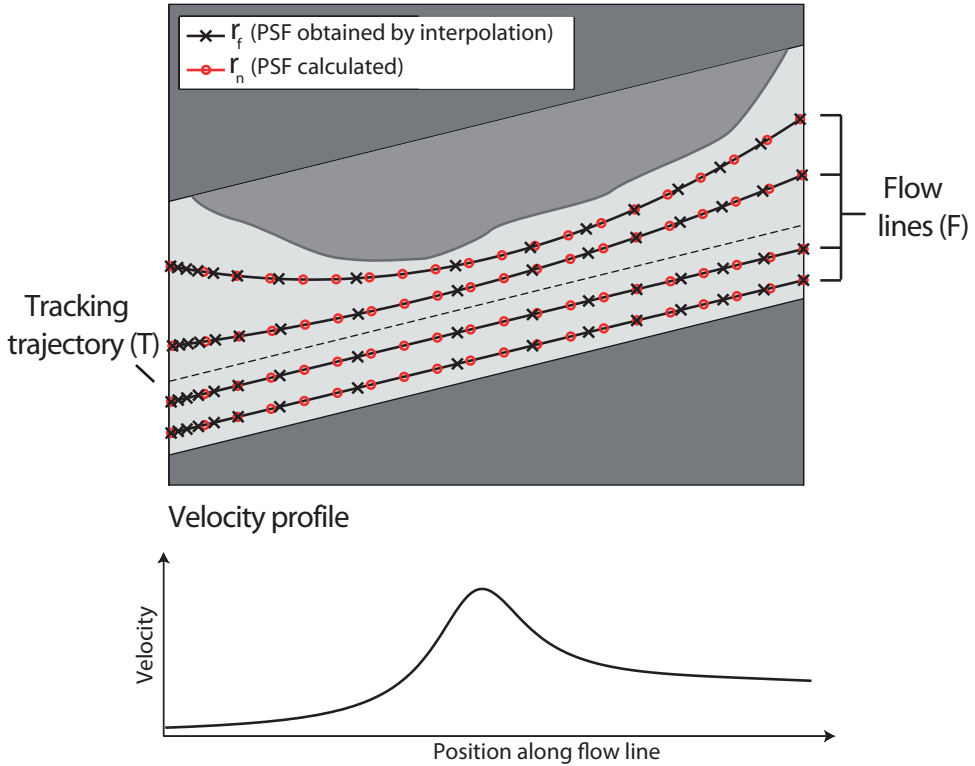


**Figure 4.3:** Illustration of the relation between the parameters used to estimate  $h_F$  in (4.6), using the simulation model. For each flow line  $F$ , the velocity profile is used to calculate the locations  $r_f$  of a scatterer at the insonation times. Point spread functions (PSF) are then calculated from scatterers at positions  $\vec{r}_n \in F$  using Field II, and interpolated to produce the point spread functions at positions  $r_f$ . Note that each flow line may have different velocity profiles.

bandwidth of the spectrum, and the bias of the estimator was used as a measure of spectral broadening.

#### 4.2.5 Transmit apodization

Using a rectangular window for transmit window results in a non-uniform beam profile due to diffraction. However, apodization may be used to obtain more homogeneous fields from the emitted plane waves in the depth range of interest (5-10 cm). The spectral broadening properties of tracking Doppler were therefore also quantified when using a Hann window, a Tukey window with taper ratio 0.45, and rectangular window on transmit.

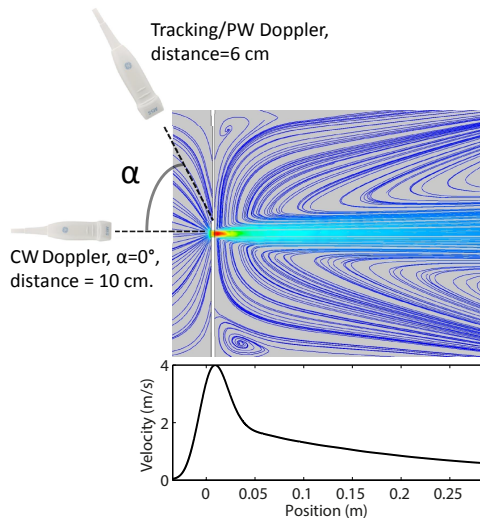


**Figure 4.4:** Illustration of imaging setup used in simulations. The flow profile shown in the lower panel was extracted from the ANSYS Fluent simulation and used as input to Field II simulations when calculating expected velocity spectra.

Parameter	Tracking	PW	CW
Probe type	Phased	Phased	Phased
Elements used on transmit	96	96	48
Pitch [ $\mu\text{m}$ ]	229	229	229
TxFrequency $f_0$ [MHz]	2	2	2
PRF [kHz]	10	10	40
Cycles @ $f_0$	1.5	6.5	200
Receive $F\#$	2.7	2.7	5.4
Ensemble length	100	100	400

**Table 4.1:** Parameters used in single flow line (jet) simulations.

#### 4.2.6 Dependency of tracking angle

The angle dependency of tracking Doppler when using a phased array probe was investigated using a simulation model of flow in a straight tube with 4 mm diameter. The point spread function was assumed to be invariant in the beam axis direction inside the tube, and separable in axial and elevation directions. The elevation amplitude profile was calculated using Field II. The signals  $h_F$  were then estimated for flow lines in a grid with resolution 0.08 mm inside the tube. Each flow line had constant velocity chosen such that the flow profile of the tube was parabolic with maximum velocity 2 m/s. Expected velocity spectra were calculated for each flow line and then summed

Parameter	Tracking/PW
Probe type	Phased
Elements used on transmit	96
Pitch [ $\mu\text{m}$ ]	229
TxFrequency $f_0$ [MHz]	2.1
PRF [kHz]	6.7
Cycles @ $f_0$	2.5
Receive $F_{\#}$	2.7
Ensemble length	73

**Table 4.2:** Parameters used in straight tube simulation.

to obtain the expected velocity spectrum for a tracking trajectory through the center of the tube. See Table 4.2 for setup parameters.

The simulated tube had a beam-to-flow angle of  $71^\circ$  and a depth of 6 cm. Tracking Doppler was performed with tracking angles between  $-80^\circ$  and  $80^\circ$ . The maximum amplitude in the spectrum, the half-power (-6 dB) and quarter power (-12 dB) thresholds were calculated for each tracking angle.

#### 4.2.7 In vitro validation

A flow phantom experiment was performed to validate the signal model. The phantom consisted of a silicon tube with an inner diameter of 4 mm, connected to a flow loop driven by a PhysioPulse 100 Flow System (Shelley Medical Imaging Technologies, London, ON, Canada). The flow system was set to output constant flow with a velocity of about 2 m/s, as measured by a CW Doppler measurement with a beam-to-flow angle of  $24^\circ$ . The probe was placed approximately 6 cm from the center of the tube, and tilted to obtain a beam-to-flow angle of approximately  $71^\circ$ .

The phantom was insonated using plane wave transmissions from a modified GE Vivid E9 scanner (GE Vingmed, Horten, Norway). Channel data were extracted from a depth range of 4.5 cm – 8.5 cm and beamformed offline, before performing the Doppler analysis using (4.1) and (4.2). The setup parameters are detailed in Table 4.3. Welch’s method was used to generate line spectra, using a window length of 73 samples (6 ms), and an window overlap of 69 samples (95 %). A temporal average of 60 spectrum estimates were used to generate the final line spectra. Clutter rejection was performed using a FIR filter with order 132 and -3 dB cutoff at 0.11 m/s.

#### 4.2.8 In vivo measurements

*In vivo* data were also acquired from aortic flow in a volunteer with a mild aortic insufficiency. The setup parameters are provided in Table 4.3. A CW Doppler recording from the apical position acquired by an experienced cardiologist was used as a ground truth measurement. Multiple recordings using plane waves were then

Parameter	In vitro	In vivo
Probe type	Phased	Phased
TxFrequency $f_0$ [MHz]	2.1	2.1
PRF [kHz]	6.7	12.1
Cycles @ $f_0$	2.5	2.5
Receive $F_{\#}$	2.7	3.8
Ensemble length	73	73

**Table 4.3:** Parameters used for *in vitro* and *in vivo* measurements.

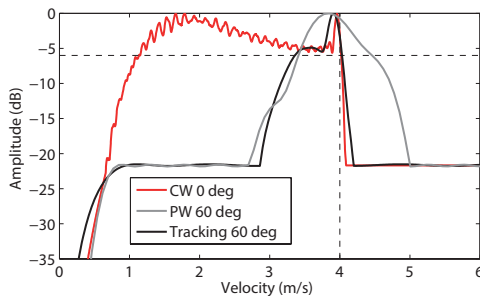


**Figure 4.5:** Simulated spectra from jet flow using CW Doppler with flow in the beam direction, and from PW Doppler and tracking Doppler with beam-to-flow angle  $60^\circ$ . The maximum velocity and the half power (-6 dB) threshold are illustrated.

made from different views before performing the Doppler analysis offline. Due to limitations in data storage capacity, only about 600 ms of data were available for each recording. Additionally, navigation had to be performed on B-mode images only during the experiment, as the modification did not allow for simultaneous color flow imaging. Tracking Doppler spectra were averaged over several tracking lines spanning a depth range of 2 cm. PW Doppler spectra were produced from the same data as tracking Doppler, and were averaged over a region of size 4 cm x 2 cm.

## 4.3 Results

### 4.3.1 Simulation results

Fig. 4.5 shows the simulated spectra for CW Doppler, PW Doppler and tracking Doppler for a single flow line with jet flow profile and maximum velocity 4 m/s. The beam-to-flow angle was  $\alpha = 60^\circ$  for PW and tracking Doppler, and  $\alpha = 0^\circ$  for CW Doppler. Using a -6dB threshold, the overestimation of the maximum velocity is approximately 1% both for CW and tracking Doppler and 10% for PW Doppler.

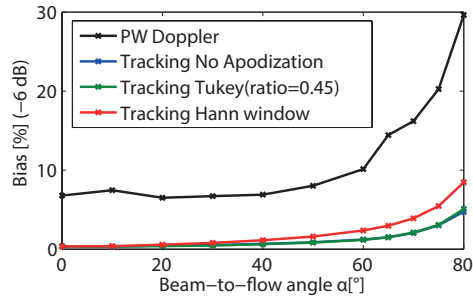


**Figure 4.6:** Bias in the maximum velocity using the half-power (-6 dB) threshold, as a function of beam-to-flow angle, for PW Doppler and tracking Doppler with three different transmit apodizations. Tracking is performed in the flow direction.

### 4.3.2 Spectral broadening vs beam-to-flow angle

The dependence between spectral broadening and beam-to-flow angle is shown in Figure 4.6, for 2-D tracking Doppler and PW Doppler. For the results shown, the scatterers are tracked along the true angle. The results show that tracking Doppler significantly reduces spectral broadening compared to PW Doppler, by a factor of more than six for all beam-to-flow angles between  $0^\circ$  and  $80^\circ$ . For a beam-to-flow angle of  $80^\circ$ , the spectral broadening is approximately 5% for tracking Doppler and 30% for PW Doppler.

### 4.3.3 Transmit apodization

Also included in Figure 4.6 is the impact of using plane waves with transmit apodization on spectral broadening. The results show that the use of a Tukey window with taper ratio 0.45 slightly increases spectral broadening, whereas the use of a Hann window substantially increases spectral broadening, especially for high beam-to-flow angles. Fig. 4.7 shows beam profiles at depth 6 cm for different transmit apodizations. It can be seen that the use of a Tukey window results in a more homogeneous field, but also a narrower beam, whereas the use of a Hann window significantly reduces the beam width.

### 4.3.4 In vitro validation

In Fig. 4.8 spectra from the flow phantom are compared with those predicted by the signal model. By visual inspection, there is good correspondence between the model predictions and the *in vitro* results.

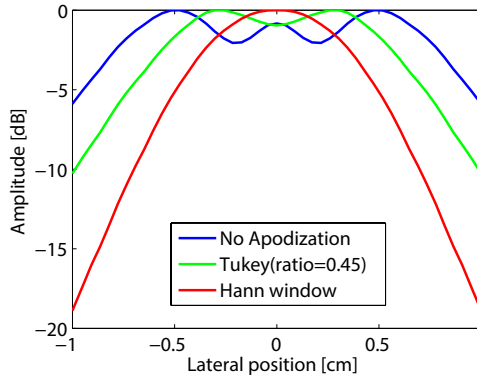


**Figure 4.7:** Beam profiles at depth 6 cm when using no transmit apodization, a tukey window with taper ratio 0.45, and a Hann window.

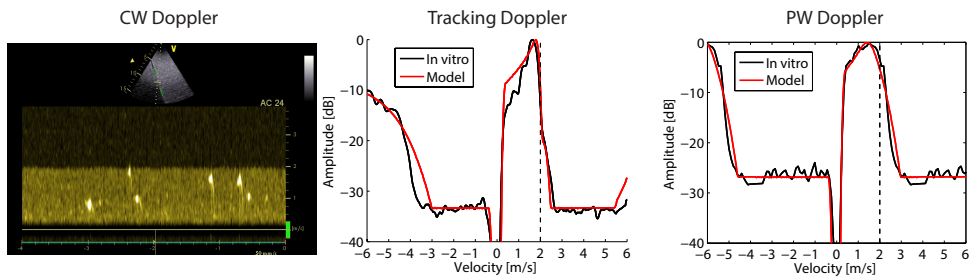


**Figure 4.8:** A comparison of in vitro measurement and model predictions. Left: Ground truth measurement using angle corrected CW Doppler spectrum with beam-to-flow angle  $24^\circ$ , showing a maximum velocity of 2 m/s. Middle: tracking Doppler spectra when tracking with beam-to-flow angle  $71^\circ$ . Right: angle corrected PW Doppler spectra with beam-to-flow angle  $71^\circ$ .

### 4.3.5 Variation with tracking angle

The left panel of Fig. 4.9 shows the maximum amplitude of the spectrum as a function of tracking angle, for simulated and *in vitro* flow in a straight tube with a beam-to-flow angle of  $71^\circ$ . The maximum amplitude is attained at the correct tracking angle. The results in the right panel of Fig. 4.9 show that, for this setup, the -6 dB and -12 dB threshold velocities, which are indicators of spectral broadening, of the model spectra and *in vitro* spectra are minimal (before angle correction) for tracking angles of  $69^\circ - 70^\circ$ . Using a tracking angle of  $69^\circ$  when the true value is  $71^\circ$  would contribute to a decrease in the estimated maximum velocity of about 9%.

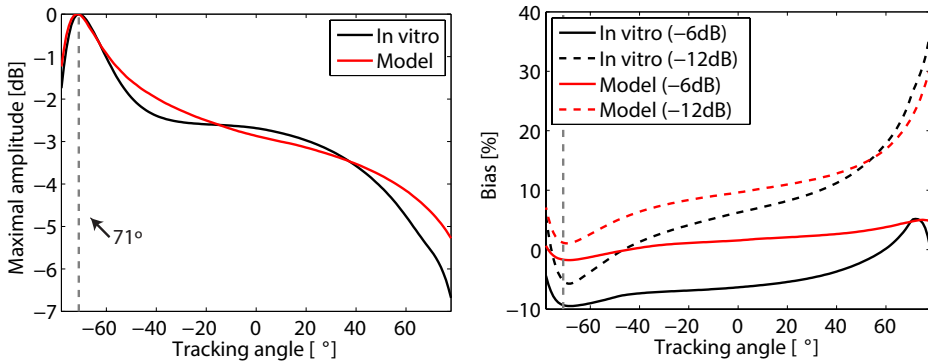


**Figure 4.9:** Candidate parameters for automatic angle correction, as a function of tracking angle. The beam-to-flow angle is  $71^\circ$ . Left: the maximum amplitude in spectrum as function of tracking angle. Right: the bias in the maximum velocity estimate as function of tracking angle, using the half power (-6 dB) and quarter power (-12 dB) thresholds.

### 4.3.6 In vivo results

*In vivo* spectra showing blood flow in a volunteer with a mild aortic insufficiency are shown in Fig. 4.10, for PW Doppler, tracking Doppler and conventional CW Doppler. Automatic angle correction was not attempted in these recordings because of movement of the jet during the heart cycle, which would require a more sophisticated algorithm. Instead the tracking angles were estimated from retrospective color flow images, shown in the left panel.

In the tracking Doppler spectrum from an apical view with a beam-to-flow angle of  $30^\circ$ , it is possible to delineate the maximum velocities, and the results are comparable to the CW Doppler measurements used as ground truth. It is also seen that tracking Doppler overcomes the Nyquist limitations seen in the corresponding PW Doppler spectrum, where delineation of the maximum velocities is difficult because of aliased clutter noise.

## 4.4 Discussion

Properties of the 2-D tracking Doppler technique using a cardiac probe have been investigated using simulations, *in vitro* and *in vivo* measurements. The results show that even though the cardiac probe has smaller aperture and the tracking regions are located deeper than in vascular imaging, the tracking Doppler method still outperforms PW Doppler in terms of spectral broadening at all investigated beam-to-flow angles.

The dependency of spectral broadening on the beam-to-flow angle was investigated in Fig. 4.6, both for PW Doppler and tracking Doppler. It is clear from the results that spectral broadening increases with beam-to-flow angle, and that this effect becomes

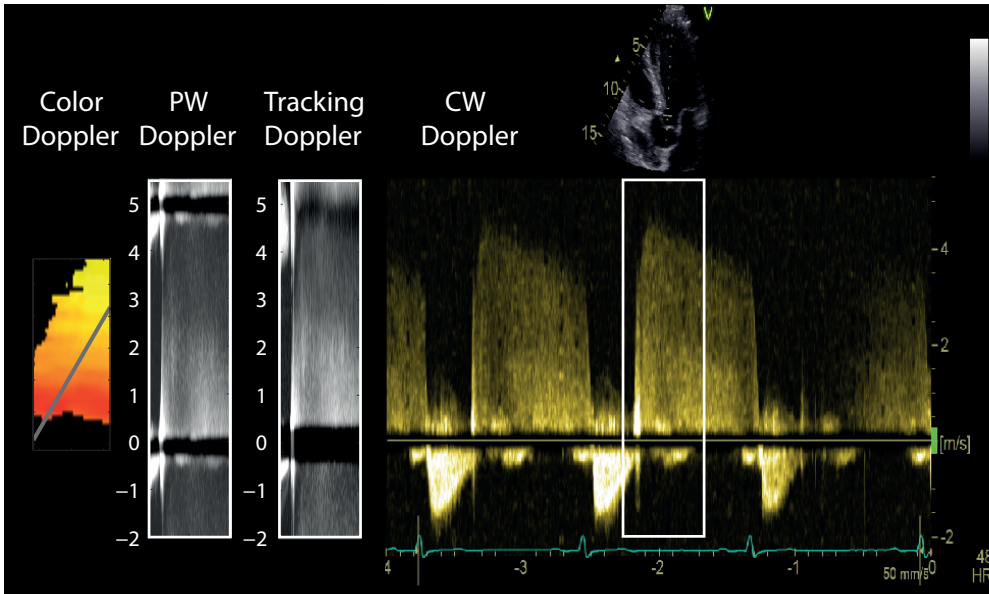


**Figure 4.10:** In vivo spectra generated using Tracking Doppler and CW Doppler. Tracking Doppler and angle corrected PW Doppler from an apical view with beam-to-flow angle of approximately  $30^\circ$ . The axes of the tracking Doppler and PW Doppler results has been scaled to match those of the CW Doppler image, and a corresponding part of the heart cycle has been highlighted in the CW Doppler spectrum. A color Doppler image including the tracking angle is shown. The dynamic range of the tracking and PW Doppler spectra is 40 dB.

increasingly important for beam-to-flow angles above  $60^\circ$ . For PW Doppler, the spectral broadening increases from 10% at  $60^\circ$  to 30% at  $80^\circ$ , which would not be acceptable for pressure gradient measurements. For tracking Doppler, however, the bias at  $80^\circ$  beam-to-flow angle is about 5%, corresponding to pressure gradient error of 10%. In fact, for beam-to-flow angles up to  $60^\circ$ , the tracking Doppler spectra are comparable to those produced by CW Doppler with a beam-to-flow angle of  $0^\circ$ . Thus, for tracking Doppler, the primary source of velocity estimation error is likely to be the determination of the correct beam-to-flow angle rather than spectral broadening. This is further discussed below.

Due to diffraction effects, the field from the emitted plane wave will not be homogeneous, an effect which is more prominent in cardiac imaging due to the small aperture size. This effect may be mitigated by using transmit apodization, as this reduces diffraction effects from the edges of the aperture. However, the results in Fig. 4.6 show that transmit apodization yields no positive effect on spectral broadening. Indeed, a significant increase in spectral broadening is observed when using a Hann window for transmit apodization. This may be explained by studying the beam profiles shown in Fig. 4.7. The significant reduction in beam width observed when using a

Hann window should lead to spectral broadening when tracking at high beam-to-flow angles. The ripples which can be observed in the beam profile when using a rectangular apodization could potentially lead to artifacts in the tracking Doppler spectrum. However, no artifacts were seen in the spectra shown in Fig. 4.5 when using a rectangular window, and this also results in the best SNR. Thus, it is not recommended to use transmit apodization for tracking Doppler in this setup.

A limitation of the simulation results for the high velocity jet flow is that only the central flow line containing the maximum velocity was included. The other flow lines contain lower velocities, and should not influence the spectral shape close to the maximum velocity. However, they may have a smaller beam-to-flow angle, thus potentially yielding a higher Doppler shift. The single flow line model is, however, still useful for comparison between the different Doppler modalities.

In the results presented in Fig. 4.6, it was assumed that tracking is performed in the flow direction. For large beam-to-flow angles ( $> 60^\circ$ ), the velocity estimates are very sensitive to errors in the tracking angle. This motivated an investigation on the potential for automatic angle correction at high beam-to-flow angles. The results in Fig. 4.9 show that, when the beam-to-flow angle is  $71^\circ$ , the highest spectral amplitude is indeed observed along the flow direction, indicating that automatic angle correction is feasible. However, without spatial or temporal averaging, the spectral amplitude estimates will have a standard deviation equal to the expectation value, and this can result in high variance in the tracking angle. In the specific case presented in Fig. 4.9, where the true beam-to-flow angle is  $71^\circ$ , the maximum amplitudes of spectras produced with tracking angles  $60^\circ - 80^\circ$  are all less than 1 dB below that of the correct tracking angle, and thus the risk of error is high unless spatiotemporal averaging is performed.

The results in the right panel of Fig. 4.9 showed that, for the current setup, using the -6 dB or -12 dB threshold for automatic angle correction would lead to a slight underestimation of the tracking angle. The small discrepancy in tracking angle would, however, contribute significantly (9%) to underestimation of the maximum velocity because of the high beam-to-flow angle. It should be noted, however, that the bias in tracking angle is dependent on scanning parameters and the geometry of the flow. Changing parameters in the scan sequence may therefore reduce or remove the bias. Another possibility is that knowledge of the bias in the tracking angle may be used for calibration of this parameter using the model.

Good correspondence was seen between the *in vitro* results and model predictions, strengthening the validity of the model and its predictions on spectral broadening and dependency on tracking angle. Some discrepancies can be seen by studying the right panel of Fig. 4.8 and the left panel of Fig. 4.9, but a possible explanation to these is that the maximum velocity in the flow phantom is lower than 2 m/s, either due to spectral broadening or erroneous angle correction in the ground truth CW Doppler measurement.

The *in vivo* results presented in Fig. 4.10 show the feasibility of using tracking Doppler to measure the maximum velocity in an aortic insufficiency. Despite some acquisition limitations, tracking Doppler spectra could be generated and the contour of the spectrum could be delineated at two times the Nyquist velocity, where the

corresponding PW Doppler spectrum was obscured by clutter or the clutter filter band. Movement of the jet during the cardiac cycle would require dynamic movement of the sampling volume to achieve optimal spectra and estimates for the tracking angle. The spatial resolution of tracking Doppler would also require additional precision of the observer when choosing the sample volume. These challenges may be addressed by either using spatial averaging or dynamic detection of jet position, but this was beyond the scope of this work. On the other hand, when using tracking Doppler, color Doppler images may be generated from the same data, and the sample volume position and the tracking angle may be adjusted after data acquisition. This may facilitate manual or automatic correction of position and tracking angle in post-processing, provided that the jet is in the imaging plane, and that the data processing is sufficiently fast for practical use.

The performance of the 2-D tracking Doppler technique, similar to PW Doppler and CW Doppler, is reduced when the flow direction is not in the imaging plane. For out-of-plane flow, the effective transit-time is limited by the size of the ultrasound field in the elevation direction, and the tracking Doppler method then has less advantage over conventional PW Doppler. Another notable limitation is that the current tracking Doppler method assumes straight flow lines. Curvilinear flow would shorten the observation time of individual scatterers and contribute to increased spectral broadening in the tracking Doppler spectra. Both the implementation of tracking Doppler on a 3-D probe, allowing tracking in the elevation direction, and tracking along curved flow lines are possible future improvements of the method.

## 4.5 Conclusion

Properties of the 2-D tracking Doppler method for cardiac applications have been investigated using a signal model. Regarding spectral broadening of simulated spectra, the tracking Doppler method clearly outperformed angle-corrected PW Doppler by reducing the spectral broadening with a factor of more than six for all beam-to-flow angles. For beam-to-flow angles below  $60^\circ$ , the spectral broadening of tracking Doppler spectra was comparable to that of CW Doppler with flow in the beam direction. In a simulation of a straight tube phantom with beam-to-flow angle  $71^\circ$ , the maximal spectral amplitude was found when the tracking angle coincided with the flow angle, whereas the minimal spectral broadening was seen when the beam-to-flow angle was  $69^\circ$ . The model was validated using an *in vitro* flow phantom measurement. *In vivo* results showed the feasibility of using the tracking Doppler technique to measure maximum flow velocities in an aortic insufficiency.

# References

- [1] L. Hatle, A. Brubakk, A. Tromsdal, and B. Angelsen, “Noninvasive assessment of pressure drop in mitral stenosis by doppler ultrasound.,” *British heart journal*, vol. 40, no. 2, pp. 131–140, 1978.
- [2] T. Skjaerpe and L. Hatle, “Noninvasive estimation of systolic pressure in the right ventricle in patients with tricuspid regurgitation,” *European heart journal*, vol. 7, no. 8, pp. 704–710, 1986.
- [3] J. Lewis, L. Kuo, J. Nelson, M. Limacher, and M. Quinones, “Pulsed doppler echocardiographic determination of stroke volume and cardiac output: clinical validation of two new methods using the apical window.,” *Circulation*, vol. 70, no. 3, pp. 425–431, 1984.
- [4] T. Skjaerpe, L. Hegrenaes, and L. Hatle, “Noninvasive estimation of valve area in patients with aortic stenosis by doppler ultrasound and two-dimensional echocardiography.,” *Circulation*, vol. 72, no. 4, pp. 810–818, 1985.
- [5] L. Hatle, B. Angelsen, and A. Tromsdal, “Noninvasive assessment of atrioventricular pressure half-time by doppler ultrasound.,” *Circulation*, vol. 60, no. 5, pp. 1096–1104, 1979.
- [6] S. Samstad, L. Hegrenaes, T. Skjaerpe, and L. Hatle, “Half time of the diastolic aortoventricular pressure difference by continuous wave doppler ultrasound: a measure of the severity of aortic regurgitation?,” *British heart journal*, vol. 61, no. 4, pp. 336–343, 1989.
- [7] H. Baumgartner, J. Hung, J. Bermejo, J. B. Chambers, A. Evangelista, B. P. Griffin, B. Iung, C. M. Otto, P. A. Pellikka, and M. Quinones, “Echocardiographic assessment of valve stenosis: Eae/ase recommendations for clinical practice,” *European Journal of Echocardiography*, 2008.
- [8] P. Lancellotti, C. Tribouilloy, A. Hagendorff, L. Moura, B. A. Popescu, J.-L. Monin, L. A. Pierard, L. Badano, J. L. Zamorano, R. Sicari, *et al.*, “European association of echocardiography recommendations for the assessment of valvular regurgitation. part 1: aortic and pulmonary regurgitation (native valve disease),” *European Journal of Echocardiography*, vol. 11, no. 3, pp. 223–244, 2010.

- 
- [9] P. Lancellotti, L. Moura, L. A. Pierard, B. A. Popescu, C. Tribouilloy, A. Hagendorff, J.-L. Monin, L. Badano, J. L. Zamorano, R. Sicari, *et al.*, “European association of echocardiography recommendations for the assessment of valvular regurgitation. part 2: mitral and tricuspid regurgitation (native valve disease),” *European Journal of Echocardiography*, vol. 11, no. 4, pp. 307–332, 2010.
- [10] C. O. Lima, D. J. Sahn, L. M. Valdes-Cruz, S. Goldberg, J. V. Barron, H. Allen, and E. Grenadier, “Noninvasive prediction of transvalvular pressure gradient in patients with pulmonary stenosis by quantitative two-dimensional echocardiographic doppler studies.,” *Circulation*, vol. 67, no. 4, pp. 866–871, 1983.
- [11] T. Loupas and R. W. Gill, “Multifrequency doppler: improving the quality of spectral estimation by making full use of the information present in the backscattered rf echoes,” *Ultrasonics, Ferroelectrics and Frequency Control, IEEE Transactions on*, vol. 41, no. 4, pp. 522–531, 1994.
- [12] H. Torp and K. Kristoffersen, “Velocity matched spectrum analysis: A new method for suppressing velocity ambiguity in pulsed-wave doppler,” *Ultrasound in medicine & biology*, vol. 21, no. 7, pp. 937–944, 1995.
- [13] D. H. Evans and W. N. McDicken, *Doppler ultrasound: physics, instrumentation, and signal processing*, pp. 155–160. Wiley Chichester, 2 ed., 2000.
- [14] T. D. Fredriksen, I. K. Ekroll, L. Lovstakken, and H. Torp, “2-D tracking Doppler: a new method to limit spectral broadening in pulsed wave Doppler.,” *Ultrasonics, Ferroelectrics and Frequency Control, IEEE Transactions on*, vol. 60, no. 9, pp. 1896–1905, 2013.
- [15] T. D. Fredriksen, J. Avdal, I. K. Ekroll, T. Dahl, L. Lovstakken, and H. Torp, “Investigations of spectral resolution and angle dependency in a 2-D tracking doppler method.,” *Ultrasonics, Ferroelectrics and Frequency Control, IEEE Transactions on*, vol. 61, no. 7, pp. 1161–1170, 2014.
- [16] B. Angelsen, “A theoretical study of the scattering of ultrasound from blood,” *Biomedical Engineering, IEEE Transactions on*, no. 2, pp. 61–67, 1980.
- [17] J. A. Jensen, “Field: A program for simulating ultrasound systems,” in *10TH NORDIC/BALTIC CONFERENCE ON BIOMEDICAL IMAGING, VOL. 4, SUPPLEMENT 1, PART 1: 351–353*, Citeseer, 1996.
- [18] J. A. Jensen, “Simulation of advanced ultrasound systems using Field II,” in *Biomedical Imaging: Nano to Macro, 2004. IEEE International Symposium on*, pp. 636–639, IEEE, 2004.
- [19] S. Ricci, R. Matera, and P. Tortoli, “An improved doppler model for obtaining accurate maximum blood velocities,” *Ultrasonics*, 2014.